The role of LRRK2 in interferon gamma-mediated neuronal immune response

Dissertation

zur Erlangung des Grades eines
Doktors der Naturwissenschaften

der Mathematisch-Naturwissenschaftlichen Fakultät
und
der Medizinischen Fakultät
der Eberhard-Karls-Universität Tübingen

vorgelegt
von

Silvia De Cicco
Aus Mailand, Italien

August, 2020

Tag der mündlichen Prüfung: .....10. Dezember 2020.....

Stellv. Dekan der Math.-Nat. Fakultät: Prof. Dr. József Fortágh

Dekan der Medizinischen Fakultät: Prof. Dr. Bernd Pichler

1. Berichterstatter: Jun. Prof. Dr. Michela Deleidi

2. Berichterstatter: Prof. Dr. Julia Skokowa

Prüfungskommission: Prof. Dr. Thomas Gasser

Prof. Dr. Stefan Liebau

Erklärung / Declaration:

Ich erkläre, dass ich die zur Promotion eingereichte Arbeit mit dem Titel:

„ The role of LRRK2 in interferon gamma-mediated neuronal immune response “

selbständig verfasst, nur die angegebenen Quellen und Hilfsmittel benutzt und wörtlich oder inhaltlich übernommene Stellen als solche gekennzeichnet habe. Ich versichere an Eides statt, dass diese Angaben wahr sind und dass ich nichts verschwiegen habe. Mir ist bekannt, dass die falsche Abgabe einer Versicherung an Eides statt mit Freiheitsstrafe bis zu drei Jahren oder mit Geldstrafe bestraft wird.

I hereby declare that I have produced the work entitled " The role of LRRK2 in interferon gamma-mediated neuronal immune response ", submitted for the award of a doctorate, on my own (without external help), have used only the sources and aids indicated and have marked passages included from other works, whether verbatim or in content, as such. I swear upon oath that these statements are true and that I have not concealed anything. I am aware that making a false declaration under oath is punishable by a term of imprisonment of up to three years or by a fine.

Tübingen, den .....4. August 2020..... .....

Datum / Date Unterschrift /Signature

Statement of contributions

Part of the thesis was published in bioRxiv, in the work "Interferon-γ signaling synergizes with LRRK2 in human neurons and microglia" from Silvia De Cicco*, Dina Ivanyuk*, Wadood Haq, Vasiliki Panagiotakopoulou, Aleksandra Arsić, David Schön dorf, Cong Yu, Maria-Jose Perez, Ruggiero Pio Cassatella, Meike Jakobi, Nicole Schneiderhan-Marra, Ivana Nikić-Spiegel, Thomas Gasser, Michela Deleidi [1]

*contributed equally to the work

In this paper, M.D., S.D.C., D.I., V.P. conceived and designed the experiments. S.D.C., D.I., and V.P. performed most of the experiments and analysed data; W.H. and D.I. designed, performed, and analysed data relative to Ca2+ measurements; C.Y. and D.S. generated and characterized LRRK2 KO iPSCs; M.J.P performed experiments and analysed data; I.N. and A.A. designed and performed dSTORM experiments; S.D.C. analysed STORM data; D.S. performed initial experiments on interferon signaling; S.D.C. and R.P.C. performed IQGAP1 experiments; N.S. and M.J. performed Multiple Elisa experiments; T.G. provided patient samples; M.D. supervised the study, acquired funding, and wrote the manuscript with contribution from all authors.

Part of the thesis is currently submitted to Nature Communications.

In this thesis, Dr. Dina Ivanyuk performed the experiments with cytosolic fractionation (figure 6C), performed and analysed staining in figure 7D, E, and performed and analysed together with Dr. Wadood Haq the live calcium imaging experiments (figure 8).

Dr. David Schöndorf generated the LRRK2 knock out lines (figure 1A) and performed the initial experiment on the interferon signaling (figure 4A).

Index

Abstract

Increasing evidence suggests a role for interferons (IFNs) in neurodegeneration. Parkinson's disease (PD) associated kinase LRRK2 has been implicated in IFN type II (IFN) response in infections and nigral neuronal loss. However, whether and how LRRK2 synergizes with IFN-γ still remains unclear. Here, we employed dopaminergic (DA) neurons differentiated from patient induced pluripotent stem cells to unravel the role of IFN-γ in LRRK2-PD. We show that IFN-γ induces LRRK2 expression in DA neurons. LRRK2 G2019S, the most common PD-associated mutation, sensitizes DA neurons to IFN-γ by decreasing AKT phosphorylation. Moreover, IFN-γ suppresses NFAT activity and synergistically enhances LRRK2-induced defects of NFAT activation. Furthermore, LRRK2 G2019S negatively regulates NFAT via calcium and microtubule dynamics, leading to defects of neurite elongation. We propose that synergistic IFN-γ/LRRK2 activation serves as a direct link between inflammation and neurodegeneration in PD.

Abstract DE

Zunehmende Beweise deuten darauf hin, dass die Interferone (IFNs) bei der Neurodegeneration eine Rolle spielen. Die Parkinson-assoziierte Kinase LRRK2 wurde bereits mit der IFN Typ II (IFN) Antwort bei Infektionen und dem Verlust der Neurone der Substantia nigra in Verbindung gebracht. Dennoch ist unklar, ob und wie LRRK2 und IFN-γ miteinander in Zusammenhang stehen. Zur Enrätselung der Rolle von IFN-γ in LRRK2-PD haben wir uns mit dopaminergen (DA) Neuronen beschäftigt, welche aus induzierten pluripotenten Stammzellen von Parkinson Patienten differenziert wurden. Wir zeigen, dass IFN-γ die LRRK2 expression in dopaminergen Neuronen induziert. LRRK2 G2019S, die am häufigsten vorkommende mit Parkinson assoziierte Mutation, macht die DA Neurone durch eine Verringerung der AKT Phosphorylierung empfindlicher für IFN-γ. Außerdem unterdrückt IFN-γ die NFAT Aktivität und erhöht die durch LRRK2 induzierten Defekte der NFAT Aktivierung. Desweiteren wirkt LRRK2 G2019S negativ regulierend auf NFAT durch Kalzium und dynamische Prozesse der Mikrotubuli, was zu einer Verkürzung der Neurite führt. Wir vermuten, dass die synergistische IFN-γ/LRRK2 Aktivierung eine direkte Verbindung zwischen Entzündungen und der Neurodegeneration in Parkinson herstellt.

1. Introduction

1.1 Parkinson's disease

Parkinson's disease (PD) is a common neurological disorder, with an overall incidence of 10-18 affected people in 100'000 people of all ages [2]. However, ageing is the main risk factor for developing PD. Indeed, PD affects about 1% of the population over the age of 60, and this percentage rises to 5% in the population older than 85 years [3]. In the majority of cases, people who develop PD before the age of 60 are carriers for a mutation in a gene that leads to familial PD, which could be either autosomal dominant (such as α-synuclein or Leucine Rich Repeat Kinase 2 -LRRK2-) or recessive (such as Parkin or PTEN-induced kinase 1 -PINK1-). Classical PD symptoms, first described by James Parkinson in 1817 in his "An Essay on the Shaking Palsy", are motor symptoms such as resting tremors, as well as bradykinesia, muscular rigidity and impaired gait and posture. Yet, non-motor symptoms are also present, including REM sleep disturbances, anosmia, constipation, pain and fatigue. Besides, cognitive symptoms such as dementia, and psychiatric symptoms such as depression and/or psychosis, also occur in PD patients. The diagnosis of PD is based on the presence of pathophysiological markers that can only be confirmed post mortem: a) the progressive degeneration of the dopaminergic (DA) neurons of the substantia nigra pars compacta (SNpc) and midbrain; b) the formation of intracellular protein aggregates called Lewy bodies (round aggregates) or Lewy neurites (spindle-like aggregates), of which the main components are α-synuclein, ubiquitin and neurofilament [4]. The depletion of DA neurons leads to a dopamine loss that affects the putamen neurons. Interestingly, motor symptoms are thought to be occurring when about 30% of the SNpc neurons have died, and a decrease of about 80% of dopamine is present in putamen neurons [5, 6]. Progression of the disease can greatly vary from person to person, but it is assumed that, on average, 12-14 years occur between the onset of the first non-motor symptoms and the motor symptoms [7]. This suggests a window of opportunity to be present for disease-modifying treatments to delay or prevent the disease, provided reliable and accessible biomarkers are found, for which different trials are ongoing.

1.1.1 Risk factors for PD

As mentioned, the major risk factor for PD is ageing. However, other important risk factors have emerged over the years. In fact, there is a known gender specific incidence, as men are 1.5-fold more likely than women to develop the disease [8], probably due to hormonal differences or to different lifestyles. Ethnicity may also play a role, since higher incidence has been found in people of Caucasian descent compared to Asian, while Africans show the lowest rate [9]. This could be

related to exposure to different environmental agents. Among the environmental factors, prior head traumas leading to concussion are among the most highly associated with disease onset [10]. Besides, viral infections have been linked as well with increased risk for PD. Indeed, viral-induced encephalopaties have been shown to cause PD-like symptoms [2, 11]. This was discovered after the influenza outbreak of 1918 left many cases of parkinsonism throughout Europe, with PD-like motor symptoms, but no Lewy bodies [12]. Besides, incidence of PD has been reported to be higher in people born during the pandemia, suggesting that maternal and early life viral infection could as well be associated with PD [13]. Apart from viral exposure, exposure to pesticides has been shown to increase the risk of developing PD. For example, paraquat, a common herbicide substance, has a remarkably similar structure to 1-methyl-4-phenyl-1,2,3,6-tetrahydropyridine (MPTP), which inhibits Complex I of the mitochondria electron transport chain. The metabolite of MPTP, 1-methyl-4-phenylpyridinium (MPP+), was found to induce rapid PD symptoms back in 1982, and has been used ever since to generate various animal models of PD [14, 15]. Moreover, exposure to the natural pesticide rotenone also increases the risk for PD [16]. However, the general consensus in the community is that environmental factors and genetic background have to coexist to lead to the development of PD. Interestingly, there are also protecting factors for PD, in particular, tobacco smoking and coffee drinking [17]. Supporting inflammation as a potential cause of PD onset and development, the usage of nonsteroidal anti-inflammatory drugs has been shown to be a protective factor [17].

1.1.1.1 Evidence for a role of the immune system in the central nervous system of PD patients

The presence of peripheral inflammation as a marker of PD is still being debated, since contradictory results have been published. In fact, analysis of cytokine profile in the serum of PD patients from various cohorts have each shown increased expression of different molecules, such as Tumor necrosis factor-α (TNF-α), interleukin-6 (IL-6) [18], interleukin-2 (IL-2) [19], RANTES [20] and of interferon-γ (IFN-γ) in the plasma [21]. Increased peripheral activation of lymphocytes has also been observed, especially in pro-inflammatory T cells, which tend to expand during/after a viral infection, consistently with the hypothesis that this has a role in the developing pathology [22-24]. Differently from the periphery, where there is no consensus yet, inflammation of the central nervous system (CNS), in terms of activation of astrocytes as well as microglia, has long been known to be present in brains of PD patients [25, 26]. Indeed, astroglial concentration in the substantia nigra of PD patients was discovered to be approximately 30% higher than in controls in post-mortem tissues [26]. In particular, astrocytes are thought to exert a neuroprotective role by detoxifying from reactive oxygen species (ROS), and are therefore accumulated in areas where

neurodegeneration is occurring, while also producing Glial-cell-line-Derived Neurotrophic Factor (GDNF) [26, 27]. Lymphocytes infiltration has also been shown in PD brains, which suggests blood-brain-barrier alterations to be a feature of the disease. In fact, mostly cytotoxic CD8+ [25] or CD4+ T cells [28] specifically localized in the substantia nigra were detected, but no B cells or natural killer cells. Microglia is usually in a resting state, if no inflammatory insult occurs [29]. However, when activated, it produces large amounts of potential neurotoxins, such as superoxide radicals and pro-inflammatory cytokines. Reactive microglia has been found in the substantia nigra of both familial [25] and sporadic [30] PD. Moreover, activated microglia has been shown to induce neurotoxicity *in vitro* [31], and it has been suggested that their ROS production might be responsible for DA neuronal death [32]. Beside ROS production, pro-inflammatory cytokines have also been detected at higher levels in basal ganglia and cerebrospinal fluid (CSF) of PD patients compared to controls, including TNF-α, interleukin-1β (IL-1β) and IL-6 [33]. Interestingly, mice who are TNF receptor knock out (KO) show no PD phenotype after exposure to MPTP [34], suggesting an important role of this cytokine in DA neurodegeneration. Furthermore, TNF-α, IL-1β and IFN-γ were also detected to be present at higher levels in the substantia nigra of PD patients [35, 36], and DA neurons express receptors for these cytokines, to which they might be sensitive to. Several SNPs in pro-inflammatory cytokines have been associated with increased risk for PD [37, 38], and, as already mentioned, there is decreased risk for PD in people who assume nonsteroidal anti-inflammatory drugs. Animal models of PD also display microglia activation: both mice [39] and monkeys [40] subjected to MPTP injection show the presence of activated microglia. Importantly, microglia activation has been shown in mice models of MPTP to precede neurodegeneration [28, 39], and that inhibiting the activation with minocycline prevents neuronal death [41]. Besides, infiltration of CD8+ T cells has also been detected in MPTP mice's substantia nigra, similarly to patients [28]. All of this taken together, suggests that the immune system has an important role in PD in the brain. Whether this role is a cause or a consequence of the DA neurons degeneration remains to be elucidated.

1.1.2 Genetics of PD

Most cases of PD are thought to be sporadic, with more than 85% unrelated to genetic mutations. However, a small percentage (10-15%) is due to a genetic mutation or duplication/triplication of a gene. The first monogenic form of PD was found in the mutation of the α-synuclein gene *SNCA* [42]. Afterwards, many genes have been correlated with monogenic PD (PARK1 to 23), of which some are autosomal dominant, such as the already mentioned *LRRK2*, some are recessive, such as *Parkin*. Recessive mutations generally lead to early onset PD, possibly due to a lack of

compensatory mechanisms. However, the onset is more variable with dominant mutations. Besides mutations leading to familial PD, to this date, 90 risk loci associated with PD linkage have been identified with genome-wide association studies (GWAS), which are estimated to explain about 36% of PD heritability [43]. Among these, the highest risk of developing PD is present in people carrying *GBA1* mutations [44]. Since the mutations in the genes encoded from these loci have incomplete penetrance, this corroborates the hypothesis that the environment also plays a role in the onset of the disease. However, the interplay between genetics and environment is far from being deciphered.

1.1.2.1 LRRK2

Mutations of the *LRRK2* gene, otherwise known as PARK8 or dardarin, are the most common cause of familial PD, being present in about 4% of cases [45]. *LRRK2* single nucleotide polymorphisms (SNPs) have also been shown to increase the risk of sporadic PD, and are present in about 1% of cases. The *LRRK2* gene encodes for a large, multi-domain protein that is involved in many different cellular pathways. The 280 kDa LRRK2 protein has 2527 aminoacids and 7 domains (Figure 1). From the N terminal to the C terminal, the domains are as follows: an armadillo domain (Arm), an ankyrin domain (Ank), a leucine rich repeat domain (LRR), a Ras of complex GTPase (Roc) domain, a C-terminus of Roc (COR) domain, a kinase and a WD40 domain. Since it has both a GTPase and a kinase domain, LRRK2 shows two different enzymatic activities. The most common mutations associated with PD are located in the catalytic sites, and alter LRRK2 function. For example, the most common PD-associated LRRK2 mutation G2019S, leads to a ~2-fold increase of protein kinase activity [46], while mutations in the GTPase domain, such as R1441C, lead to a decreased GTPase activity [47]. Recently, a 3D model of LRRK2 has been proposed, in which the protein-protein interaction is determinant for stabilizing the catalytic part of the dimer [48].

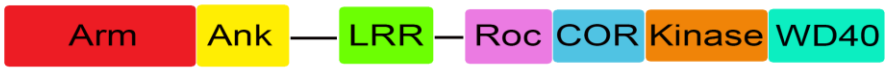

Figure 1. Scheme of LRRK2 protein domains. Arm: armadillo domain; Ank: ankyrin domain; LRR: leucine rich repeat domain; Roc: Ras of complex GTPase domain; COR: C-terminus of Roc domain.

LRRK2 is ubiquitously expressed, but it has been found to be highly expressed in lungs, kidney and the brain [49, 50]. In particular, it has been shown that LRRK2 is expressed in human brain in the striatum, as well as the substantia nigra, with similar expression levels between healthy controls and patients carrying the G2019S mutation [51]. LRRK2 has been found to have several interactors with different methods, including various Rab GTPases (with mass spectrometry as well as yeast two-

hybrid screenings) [52, 53] and members of the mitogen activated protein kinase family [54]. LRRK2 is generally found as a homodimer in the proximity of membrane compartments [55]. When mutated, or after treatment with kinase inhibitors, LRRK2 has been detected in inclusions associated with microtubules [56]. LRRK2 is regulating cellular homeostasis in different ways: to name a few, by modulating vesicles and mitochondrial dynamics, as well as the cytoskeleton. LRRK2 has a key role in regulating vesicles sorting and transport, also by direct phosphorylation of several Rab GTPases [52]. In particular, LRRK2 has been shown to directly interact with Rab5 [57], Rab32 [53], Rab7L1 (Rab29) [58] and, importantly, phosphorylates Rab10, which has been proposed as a potential biomarker for LRRK2 activity in clinical trials [59, 60]. The interaction of LRRK2 with these GTPases regulates the endolysosomal system from early sorting to secretion, and increased levels of LRRK2 wild type (WT) expression, as well as its mutated form, have been shown to alter the pathway [57]. LRRK2 has been proposed to be involved with regulating vesicles dynamics also at the autophagy level [61], by phosphorylating Beclin [62]. However, there is no consensus about whether LRRK2 is increasing or decreasing autophagy, as opposite results were reported [63-65]. Importantly, LRRK2 affects mitochondria homeostasis by interacting with dynamin- related protein 1 (DRP1), OPA1 and Mitofusin [66, 67]. Interestingly, LRRK2 is often found in the proximity of the mitochondria membrane [50]. A current hypothesis is that it might work as a scaffolding protein for the modulation of mitochondria fission and fusion. Indeed, various LRRK2 mutant models have shown mitochondria fragmentation [67-70]. Besides, mitophagy could be modulated by LRRK2 indirectly, by phosphorylation of specific Rabs, as well as directly, by regulating Miro degradation [71]. Furthermore, LRRK2 has an effect on intracellular calcium homeostasis. In fact, neurons derived from mice carrying the LRRK2 G2019S or R1441C mutations showed reduced ability in calcium buffering as well as mitochondrial impairment [72], accompanied by an elicited mitochondria calcium uptake [73]. Moreover, a reduced calcium response to KCl depolarization was recorded in LRRK2 G2019S mutant human induced pluripotent stem cells (iPSCs, see chapter 1.4)-derived sensory and DA neurons [74, 75]. Lastly, LRRK2 has been discovered to regulate microtubules by phosphorylation [76] and acetylation of tubulin [77]. Direct phosphorylation of tubulin by LRRK2 has been proposed to stabilize microtubules by increasing its polymerization [78]. Indeed free tubulin levels are inversely correlated to LRRK2 kinase activity in mice models [78]. Moreover, tubulin acetylation has been found to be decreased in peripheral blood mononuclear cells (PBMCs) of sporadic as well as LRRK2 G2019S mutant PD patients [79]. Interestingly, LRRK2 R1441C mutant primary neurons showed defective microtubules acetylation and stabilization [80]. All these functions are very important in post-mitotic neurons of the SNpc. If we consider that LRRK2 has a role in regulating a) vesicular

sorting, which suggests that neurotransmitters release could be controlled by it, b) mitochondria/calcium homeostasis, which is particularly sensitive for DA neurons that need tight regulation of cellular stress to survive, and c) the cytoskeleton, so that neurite morphology could depend on it, it might explain why mutations of the protein lead to such specific neurodegeneration. However, LRRK2 G2019S overexpressing mice don't show overt DA neuronal loss. Nonetheless, they show reduced dopamine transmission in the striatum, as well as decreased motor performances [81], and mitochondrial and autophagy alterations, together with reduced neurite complexity in primary cultures [82]. The lack of the main characterizing PD feature suggests that a second hit is necessary for neurodegeneration to occur, and that other models might be needed to investigate it.

1.1.3 Therapeutic approaches

To this date, there is no cure for PD. However, treatments targeting the symptoms are available. The standard therapy is based on dopamine supplementation, with drugs developed like levodopa, dopamine agonists and monoamine oxidase (MAO) inhibitors, which are treating the motor symptoms like rigidity and bradykinesia well. On the other hand, tremor necessitates further medicines to be under control, such as clozapine. However, several adverse effects are common for dopamine agonists. For example, they are associated with high onset of hallucinations, which is why they are not recommended for patients who have impulse control issues. Besides, these drugs may have other adverse reactions, such as nausea and oedemas. Especially in the case of levodopa, one of the main issues is that long term therapy often leads to fluctuation of dopamine concentration that leads to dyskinesia and psychosis. Since levodopa is the most efficient drug, the tendency is to start treatment with a combination of levodopa at lower dosage, combined with dopamine agonists or a MAO inhibitor. Generally, PD-associated psychosis is treated with clozapine or the serotonin agonist primavanserin. Depression symptoms, which are commonly associated with PD, are cured with tricyclic antidepressants or serotonin reuptake inhibitors. In late stages of the disease, neuronal loss-associated dementia is treated with cholinesterase inhibitors such as rivastigmine. Lately, surgical deep brain stimulation of the thalamus has become more established for treating moderate to severe PD motor symptoms, when dyskinesia becomes debilitating. Interestingly, a study by the EARLYSTIM study group showed that early deep brain stimulation after PD diagnosis led to higher beneficial effects in the patients quality of life later [83]. However, as mentioned, none of these therapies cure the disease. Efforts have been made to develop alternative strategies to achieve the final goal of curing the disease, with several studies on stem cells-derived DA neurons transplantation [84-86], as well as clinical trials ongoing utilizing gene therapy [87],

glucosylceramide synthase inhibitors [88, 89] and LRRK2 kinase inhibitors [90]. Unfortunately, there is still a lot be uncovered about PD pathogenesis.

1.2 LRRK2 in the immune system

LRRK2 displays high expression levels in cells of the innate immune system, including monocytes, macrophages and microglia [91], though, for this cell type, the protein expression is still under discussion. Curiously, monocytes belonging to the pro-inflammatory subtype CD14/CD16 double positive have shown the highest expression levels of LRRK2 [92]. Higher expression of LRRK2 has also been detected in neutrophils, B cells, T cells and CD16 positive monocytes from sporadic PD patients compared to controls [59, 93]. Interestingly, healthy subjects carrying the LRRK2 G2019S mutation showed increased expression levels of IL-1β in the serum compared to WT controls [94], suggesting a role for the kinase activity of LRRK2 in regulating inflammatory responses. From the genetic point of view, *LRRK2* SNPs have been associated with increased susceptibility for several immune related disorders, such as inflammatory bowel disease (IBD), Crohn's disease, ulcerative colitis and leprosy [95-98]. Notably, LRRK2 expression is induced in immune cells upon stimulation with the classic pro-inflammatory bacterial protein lipopolysaccharide (LPS) [99], as well as upon pathogen exposure [91]. Furthermore, LRRK2 expression is induced in human monocytes and macrophages by stimulation with IFN-γ [92, 100, 101]. Besides, LRRK2 has been shown to have a IFN-γ responsive element at the promoter level [100], which suggests direct regulation of its expression is occurring. Moreover, PD patients with LRRK2 mutations showed an altered cytokine profile in the serum [102]. Interestingly, LRRK2 KO mice showed a propensity to develop stronger IBD-like symptoms upon stimulation with the bacteria *Listeria monocytogenes* [103]. Of note, LRRK2 has also been found to regulate the cellular localization of the Nuclear Factor of Activated T-cells (NFAT), and this mechanisms might have many implications for the immune system regulation [104, 105]. For example, Liu and colleagues reported that LRRK2 KO mice had more severe inflammatory reactions to experimental colitis, mediated by the deregulation of NFAT [104]. Moreover, LRRK2 has been shown to control the response of dendritic cells to fungal infections from *Aspergillus* by modulating NFAT translocation [105]. In addition, LRRK2 has also been found to modulate NF-kB activity, an important transcription factor involved, for example, in the production of cytokines such as IL-1β upon LPS-mediated activation of microglia [106], thus suggesting LRRK2 as a pivotal player in microglia activation. Indeed, various experiments in mice-derived primary microglia have demonstrated a reduced production of pro-inflammatory cytokines upon LRRK2 knockdown, KO or kinase inhibition [106, 107]. Besides, LRRK2 has been shown to be of importance for microglia migration,

as Choi et al. have demonstrated that the G2019S mutation inhibits Focal Adhesion Kinase (FAK) activity [108], while Ma et al. have shown that LRRK2 expression regulates Chemokine (C-X3-C) receptor 1 (CX3CR1), which promotes microglia migration [109]. Furthermore, primary microglial cells derived from LRRK2 R1441G mutant mice have shown increased levels of released pro-inflammatory cytokines, and, upon LPS activation, their supernatant caused neurotoxicity [99].

1.2.1 LRRK2 role in infections

Recently, LRRK2 has been shown to have important roles in the clearance of bacterial infections. For instance, Toll-like receptor activation leads to LRRK2 phosphorylation, and subsequent activation [110]. Moreover, LRRK2 KO mice have shown higher infective burden after exposure to *Salmonella Typhimurium*, connected to the absence of LRRK2-dependent NLRC4 activation and IL-1β production [111]. Interestingly, LRRK2 G2019S mice showed improved clearance of *Salmonella Typhimurium*, but not of Reovirus [112]. On the other hand, lack of LRRK2 activity has been found to be both helpful upon *Mycobacterium tuberculosis* infection, by limiting its replication [113], and harmful, by increasing the inflammatory state [114]. Therefore, while it is clear that LRRK2 plays a role in bacterial infections, this role might be pathogen-dependent.

1.3 Role of interferon gamma in PD

The main sources of IFN-γ, or interferon type II, are T cells and natural killer cells [115], but IFN-γ has been shown to be produced also by microglia *in vitro* [116, 117]. IFN-γ is usually produced in response to specific viral, bacterial or protozoal infections, and is involved in both innate and adaptive immune response, where it exerts several activities. Among others, IFN-γ upregulates antigen presentation on the surface of antigen presenting cells. In the brain, interferon type I and II have multiple roles in homeostasis regulation, and the ratio between the two has to be kept tightly controlled [118]. Interestingly, GWAS studies have implicated the IFN-γ signaling to be correlated with neurodegeneration [119, 120]. Moreover, a recent paper has pinpointed IFN-γ response as risk loci for PD [43]. However, IFN-γ has been thought to be involved in PD pathogenesis for some years. Indeed, PD patients show increased IFN-γ levels at plasma level [21], as well as in post mortem brain in the substantia nigra [36], and in glial cells of the substantia nigra [35]. Besides, IFN-γ expression has been found to be correlated with α-synuclein expression in PD patients substantia nigra [121]. Importantly, PD animal models have also suggested involvement of IFN-γ in neurodegeneration. In fact, numerous studies have found that IFN-γ leads to a selective DA neurons cell death. Mount and colleagues have reported that IFN-γ KO mice showed less sensitivity to MPTP treatment, with significantly more DA neurons present in their substantia nigra compared to

controls treated [21]. Moreover, Chakrabarty and colleagues showed that overexpression of IFN-γ in mice brain led to an age-progressive DA cell death dependent on the presence of astrogliosis and microgliosis [122, 123]. Furthermore, Kozina and colleagues have discovered that LPS-mediated cytokine release in the brain is accelerated in the presence of mutant LRRK2, leading to a faster selective DA loss mediated by IFN-γ responsive genes [124]. Another experimental model has corroborated the role of IFN-γ in PD. In fact, macaques affected by chronic PD displayed higher IFN-γ levels in serum and in the CNS, coupled with increased expression of TNF-α and increased astrocytes and microglia activation [125]. Mice models KO for IFN-γ as well as TNF-α showed that glial activation was dependent on the presence of the cytokines taken into consideration [125]. However, neurons, as well as microglia, express IFN-γ receptors subunits [126], but very little is known about the cell autonomous role of IFN-γ on neurons. Based on these premises, this project aimed at investigating the effect of IFN-γ chronic exposure on neurons.

1.4 iPSC-based modeling of PD

Due to the limited availability of brain samples, modeling neurological disorders in vitro has been challenging. Therefore, the possibility of generating induced pluripotent stem cells (iPSCs) from somatic cells has been fundamental to improve our knowledge of the pathophysiology of many neurological diseases, including PD [127]. iPSCs are able to differentiate in many cell types of the body, including but not limited to neurons and glial cells. IPSCs generation was first reported in 2006 by Takahashi and Yamanaka [128]. Indeed, they were able to induce stemness, with a process called cellular reprogramming, by transducing mouse fibroblasts with retroviral vectors expressing 4 pluripotency factors: Oct-4, Sox-2, c-Myc and Klf-4. These cells were then able to lead to embryonic development, when introduced into blastocysts, and to differentiate into cells of the three germinal layers after subcutaneous transplantation [128]. The same group was able to replicate this process in human fibroblasts [129]. Over the years, different reprogramming methods have been implemented: 1) by using different somatic cells, such as blood cells and keratinocytes [130, 131]; 2) by using different combination of genes ectopically expressed, such as Oct-4, Sox-2, c-Myc, Klf-4, NANOG, LIN-28, l-Myc [132, 133]; 3) by using delivery systems. For example, retroviruses have been employed first. However, they can only enter replicating cells, as well as having the tendency to integrate near a transcription starting site, leading to possible tumorigenesis [134]. For these reasons, alternative vectors have been investigated, such as lentiviral ones with a safer integration profile [134], which are able to reach the chromatin at all cellular mitotic stages [135]. Other non-integrating methods have been used successfully, such as adenoviral vectors [136], Sendai vectors [137], episomal vectors [138], supplement of the reprogramming proteins [139], and

transfecting modified mRNAs [140]. In principle, iPSCs circumvent the technical, as well as ethical, issues of using embryonic stem cells (ESCs), because they provide a potential unlimited cellular source for research, drug screening and eventually patient-specific cell therapy (Figure 2).

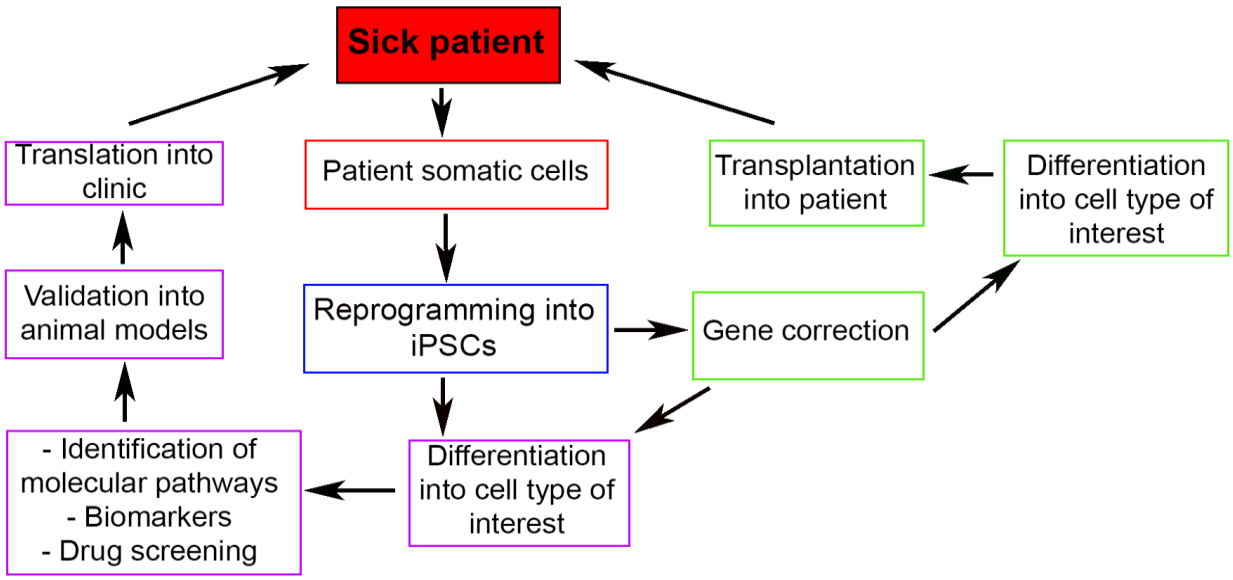

Figure 2. IPSC technology allows the reprogramming of virtually any kind of somatic cells, such as skin and blood-derived cells, into stem cells that can be differentiated into relevant cell types for the disease of interest. These patient-derived cells have the same genetic background. This might lead to the identification of molecular pathways involved in the disease, as well as possible biomarkers. IPSC-derived cells can be used for drug screening, from which potential targets should be validated in animal models, and, when successful, in clinical trials in humans (purple path). Patient derived cells might even be used as a source of autologous transplant of gene-corrected cells (green path).

IPSCs are a useful tool for PD modelling. Different protocols exist for the differentiation of iPSCs into DA neurons, the most affected neurons of the disease. Since the molecules responsible for the DA neurons generation during embryonic development are well established, protocols usually aim at recapitulating this process by exposure of the cells to a combination of small molecules similar to the developmental process [141, 142]. In particular, important molecules for the DA determination of proliferating neural progenitors are sonic hedgehog (Shh) and fibroblast growth factor 8 (Fgf-8), which are produced by the floor plate of the ventral and midbrain border. IPSCs have been generated from patients carrying the most common mutations for α-synuclein, Parkin, PINK1, DJ-1, GBA1, as well as LRRK2. For each mutation, altered phenotypes that might be correlated with the onset of PD pathology have been discovered in cells differentiated from iPSC. For example, iPSC-derived neural precursors cells (NPCs) with triplication of *SNCA* gene encoding for α-synuclein have been found to have reduced viability and growth, as well as impaired response to stress, when

challenged, reversed with knockdown of α-synuclein by short hairpin RNAs (shRNAs) [143]. Furthermore, iPSC-derived neurons carrying the same triplication showed delayed maturation, in terms of less DA neurons, with reduced neurite outgrowth and neuronal activity, compared to controls [144]. Besides triplications, point mutations of α-synuclein also lead to protein misfolding and accumulation in Lewy bodies. The group from Jaenisch generated iPSCs from patients carrying the A53T mutation in SNCA, and gene corrected it by exploiting the Zinc Finger Nucleases (ZFNs) technology. Neurons differentiated from these cells displayed increased endoplasmic reticulum (ER) stress and nitrosative stress when the mutation was present [145], as well as increased S-nytrosilation, which leads to altered mitochondria biogenesis and higher apoptotic rate [146]. IPSC-derived neurons from patients carrying *Parkin* mutations showed a significant increase in oxidative stress dependent on the increased expression of Monoamine Oxidases A and B (MAO A and MAO B), and DA transmission disruption [147]. Besides, morphological alterations were identified in *Parkin* mutant DA neurons, such as reduced neurite length and complexity due to microtubules instability [148]. Furthermore, abnormal mitochondria morphology was observed in iPSC-derived *Parkin* mutant neurons [149]. *PINK1* mutations lead as well to mitochondrial abnormalities, but also to increased cytosolic dopamine levels in DA neurons [150]. Moreover, it was shown that complex I activity was reduced in neurons carrying *PINK1* mutation, leading to reduced mitochondrial membrane potential, and consolidating PINK1 as an important mitochondria regulator protein [151]. IPSC-derived DA neurons carrying a *DJ-1* mutation showed neuromelanin-like aggregation, as well as increased oxydation of dopamine. This, in turn, leads to impaired GBA1 activity and lysosomal dysfunction, which contribute to α-synuclein aggregation [152]. These observations indicate that DJ-1 is important in DA neurons for the handling of oxydative stress. IPSCs carrying mutations of *GBA1*, the most common risk factor for PD, were generated in our lab, with corresponding isogenic controls. DA neurons differentiated from these iPSCs showed increased levels of α-synuclein, dysregulation of the autophagic/lysosomal pathway, altered calcium homeostasis [153], as well as ER stress increase, mitochondrial function and NAD+ metabolism alterations [154]. As for *LRRK2*, many groups have generated iPSCs from PD patients carrying mutations for the gene, with studies mainly focusing on the G2019S mutation. The first report was from Nguyen et al. in 2011, which showed increased α-synuclein levels and sensitivity to oxidative stress in iPSC-derived mutant neurons [155]. Interestingly, another study demonstrated that the toxicity of the G2019S mutation in neurons depends on the levels of both α-synuclein and LRRK2 itself, independently of the kinase activity [156]. Besides, multiple studies showed that LRRK2 mutant iPSC-derived neurons have reduced number of arborizations and neurites, as well as reduced length of the latter [75, 157, 158]. Moreover, mitochondrial abnormalities have been documented

also in *LRRK2* mutant neurons, including increased mitochondrial DNA damage [159] and altered mitochondria transport along the microtubules [71]. Lately, it has become evident that different mutations lead to the alteration of common pathways, suggesting these might be the pathways overall impaired in the disease.

However, there are some drawbacks for studying PD with iPSCs. First of all, it is very difficult to replicate the complexity of a 3D environment such as the brain, even if the application of the technique to generate "midbrain-like" organoids from iPSCs has much improved lately [160]. Most importantly, the reprogramming cancels any epigenetic memory [161], therefore nullifying the environmental component which plays a role in the development of the disease. Besides, neurons that have accumulated age-related issues are the target cells to consider with neurodegenerative diseases such as PD, which usually develop late in life. Moreover, it is important to keep in mind that proper controls are needed to be able to trust results generated with iPSCs. In fact, it is now established that iPSCs differentiation ability is extremely variable, due to a different epigenetic state and/or profile of gene expression present in the different cell lines. These variations could also affect different clones derived from the same sample [162, 163]. Importantly, a large study on 317 iPSC lines generated from 101 subjects showed that about 50% of the expression differences were due to genetic variability across individuals [164]. Besides, another study by Kilpinen and colleagues on 711 iPSCs derived from 301 subjects confirmed that 5 to 46% of differences in differentiation ability and morphology were arising from genetic variability [165]. To reduce the genetic bias, it is therefore important to generate isogenic control lines, and, if possible, to work with different clones from the same line. Thus, the analysed iPSC lines will have the same genetic background, and any detectable phenotype could be reliably identified as a consequence of the presence of the mutation of interest. Despite these shortcomings, due to their potential to scale up for high throughput screening, iPSCs can be an invaluable tool of new drug discovery, as well as for elucidating the still not well-known pathophysiology of PD.

2. Materials and methods

2.1 Cell culture

All the fibroblasts from which iPSCs were generated for this study are derived from patients that signed an informed consent, with approval of all protocols by the Ethics Committee of the University Hospital Tübingen and of the Medical Faculty. IPSCs carrying the G2019S mutation in LRRK2 (G2019S), as well as isogenic lines (CTRL, see table 1) were previously generated [158], and differentiated into NPCs and subsequently into dopaminergic neurons following a published protocol [142]. LRRK2 knockout (KO) lines were generated by Dr. David Schöndorf.

Control (CTRL)	One healthy control	2 gene corrected lines [158]
LRRK2 mutant (G2019S)	One artificial mutant [158]	2 patient derived lines
LRRK2 knock out (KO)	2 lines generated by ZFN technology from the healthy control (paper under revision)	

Table 1. IPSC lines used to perform experiments in the study.

Briefly, iPSCs were maintained in culture on mytomycin-inactivated CF-1 mouse embryonic fibroblasts (Globalstem MTI ThermoFisher), and split manually when needed (based on morphology of colonies, with brightfield images showing a dark centre due to density of the cells, without proliferation of differentiated cells at the borders), in medium containing 10 μM Rock Inhibitor Y-27632 2HCl (Selleckchem). Medium for iPSCs was as follows: knockout DMEM (Gibco Life Technologies), supplemented with 20% Knockout Serum replacement (Gibco Life Technologies), 500 μM β-mercaptoethanol (Sigma-Aldrich), 1% non-essential amino acids (Gibco Life Technologies), 1% penicillin/streptomycin (P/S, Merck Millipore), 1% GlutaMAX Supplement (Gibco Life Technologies), with the addition of 10 ng/mL FGF2 (Peprotech) to maintain stemness. NPCs generation was based on Reinhardt et al. protocol [142]. NPCs were maintained in culture on Matrigel-coated plates, and split with Accutase (Sigma-Aldrich) when confluency was reached, usually once every 5-6 days, at a 1:10-1:15 ratio, in medium containing 10 μM Rock Inhibitor Y-27632 2HCl (Selleckchem). Medium for NPCs was as follows: half DMEM/F12 (Gibco Life Technologies), half Neurobasal (Gibco Life Technologies), N-2 supplement 200x (Gibco Life Technologies), B-27 supplement 100x (Gibco Life Technologies), 1% P/S (Merck Millipore), 1%

GlutaMAX Supplement (Gibco Life Technologies), with NPCs maintaining factors 3 μM CHIR 99021 (CHIR, Axon Medchem), 150 μM ascorbic acid (AA, Sigma-Aldrich) and 0.5 μM purmorphamine (PMA, EMD). Differentiation of NPCs towards dopaminergic neurons was started when cells reached about 70% confluency, with medium change from the maintaining one to the differentiation medium, which consists of the NPCs medium, supplemented with differentiation factors 100 ng/mL FGF8 (Peprotech), 200 μM AA and 1 μM PMA. After 8 days of medium change with differentiation medium every other day, medium was changed to maturation medium, which consists of NPCs medium supplemented with maturation factors 20 ng/mL BDNF (Peprotech), 20 ng/mL GDNF (Peprotech), 500 μM dbcAMP (Applichem), 200 μM AA, 1 ng/mL TGFβ3 (Peprotech), plus 0.5 μM PMA for 2 more days only. Along the differentiation and maturation, cells were passaged when confluency was reached, and plated in the corresponding medium on Matrigel-coated plates for experiments. Experiments were performed after at least 2 weeks of exposure of the cells to maturation medium. Cells were regularly checked for identity with Sanger sequencing, for mycoplasma absence, and for quality of differentiation with immunocytochemistry for Tyrosine Hydroxylase (TH) and β-III Tubulin.

2.2 iPSC LRRK2 knock out generation and characterization

David Schöndorf generated the lines. Briefly, homologous constructs carrying the premature stop codon on exon 41 of LRRK2 were generated with antibiotic resistance against Neomycin (G418) and Blasticidin. Nucleofection of CTRL-1 iPSCs with 2 μg of each zinc finger nuclease (ZFN) construct and 2 μg of homologous construct carrying Neomycin resistance was performed with Amaxa 2D Nucleofector (Lonza, program B016) and Nucleofection Solution from human stem cells kit 2 (Lonza). The first selection step was performed with 50 μg/mL G418 (PAA). Resistant colonies were picked and expanded. iPSCs were then subjected to a second nucleofection of ZFN constructs and 2 μg of homologous construct carrying Blasticidin resistance. After selection with 100 μg/mL of Blasticidin, resistant colonies were clonally expanded on MEFs. Genomic integration of the homologous construct was confirmed by Sanger sequencing, with the following primers: LRRK2 exon 41 FW GCACAGAATTTTTGATGCTTG, LRRK2 exon 41 RV GAGGTCAGTGGTTATCCATCC. Absence of LRRK2 protein expression was confirmed by western blot with antibodies binding is different regions of the protein. Genomic integrity of the selected clones was assessed by high-density genotyping using the Illumina HumanOmni2.5-8 (Omni2.5) array.

2.3 Image stream

Cells were fixed in 1% paraformaldehyde (PFA) for 10 minutes, then blocked with PBS 1% Triton X-100 (PBST) with 10% Fetal Bovine Serum (FBS, Gibco). Intracellular staining was performed with antibodies anti NFAT1-Alexa Fluor488 (Cell signaling technology, #14324) and anti β-III tubulin-Alexa Fluor647 (Cell signaling technology, #3624S) antibodies in PBST with 1% FBS. Cell nuclei were counterstained with DAPI (Biozol). Images were acquired with a 40x magnification on an Amnis ImageStream 100 imaging flow cytometer (EMD Millipore). A minimum of 10,000 events were acquired per sample. A compensation matrix was created by using single stained samples. β-III tubulin positive cells (in all the experiments more than 85%) were selected for analysis. Double positive cells for NFAT1/DAPI were gated, and Similarity morphology feature was applied to calculate NFAT1 translocation score with Amnis IDEAS software (EMD Millipore). Cells treated with 1 μM ionomycin (Sigma Aldrich) for 30 minutes were used as positive control.

2.4 Live imaging of neurite outgrowth

Cells were plated on Matrigel-coated 15μ-Slide 8 well (Ibidi) at the density of $3*10^5$ cells/well in maturation medium supplemented with 10 μM Rock inhibitor Y-27632 2HCl (Selleckchem) with or without stimuli for 24 hours. Neurite outgrowth was measured using an Axiovision microscope and a live-cell chamber. Pictures were taken every 5 minutes over a total time of 30 minutes and analyzed with ImageJ using the plugin MTrack2.

2.5 THP-1 differentiation and treatment for experiments

Human THP-1, a suspension monocytic cell line (Sigma Aldrich), is cultured in RPMI 1640 (Life technologies), 10% FBS (Gibco Life Technologies), 1% P/S (Merck Millipore) and 1% GlutaMAX Supplement (Gibco Life Technologies). THP-1 monocytes were differentiated into macrophages by exposure of the cells for 48 hours to 25 ng/mL of phorbol 12-myristate 13-acetate (THP-1-PMA, Sigma). THP-1-PMA was then removed, and cells were left to stabilize for 48 hs before experiments were carried out. Where indicated, cells were treated with 200 IU/mL IFN-γ for 72 hours, or 1 μM Ionomycin (Sigma Aldrich) for 30 minutes, before fixation with 4% PFA.

2.6 THP-1 LRRK2 knockdown generation and characterization

LRRK2 knockdown was generated on THP-1 monocytes by lentiviral infection with spinfection at MOI 10, by using these lentivirus from the Sigma Mission Library: SHC002V non-target control, TRCN0000021460 10^8 TU vector pLK0.1, and TRCN0000021462 10^8 TU vector pLK0.1. Selection was performed for 21 days with 10 μg/mL Puromycin (Invivogen). The lower expression

of LRRK2 was then verified by Western blot. THP-1 were then differentiated into macrophages as above

2.7 Plasmids

The plasmid pEGFP-C1 NFAT3 for overexpression of NFAT3-GFP for NFAT3 nuclear localization analysis was purchased by Addgene (#10961). The plasmid for overexpression of LRRK2 wild type (WT) or mutant for luciferase assay and microtubule analysis is a Strep-Flag (SF)-tagged plasmid expressing LRRK2 WT or LRRK2 G2019S, kindly gifted to us from Dr. Christian Johannes Gloeckner.

2.8 HEK NFAT Reporter IQGAP1 knockdown generation and characterization

NFAT Reporter HEK 293 Cell Line (PKC/ Ca2+ Pathway) (TebuBio, # 79298), were cultured in Dulbecco's MEM (Merck), 10% FBS (Gibco Life Technologies) and 400 μg/mL of Geneticin (Life technologies). IQGAP1 knockdown was generated on HEK NFAT reporter by lentiviral infection at MOI 1, by using these lentiviruses from the Sigma Mission Library: SHC002V non-target control, TRCN0000047486 10^8 TU vector pLK0.1 and TRCN0000047487 10^8 TU vector pLK0.1. Selection was performed for 5 days with 10 μg/mL Puromycin (Invivogen). The lower expression of IQGAP1 was then verified by Western blot.

2.9 Luciferase assay

For luciferase assay, SF-tagged LRRK2 WT, or SF-tagged LRRK2 G2019S plasmid DNA (8 μg for a 10 cm^2 dish) were introduced into HEK NFAT reporter cells via polyethyleneimine (Polysciences) solution. After 24 hours from transfection, cells were treated or untreated, as indicated, with 40 ng/mL THP-1-PMA and 1 μM Ionomycin (Sigma Aldrich), and/or 200 IU/mL IFN-γ for 24 hours. Where specified, cells were treated with Colchicine (Sigma) 100 μM for 30 minutes at 37 °C. Luciferase assay was performed 48 hours after transfection, according to protocol from the Dual-Luciferase Reporter Assay System (Promega).

2.10 NFAT3 nuclear localization in iPSC-derived neurons

Neurons were transfected with 500 ng of pEGFP-C1 NFAT3 plasmid per coverslip by using ViaFect Transfection Reagent (Promega). Where indicated, after 24 hours cells were stimulated with 200 IU/mL of IFN-γ. After 48 hours from transfection, cells were fixed with 4% PFA, and immunocytochemistry was performed. Analysis was performed by using ImageJ.

2.11 Western blot

For whole cell protein extraction, cell pellets were resuspended with Tris Buffered Saline 1x (TBS) 0,5% NP40, supplemented with protease and phosphatase inhibitors 1:10 (Roche) on ice, kept at least one hour on a rotating wheel at 4 degrees, then centrifuged for at least 30 minutes at maximum speed in a microcentrifuge at 4 degrees. Protein concentration was then determined with BCA assay (Pierce). Polyacrylamide gels were either self-made (with acrylamide concentration between 7% to 12%) or NuPAGE 4-12% Bis-Tris Protein Gels (Thermo Fisher Scientific), depending on the experiment, and 50 to 100 µg of protein were loaded. Transfer was performed overnight on methanol activated PVDF membranes (Millipore), followed by blocking for one hour with TBS plus 0,1% Tween (TBS-T) with 5% Milk or 5% BSA (both Sigma Aldrich) depending on the antibody. The primary antibody of interest (see Table 2) was therefore diluted in TBS-T plus 10% Roche Blocking solution (Roche), and the membranes were incubated overnight at 4 degrees. The secondary antibody of the corresponding species (HRP- conjugated, Sigma Aldrich) was diluted 1:10'000 in 5% milk or 5% BSA, and membranes were incubated one hour at room temperature. To develop, blot membranes were exposed to Amersham ECL Western Blotting Detection Reagent (GE healthcare), and Amersham Hyperfilm (GE healthcare) were used to detect the proteins. Densitometric analysis of the bands was performed by using ImageJ software. For proteasomal inhibition, cells were treated with 20 nM MG132 (Sigma Aldrich) for 24 hours.

Experiments with cytosolic fractionation were performed by Dina Ivanyuk, by using NE/PER Nuclear and cytosolic extraction kit (Thermo Fisher Scientific). Cells were detached with Accutase (Sigma-Aldrich), and then resuspended with cold PBS. After centrifugation, the pellet was resuspended with CER I buffer plus protease and phosphatase inhibitors (Roche), then lysed with CER II buffer. Afterwards, centrifugation at 12000 g for 10 minutes was performed, and supernatant was put aside as the isolated cytosolic fraction. After 2 washing steps with cold PBS, NER buffer plus protease and phosphatase inhibitors (Roche) was used to resuspend the pellet. The solution was then vortexed repeatedly, and immediately put on ice for 40 minutes, every 10 minutes. Protein concentration was then determined with BCA assay (Pierce). 10 µg of protein was loaded on a NuPAGE 4-12% Bis-Tris Protein Gels (Thermo Fisher Scientific), and then western blot was developed for NFAT3, Hsp90 for the cytosolic compartment and PARP1 for the nuclear compartment (see Table 2).

2.12 Immunocytochemistry

Fixation of cells on coverslips was performed with 4% PFA in PBS for 15 minutes. Coverslips were then blocked for 30 minutes at room temperature with PBS 10% Normal goat serum (NGS) 0,1% Triton X-100 for permeabilization (blocking solution). Primary antibodies (see Table 2) were then diluted in blocking solution and coverslips were incubated overnight at 4 degrees. The next day, secondary antibodies of the corresponding species, conjugated to the fluorophores 488, 568 or 647 (Invitrogen), were resuspended in PBS 1% NGS 0,1% Triton X-100, and applied on the coverslips for one hour at room temperature. DAPI (Biozol) 1:10'000 in PBS was used to counterstain the nuclei of the cells. A Zeiss Imager Z1 with Apotome (Carl Zeiss) microscope was used to acquire pictures. For the neurite length analysis experiment, the Simple Neurite Tracer plugin of Fiji ImageJ was used to quantify the images.

Antibody list	Host	Dilution	Use	Brand	Catalogue number
LRRK2 UDD3	rabbit	1:500	WB	Abcam	Ab133518
LRRK2	rat	1:50 (2 µg)	WB, CoIP	gift from J. Gloeckner	24D8
LRRK2 MJFF2	rabbit	1:1000	WB	Abcam	Ab133474
Pan phospho AKT (Ser473)	rabbit	1:1000	WB	Cell Signaling Technology	4060
Pan AKT	rabbit	1:1000	WB	Cell Signaling Technology	9272
AKT3	rabbit	1:1000	WB	Cell Signaling Technology	4059
NFAT3 (23E6)	rabbit	1:1000	WB	Cell Signaling Technology	2183
PARP1	rabbit	1:8000	WB	Cell Signaling Technology	9542
HSP90	rabbit	1:20000	WB	Enzo	ADI SPA 836F
β-Actin	mouse	1:20000	WB	Sigma Aldrich	A5441
IQGAP1	rabbit	1:500	WB	Cell Signaling Technology	2293
ß-III Tubulin	mouse	1:1000	ICC	Covance	14945202
Tyrosine Hydroxylase	rabbit	1:500	ICC	Pel-Freeze	P40101-150
NFAT1(D43B1) XP	rabbit	1:100	ICC	Cell Signaling Technology	5861
β-tubulin	mouse	1:1000	ICC	Sigma Aldrich	T8328
anti-DYKDDDDK Tag (D6W5B)	rabbit	1:1000	ICC	Cell Signaling Technology	14793S

Table 2. List of primary antibodies for western blot (WB) or immunocytochemistry (ICC) used in the project.

2.13 Cell treatments for neurite length experiments

Where indicated, cells were treated with IFN-γ 200 IU/mL for 24 hours before being fixed. To inhibit NFAT translocation, 500 nM MCV1 (HPVIVIT, Calbiochem Cat. No. 480404) was applied

on neurons for 24 hours. For rescue experiments, cells were stimulated for 48 hours with 200 ng/mL of recombinant human NRG1 (BioLegend, Cat. No. 551904), and after 24 hours treated with IFN-γ 200 IU/mL or 500 nM MCV1, as indicated, for another 24 hours.

2.14 Quantitative RT-PCR

To extract cDNA from samples, RNeasy Mini kit (Qiagen) was used for mRNA isolation, and QuantiTect Reverse Transcription kit (Qiagen) was used for reverse transcription. Quantitative RT-PCR (qRT-PCR) was performed with QuantiTect SYBR GREEN I kit (Qiagen), and the machine Viia7 Real time PCR system (Applied Biosystems) was used. For reference, housekeeping genes were added to each experiment as follows: Hydroxymethylbilane Synthase (HMBS) for IFN-γ pathway analysis; β2-microglobulin for THP-1 experiments; ribosomal protein large P0 (Rplp0) for the rest. To quantify gene expression fold changes, the 2^{-ddCt} method was used, with normalization on housekeeping genes as well as reference samples (generally untreated samples).

Primers used for qRT-PCR (5'-3')		
RPLP0	FW	CCTCATATCCGGGGGAATGTG
	RV	GCAGCAGCTGGCACCTTATTG
HMBS	FW	ATGCCCTGGAGAAGAATGAAGT
	RV	TTGGGTGAAAGACAACAGCATC
LRRK2	FW	TCCCTGCCATACGAGATTACC
	RV	GCACATTTTTACGCTCCGATA
NFAT1	FW	AGAAACTCGGCTCCAGAATCC
	RV	TGGTTGCCCTCATGTTGTTTTT
NFAT2	FW	GCCGCAGCACCCCTACCAGT
	RV	TTCTTCCTCCCGATGTCCGTCTCT
NFAT3	FW	TCAGAAGACACGGCGGACTTCC
	RV	TGAACATCTGTAGGGTCAGTGG
NFAT4	FW	ACCAGCCCGGGAGACTTCAATAGA
	RV	AAATACCTGCACAATCAATACTGG
PLGC2	FW	GACTCTTCATCAAACTACGACCC
	RV	GGAGTAAAGTTCCTCTTCGC
IFNGR1	FW	CATCACGTCATACCAGCCATTT
	RV	CTGGATTGTCTTCGGTATGCAT
SRC	FW	GCTCGTTCATCCACATTGCC
	RV	ACTACTTGTCATGCCAACGG
PIK3CB	FW	CTAATGTGTCAAGTCGAGGTGGAA
	RV	GGAAAATCTCTCGGCAGTCTTGT
IFNG	FW	TGACCAGAGCATCCAAAAGA
	RV	CTCTTCGACCTCGAAACAGC
MAPK14	FW	TTCTGTTGATCCCACTTCACTGT
	RV	ACACACATGCACACACACTAAC
AKT1	FW	ATGAGCGACGTGGCTATTGTGAAG
	RV	GAGGCCGTCAGCCACAGTCTGGATG
EP300	FW	AAACCCACCAGATGAGGAC

	RV	TATGCACTAGATGGCTCCGCAG
AKT2	FW	ATGAATGAGGTGTCTGTCATCAAAGAAGGC
	RV	TGCTTGAGGCTGTTGGCGACC
CAMK2G	FW	TCCCGAGCATCTCTTACCTG
	RV	CCACCCTTCTTCCGAATGTA
PIK3CD	FW	CAACCAGACAGCGGAGCAGCAAGA
	RV	CACTTCTGGGTCGCACAAGGAGTCAA
PIK3R1	FW	TGACGCTTTCAAACGCTATC
	RV	CAGAGAGTACTCTTGCATTC
MAP2K1	FW	CCAGAGAACCCTGAGGGAGA
	RV	TGTTGAGCAGCAGGTTGGAA
IFNGR2	FW	GCTGCTCGGAGTCTTCGCCG
	RV	GGACTGGCGGCAGTGAAGTC
CBL	FW	CGGTAATTGTTGCGTTTCCA
	RV	ACAGCTC-GCTCCCGAAGAA
CDKN1A	FW	GGCAGACCAGCATGACAGATT
	RV	GCGGATTAGGGCTTCCTCT
MAP2K6	FW	GGTTGTCTGGTCACTGAGGTCAC
	RV	CAGGGAACCTGAGACAGGCTAC
MYC	FW	GGCCCCCAAGGTAGTTATCCTT
	RV	CGTTTCCGCAACAAGTCCTCT
PRKCD	FW	CCCTTCTGTGCCGTGAAGAT
	RV	GCCCGCATTAGCACAATCTG
MAPK3	FW	CTGGATCAGCTCAACCACATT
	RV	AGAGACTGTAGGTAGTTTCGGG
CREBBP	FW	CACAGCGACGACTGCAAGATCC
	RV	CTTGAACAAGTTCCGCAGGGTG
SMAD7	FW	TACCGTGCAGATCAGCTTTG
	RV	TTTGCATGAAAAGCAAGCAC
PTPN11	FW	GTGGAGGAGAACGGTTTGATTC
	RV	CCAATGTTTCCACCATAGGATTC
BRCA1	FW	GGCTATCCTCTCAGAGTGACATTT
	RV	GCTTTATCAGGTTATGTTGCATGGT
CEBPB	FW	CACAGCGACGACTGCAAGATCC
	RV	CTTGAACAAGTTCCGCAGGGTT
JAK2	FW	GATAAAGCACACAGAAACTATTCAGAGTC
	RV	AGAATATTCTCGTCTCCACAAAC
eIF2AK2	FW	TCTTCATGTATGTGACACTGC
	RV	CACACAGTCAAGGTCCTTAG
AKT3	FW	ATGAGCGATGTTACCATTGT
	RV	CAGTCTGTCTGCTACAGCCTGGATA
ICAM1	FW	AGGCCACCCCAGAGGACAAC
	RV	CCCATTATGACTGCGGCTGCTA
SOCS1	FW	TGGTAGCACACAACCAGGTG
	RV	GAACGGAATGTGCGGAAGT
IRF1	FW	TGCATTTATTTATACAGTGCCTTGCT
	RV	CCCTCCCTGGGCCTGTTGAG
STAT1	FW	CTAGTGGAGTGGAAGCGGAG
	RV	CACCACAAACGAGCTCTGAA

β2-microglobulin	FW	GATAGTTAAGTGGGATCGAG
	RV	GCAAGCAAGCAGAATTTGGA
IQGAP1	FW	GGAGCACAATGATCCAATCC
	RV	ATGGTTCGAGCATCCATTTC

Table 3. Primers used for qRT-PCR in the study.

2.15 Live imaging of calcium

Dr. Wadood Haq and Dina Ivanyuk performed and analysed the experiments. Bessel medium supplemented with Fura-2-AM 0,27 μM and Pluronic F127 in a 1:1 ration (Thermo Fisher Scientific) was used to incubate neurons slides for 40 minutes at 37 degrees in a 5% CO_2 incubator. An upright fluorescence microscope (BX50WI, Olympus) was used for ratiometric recordings, by exploiting the following features of the microscope: a CCD camera (RETIGA-R1, 16 bit, 1360×1024 pixels), a polychromator (VisiChrome, Till Photonics) and a 20X water immersion objective (LUMPlan FL, 20X/0.80W, ∞/0, Olympus). After setting the focal plane, two-channel stacks were acquired with VisiView software (Till Photonics) of the Fura-2 fluorescence at 2 Hz, with λ of excitation 340 nm and 380 nm, with an exposure time of 40 ms and an 8 pixel binning (Olympus U-MNU filter set). The recording of the Ca2+ activity was carried out for 20 minutes, with 5 minutes control recording for baseline, and 15 minutes of recording after stimulation. Stimulation with 20 mM KCl (Sigma-Aldrich) was applied for one minute, followed by washout for 3 minutes (2 mL/min). Stimulation with 500 nM of Thapsigargin (Sigma-Aldrich) was not washed out after application. IFN-γ 200 IU/mL was applied for the 24 hours previous analysis of the Ca2+ activity, as a measure of chronic IFN-γ stimulation effect. The reagents were applied to the temperature controlled (37 degrees) recording chamber with a micro pipette (amount of 200 μL) near the objective, so as to reach the cells immediately. The ratio between the fluorescence images pictured at wavelength of F340 over F380 were generated, as ratio-stacks of Ca2+ activity. In this ratio-stacks, cells of interest were manually encircled as regions of interest (ROIs) with defined coordinates, which were used to generate calcium traces with a custom ImageJ macro. These data were scaled as 0,1 matrix values for further processing (y=(x-min(min(x)))/(max(max(x))-min(min(x))), and analysed by a custom made Matlab script (Mathworks). Baseline values were calculated as mean of each timepoint (n=5, one per minute, in 5 minutes recording). The delta Ca2+ influx and release were calculated as the difference between the peak Ca2+ value after stimulation and the baseline value. The recovery after KCl stimulation was considered as baseline value ± 5%.

2.16 dSTORM super-resolution imaging

HEK 293 were cultured in Dulbecco's MEM (Merck), 10% FBS (Gibco Life Technologies), 1% P/S (Merck Millipore) and 1% GlutaMAX Supplement (Gibco Life Technologies) and split with Accutase (Sigma-Aldrich) when confluent. SF-tagged LRRK2 WT, or SF-tagged LRRK2 G2019S plasmid DNA were introduced into HEK 293 cells via polyethyleneimine (Polysciences) solution. Where specified, treatment with colchicine (Sigma) 100 μM for 30 minutes at 37 °C was used as a control. After 48 hours from transfection, cells were first treated for 10 seconds with a microtubules preserving buffer composed of 80 mM PIPES, 5 mM EDTA pH 6.8, 1 mM $MgCl_2$, plus 0,5% Triton X-100, then fixed at minus 20 degrees with MetOH for 10 minutes. Immunocytochemistry was performed as per paragraph 2.12, with primary antibodies against Flag tag (with secondary antibody Alexa Fluor 488) to identify cells expressing tagged LRRK2 after transfection, and β-tubulin (with secondary antibody Alexa Fluor 647) for microtubule staining. Imaging was performed on a Nikon N-STORM 4.0 microscope. Reference images were acquired before dSTORM imaging, by using fluorescent lamp, Cy5 (for β-tubulin) and 488 (for Flag tag) filter cubes. NIS-Elements AR software (Nikon Instruments) was used to control the setup. Filter cubes to filter the fluorescent light were used as follows: Cy5 (AHF; EX 628/40; DM660; BA 692/40), 488 (AHF; EX 482/18; DM R488; BA 525/45) and Nikon Normal STORM cube (T660lpxr, ET705/72m). ORCA-Flash 4.0 sCMOS camera (Hamamatsu Photonics) was used to image filtered emitted light. A fluorescent lamp (Lumencor Sola SE II) was used for epifluorescent widefield imaging. Continuous 647 nm laser illumination at full power was applied to perform dSTORM imaging in highly inclined and laminated sheet microscopy (HiLo) or total internal reflection fluorescence (TIRF) mode. For fluorophore reactivation, 405 nm laser at 1% power was applied. For dSTORM images, 30'000 frames were obtained at 33 Hz with a Nikon Normal STORM cube (T660lpxr, ET705/72m), image depth of 16 bit and a frame size of 256x256 pixels. NIS-Elements AR software was exploited to process the images as follows. Default settings for molecule identification were: maximum width 400 nm, minimum width 200 nm, max axial ratio 1.3, max displacement 1, initial fit width 300 nm, and minimum height for peak detection 150. Overlapping peaks algorithm was used for localization analysis. Gaussian rendering size of 18 nm was used to reconstruct dSTORM images. Gaussian rendering intensity was used to adjust brightness and contrast from 0 to 50. Tiff images were then generated from the processed dSTORM images. Analysis of the dSTORM images was then performed with the Matlab-based open source software from Zhang et al. SMLM image filament network extractor (SIFNE) [166]. Otsu's threshold was selected based on the image with the lowest staining intensity of β-tubulin in each set of experiments, with 5 or more cells per condition per experiment. Default parameters for SIFNE

analysis were as follows: junction size 7 pixels, registration of tip direction no multi-core, 5 iterative extractions of fragments, gap orientation 28.6479 degrees, search angle for curvature grouping 57.2958 degrees, maximal curvature of 1 rad/um, search radius 50 pixels. Short filaments (< 1 μm) were excluded from the analysis.

2.17 LDH assay

Lactate dehydrogenase (LDH) assay was performed on iPSC-derived neurons with or without treatment with IFN-γ at different concentrations (100 IU/mL, 200 IU/mL or 400 IU/mL), with the Cytotoxicity Detection KitPLUS (LDH) (Merck), following manufacturer's instructions. As a control, cells were treated with 1% Triton X-100.

2.18 Statistical analysis

Data were analysed with GraphPad Prism version 7.00 (GraphPad Software) and expressed as mean + SEM (or + SD) as indicated. Two-tailed Student's t-test or One-way Anova followed by Bonferroni multiple comparison test were used for statistical analysis (statistical significance $p<0.05$). The number of samples and the statistical test used are indicated in the figure legend.

3. The role of LRRK2 in interferon gamma-mediated neuronal immune response

3.1 IFN-γ increases LRRK2 expression in iPSC-derived neurons

As mentioned in paragraph 1.3, IFN-γ role in PD pathogenesis is being investigated, especially in the context of the immune system. Interestingly, IFN-γ increases LRRK2 expression in immune cells [100, 101]. Moreover, IFN-γ has been shown to lead to selective dopaminergic neuronal death in mice models [122, 123], provided microgliosis and astrogliosis are present. Therefore, our aim was to examine the potential cell autonomous effect of IFN-γ on dopaminergic neurons. To do this, we employed iPSC-derived NPCs that we then differentiated into dopaminergic neurons. These lines were derived from one healthy control, on which an artificial mutant carrying the G2019S mutation in LRRK2 [158] and two LRRK2 KO lines were generated by David Schöndorf (Figure 1), and two PD patient-derived lines carrying the G2019S mutation in LRRK2, from which gene corrected isogenic controls were previously generated (see also Table 1 in Materials and methods) [158]. LRRK2 knockout iPSC lines were generated by exploiting the Zinc Finger Nucleases (ZFNs) technology targeting exon 41 of LRRK2, the one where the G2019S mutation occurs, and inserting an homologous construct carrying a premature stop codon, with efficient results (Figure 1A-D).

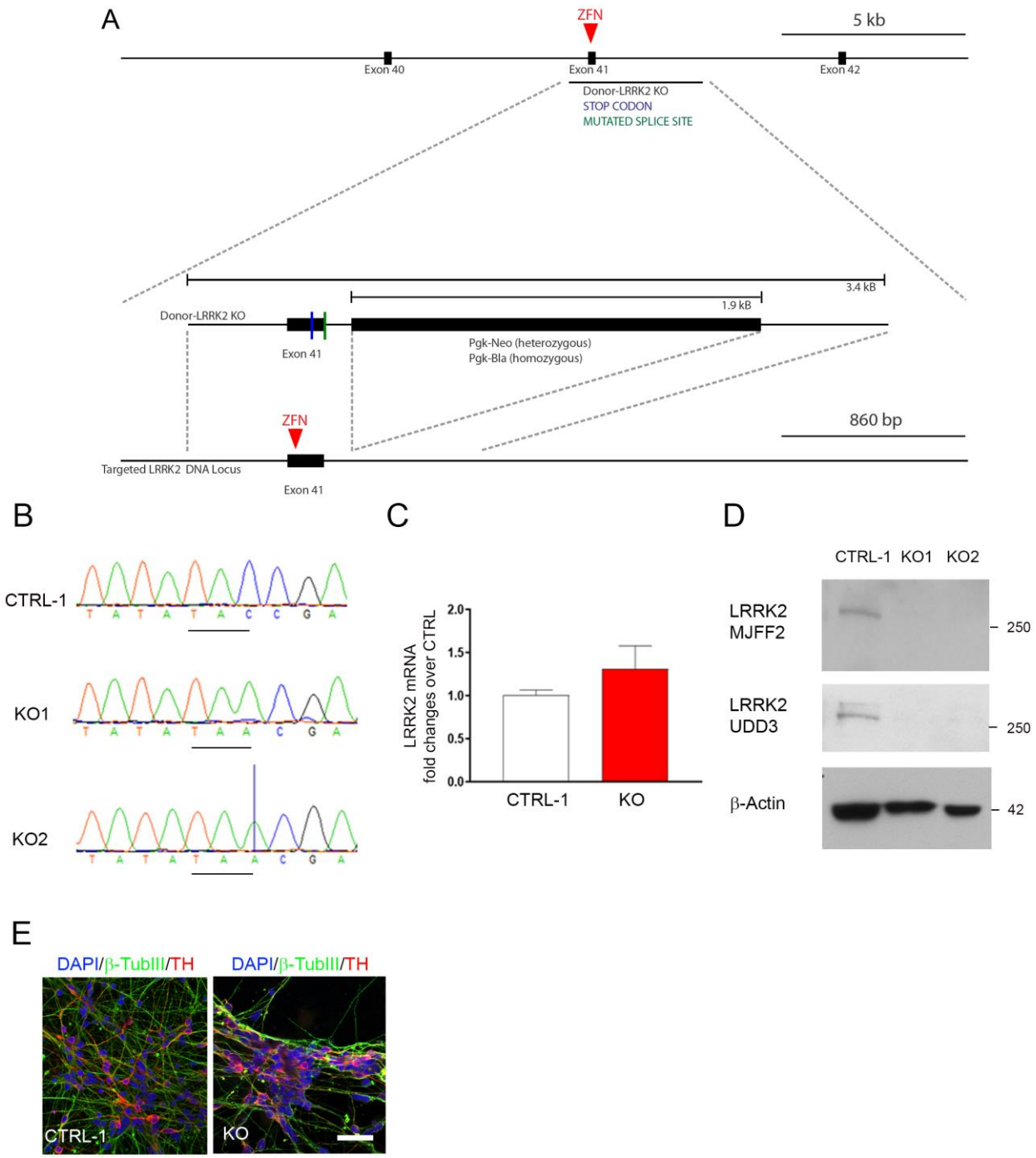

Figure 1. Generation and characterization of LRRK2 KO lines. (A) Schematic representation of generation of LRRK2 KO by exploiting ZFNs and an homologous construct carrying a premature stop codon and a mutated splice site, together with antibiotic resistance cassettes for Neomycin (Pgk-Neo) or Blasticidin (Pgk-Bla). **(B)** Sanger sequencing of LRRK2 KO clones 1 and 2, underlined is the premature stop codon inserted in homozygosity. **(C)** LRRK2 mRNA levels in iPSC-derived neurons in LRRK2 KO lines expressed as fold over CTRL (mean + SEM; n=3). **(D)** Representative western blot showing no LRRK2 protein expression in iPSC-derived neurons from LRRK2 KO lines. **(E)** Representative pictures of β-tubulin III

(green) / TH (red) staining of iPSC-derived neurons from LRRK2 KO and isogenic control at basal conditions. Nuclei were counterstained with DAPI (blue). Scale bar of 20 μm.

As previously shown, no differences in differentiation potential were observed for all the cell lines (Figure 1E, 2A) [158]. Moreover, no differences in expression levels of LRRK2 were detected at the neuronal stage in mutant cells (Figure 2B). First of all, we wanted to determine if chronic exposure of dopaminergic neurons to IFN-γ for 24 hours lead to neuronal death *in vitro*, in the absence of reactive gliosis. As expected, we did not detect an increase in apoptosis after IFN-γ stimulation of our neurons at different concentrations (selected based on previous reports [101]), as detected with LDH assay (Figure 2C). Similarly, we did not detect changes in differentiation potential after stimulation (Figure 2D). Therefore, IFN-γ does not affect cellular viability and the ability to differentiate.

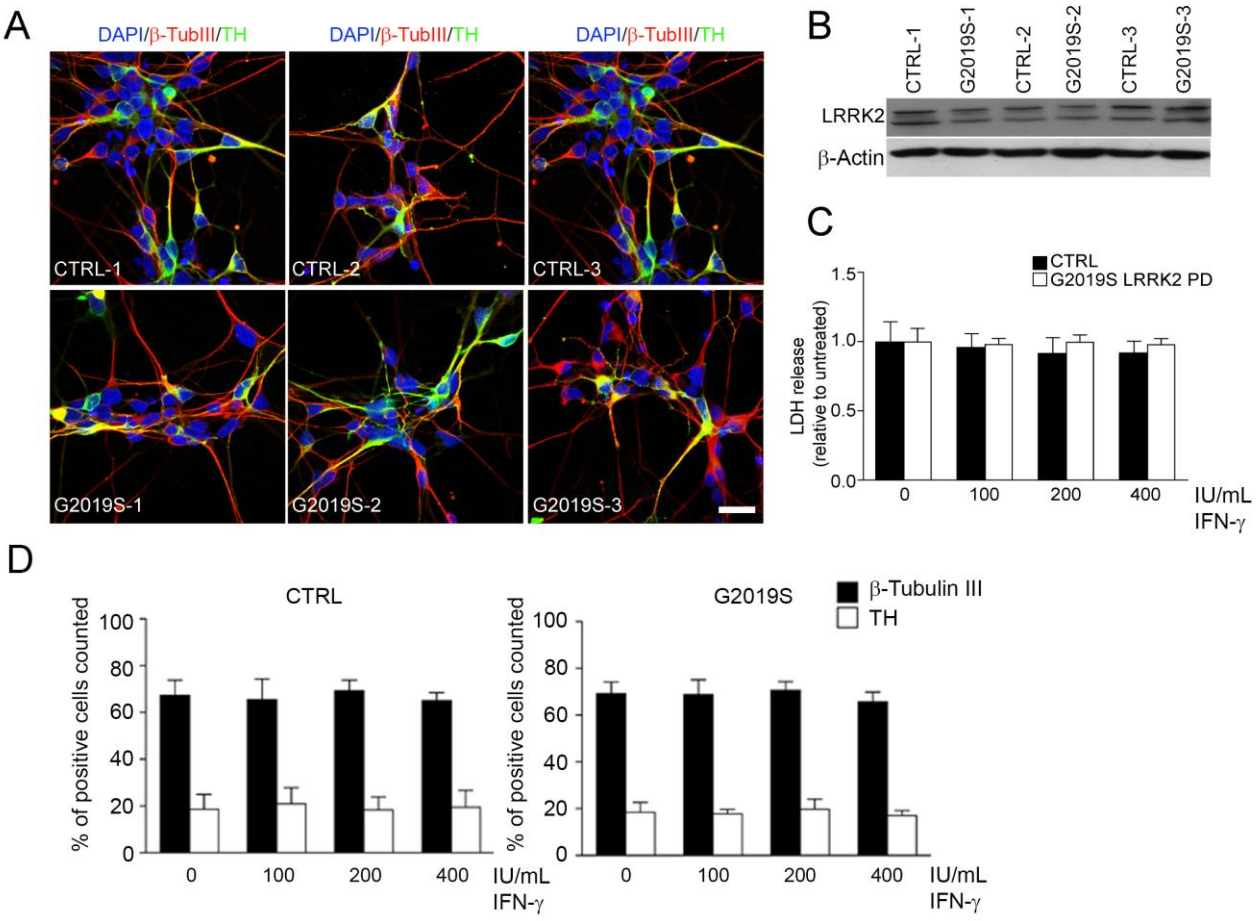

Figure 2. iPSC-derived dopaminergic neurons differentiation potential and viability after IFN-γ stimulation. (A) Representative pictures of β-tubulin III (red) / TH (green) staining of iPSC-derived neurons from LRRK2 G2019S mutant and isogenic controls at basal conditions. Nuclei were counterstained with DAPI (blue). Scale bar of 20 μm. **(B)** Representative western blot showing basal LRRK2 expression levels in iPSC-derived neurons isogenic couples. **(C)** Cytotoxicity of IFN-γ measured with activity of LDH released

in the medium after treatment at different concentrations (mean + SEM, n=3). **(D)** β-tubulin III and TH positive cells detected by immunocytochemistry after IFN-γ treatment at different concentrations in CTRL and LRRK2 G2019S iPSC-derived cells (mean + SEM, n=3).

After having established there is no toxicity of IFN-γ on neurons *in vitro*, we investigated whether LRRK2 expression was increased in our iPSC-derived neurons upon treatment. Indeed, we found a significant increase in mRNA, as well as protein levels of LRRK2 in our control cell lines after stimulation for 24 hours with IFN-γ (Figure 3A, B). Moreover, this increase was specific for IFN-γ (200 IU/mL), as treatment with other pro-inflammatory stimuli as LPS (100 ng/mL) and IL-1β (100 IU/mL) for 24 hours did not increase LRRK2 mRNA levels (Figure 3C). Besides, neurons carrying the G2019S mutation in LRRK2 responded in a similar way to IFN-γ, also showing increased levels of LRRK2 at mRNA and protein levels (Figure 3D, E). From these data, we gathered that a similar effect on LRRK2 was occurring at the different concentrations, therefore we carried on all the remaining experiments at the concentration of IFN-γ of 200 IU/mL.

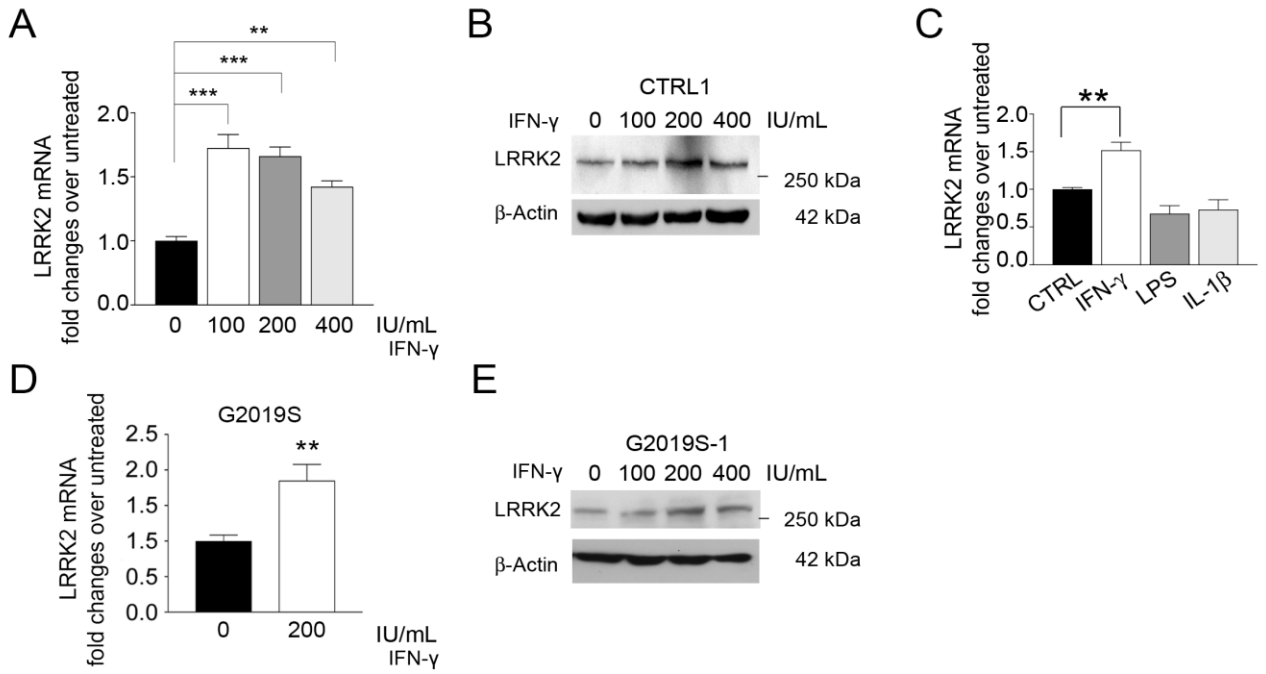

Figure 3. IFN-γ increases LRRK2 expression in iPSC-derived neurons. (A) qRT-PCR showing LRRK2 mRNA levels in control neurons treated for 24 hours at the different concentrations of IFN-γ indicated in the graph. Data are expressed as fold changes over untreated (mean + SEM, one-way ANOVA, Bonferroni post hoc, ***P < 0.001, **P < 0.01; n=3). **(B)** Representative western blot of LRRK2 protein levels in control neurons treated for 24 hours at the different concentrations of IFN-γ indicated. **(C)** qRT-PCR showing LRRK2 mRNA levels in control neurons treated for 24 hours with 200 IU/mL of IFN-γ, 100 ng/mL of LPS or 100 IU/mL of IL-1β. Data are expressed as fold changes over untreated (mean + SEM, one-way ANOVA, Bonferroni post hoc, **P < 0.01; n=3). **(D)** qRT-PCR showing LRRK2 mRNA levels in G2019S neurons

treated for 24 hours with 200 IU/mL of IFN-γ. Data are expressed as fold changes over untreated (mean + SEM, t-test, **P < 0.01; n=3). **(E)** Representative western blot of LRRK2 protein levels in G2019S neurons treated for 24 hours at the different concentrations of IFN-γ indicated.

3.2 LRRK2 G2019S neurons show altered AKT response to IFN-γ

Next, we investigated if IFN-γ response pathway was altered in neurons carrying the LRRK2 G2019S mutation. To do so, we selected a panel of IFN-γ dependent genes to screen by qRT-PCR from the INTERFEROME gene expression database (Interferome DB v2.0) [167]. By using control cell lines, we demonstrated that gene expression after treatment with 200 IU/mL of IFN-γ remained stable for some genes, while for a few (Interferon Gamma Receptor 1 (*IFNgR1*), SRC proto-oncogene, non-receptor tyrosine kinase (*SRC*), and mitogen-activated protein kinase 14 (*MAPK14*)) it was significantly downregulated (Figure 4A). However, some genes were significantly upregulated after treatment, in particular Janus kinase 2 (*JAK2*), eukaryotic translation initiation factor 2 alpha kinase 2 (*EIF2AK2*), AKT serine/threonine kinase 3 (*AKT3*), signal transducer and activator of transcription 1 (*STAT1*), suppressor of cytokine signaling 1 (*SOCS1*), intercellular adhesion molecule 1 (*ICAM1*), and interferon regulatory factor 1 (*IRF1*) (Figure 4B, C). To understand if the presence of the LRRK2 G2019S mutation has an effect on IFN-γ response, we performed further qRT-PCR analysis on the more significantly upregulated genes, by comparing their expression after treatment between LRRK2 G2019S carrying neurons and corresponding isogenic controls (Figure 4D). Indeed, we found that AKT3 was the only one altered, with significantly higher upregulated mRNA expression levels in LRRK2 mutant neurons in all isogenic couples upon IFN-γ stimulation (Figure 4D, E). However, AKT3 protein levels were slightly, but not significantly, upregulated upon treatment (Figure 4F). We next sought to investigate whether the activity of AKT3 was affected by the mutation, by checking its phosphorylation state. Since no good antibodies are available for phosphorylated AKT3 specifically, we performed the experiment with an antibody targeting all the isoforms of AKT when phosphorylated (AKT1, AKT2 and AKT3, which have all a similar phosphorylation site at Ser473). Interestingly, upon IFN-γ treatment, the phosphorylation was decreased in all iPSC-derived neurons, but a significantly lower phosphorylation was present in LRRK2 G2019S neurons compared to their isogenic control (Figure 4G, H). This suggests that AKT might be less active when the mutation is present. AKT is a kinase involved in many different cellular pathways, but one in particular came to our attention. When active, AKT negatively phosphorylates GSK3β at Ser9, rendering GSK3β inactive [168]. One of the important activities of GSK3β is its negative phosphorylation of NFAT while in the nucleus, leading to the masking of its nuclear localization factor, and therefore cytoplasmic translocation of

the factor itself [169]. We therefore focused next on the possible effect of the reduced AKT phosphorylation on NFAT translocation and activity.

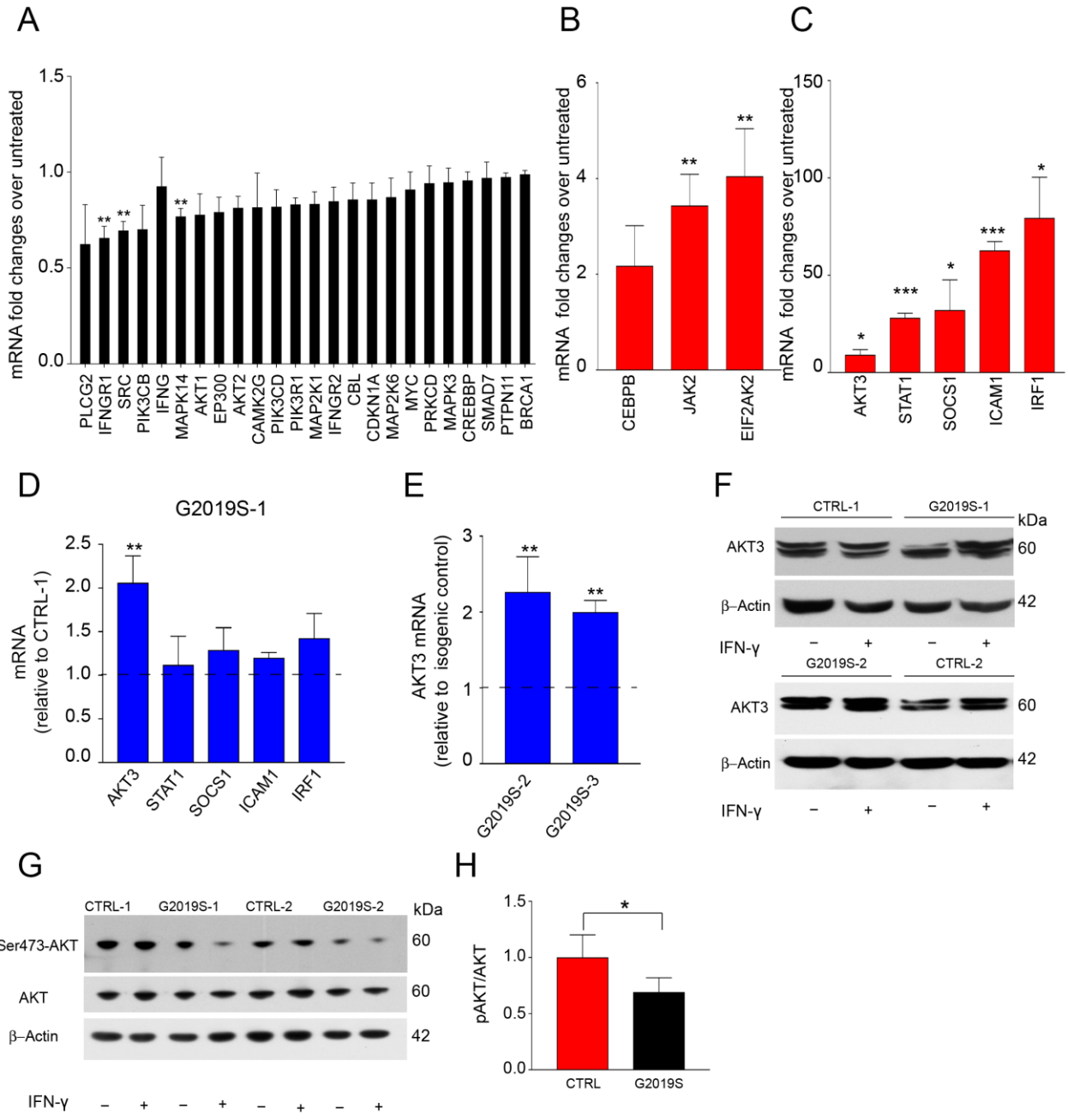

Figure 4. LRRK2 G2019S mutation alters AKT response to IFN-γ. (A) qRT-PCR showing IFN-γ response genes that are stable or downregulated in IFN-γ treated iPSC-derived CTRL neurons. Data are expressed as fold changes over untreated (mean + SEM, t-test treated vs untreated, **P<0.01; n=3). **(B, C)** qRT-PCR showing IFN-γ response genes that are upregulated in IFN-γ treated iPSC-derived CTRL neurons. Data are expressed as fold changes over untreated (mean + SEM, t-test treated vs untreated, ***P<0.001, **P<0.01, *P<0.05; n=3). **(D)** qRT-PCR showing mRNA expression of the genes in (C) in IFN-γ treated iPSC-derived LRRK2 G2019S-1 neurons compared to CTRL-1. Data are expressed as fold of IFN-γ treated mutant over treated CTRL (mean + SEM, t-test, **P<0.01; n=3). **(E)** qRT-PCR showing mRNA expression

of AKT3 in IFN-γ treated iPSC-derived LRRK2 G2019S neurons compared to their isogenic controls. Data are expressed as fold of IFN-γ treated mutant over corresponding treated isogenic control (mean + SEM, t-test, **P<0.01; n=3). **(F)** Representative western blot showing AKT3 protein expression in iPSC-derived neurons from the cell lines indicated in the figure, with or without IFN-γ treatment. **(G)** Representative western blot showing phosphorylated Akt (p-Akt) and total AKT protein expression in iPSC-derived neurons from the cell lines indicated in the figure, with or without IFN-γ treatment. **(H)** Quantification of levels of p-Akt/total Akt in iPSC-derived neurons from LRRK2 G2019S and controls (mean + SD, treated vs untreated, t-test, *P<0.05; n= 4 independent experiments).

3.3 LRRK2 G2019S and IFN-γ synergise to reduce NFAT nuclear localization

First of all, we wanted to check in a simpler system whether NFAT localization was affected by the presence of LRRK2 mutant. Therefore, we obtained a HEK NFAT reporter cell line from TebuBio to test this hypothesis. HEK cells were transfected with SF-tagged LRRK2 WT or LRRK2 G2019S, and NFAT transcriptional activity was measured with luciferase assay at basal condition or after stimulating translocation with THP-1-PMA and Ionomycin (see Materials and Methods 2.9). Indeed, already in the presence of overexpressed LRRK2 WT, NFAT activity was reduced, according to literature (Figure 5A) [104]. Moreover, with overexpression of LRRK2 G2019S, a significantly lower translocation was present (Figure 5A). Next, we checked the effect of IFN-γ treatment after stimulation with THP-1-PMA and Ionomycin. In the presence of the cytokine, NFAT activity was even further reduced, with the more severe decrease happening in cells overexpressing LRRK2 G2019S (Figure 5B). Having established that LRRK2 G2019S affects NFAT activity in a simple model, we next checked for the mRNA expression of the different isoforms of NFAT in our iPSC-derived neurons. The most expressed isoform was NFAT3, which is, according to literature, important for neurite length and development (Figure 5C) [170, 171]. Since there are no good antibodies for immunocytochemistry for NFAT3, to check NFAT3 translocation we decided to transfect our neurons with a plasmid expressing NFAT3 tagged with GFP, and then quantified the intensity of the signal in the nuclei versus in the total cell body (Figure 5D-F). In line with the luciferase assay results, a decreased NFAT3 nuclear localization was observed in neurons carrying the LRRK2 G2019S mutation compared to controls, and, importantly, it was further exacerbated with IFN-γ treatment (Figure 5D-F). No effect of IFN-γ was present in LRRK2 KO derived neurons (Figure 5G, H), suggesting that the IFN-γ effect is dependent on LRRK2.

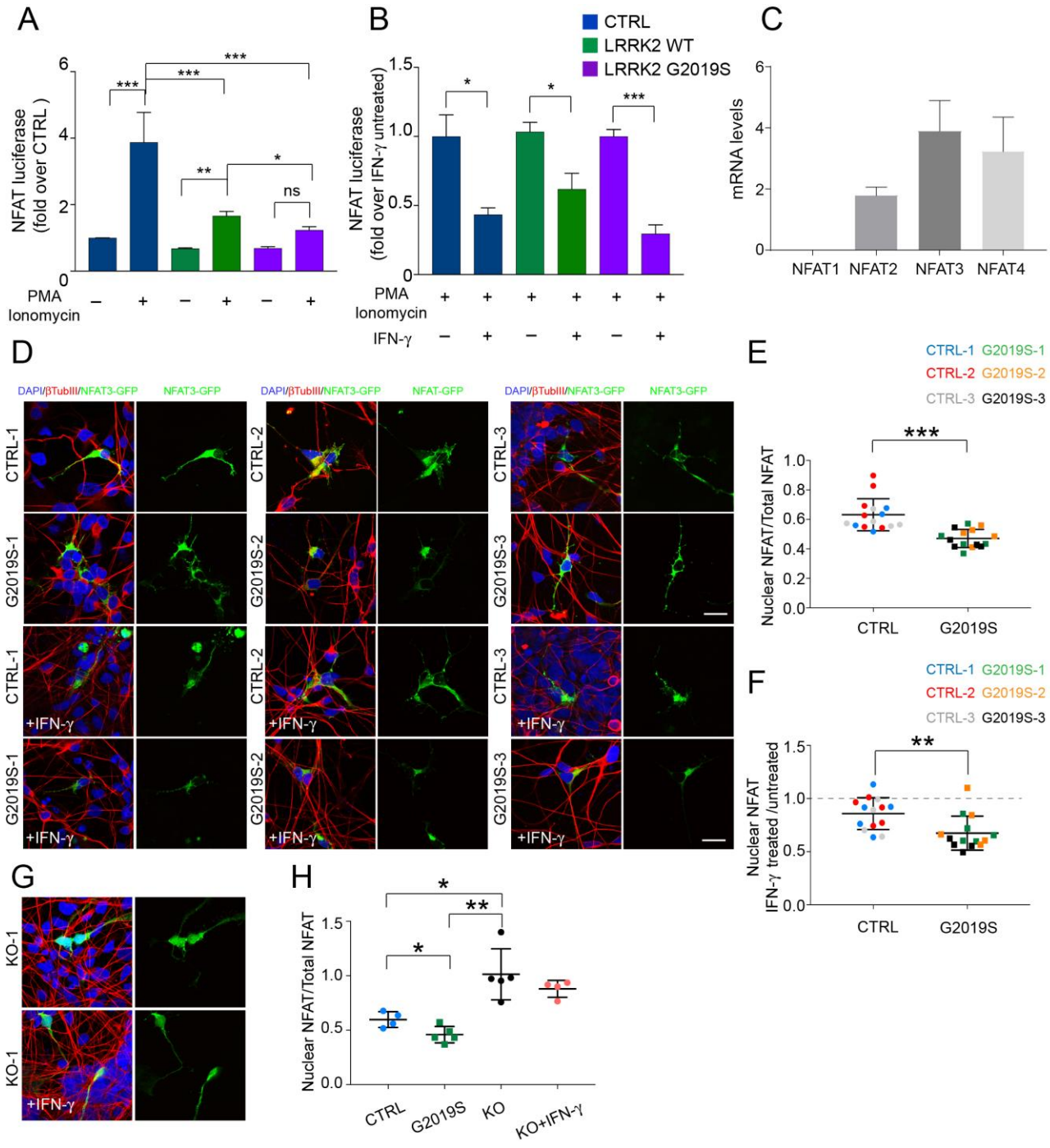

Figure 5. LRRK2 G2019S reduced NFAT activity in HEK NFAT reporter and NFAT3 translocation in iPSC-derived neurons. (A) Luciferase activity assay in HEK NFAT reporter cells with or without transfection with SF-tagged LRRK2 wt or G2019S. Where indicated, cells were stimulated with THP-1-PMA 40 ng/mL and Ionomycin 1 μM for 24 hours (mean + SD, one-way ANOVA, Bonferroni post hoc, ***P<0.001, **P<0.01, *P<0.05; n=3). **(B)** Luciferase activity assay in HEK NFAT reporter cells stimulated with THP-1-PMA 40 ng/mL and Ionomycin 1μM for 24 hours, with or without transfection with SF-tagged LRRK2 wt or G2019S. Where indicated, cells were treated with 200 IU/mL of IFN-γ for 24 hours. Data are expressed as fold changes over corresponding IFN-γ untreated cells (mean + SD, t-test, ***P<0.001, *P<0.05; n=3). **(C)** qRT-PCR showing mRNA levels of the different NFAT isoforms in iPSC-derived CTRL

neurons at basal level (mean + SEM, n=3). **(D)** Representative pictures of iPSC-derived neurons CTRL and G2019S transfected with NFAT3-GFP plasmid (green) untreated or treated with 200 IU/mL of IFN-γ for 24 hours. Red β-Tubulin III, blue DAPI. Scale bars 20 μm. **(E)** Quantification of NFAT3 nuclear fluorescent intensity over total cell body fluorescent intensity in transfected iPSC-derived neurons at basal level (mean ± SD, t-test, ***P<0.001; n=5 independent experiments). **(F)** Quantification of NFAT3 nuclear fluorescent intensity in transfected iPSC-derived neurons after IFN-γ treatment. Data are expressed as fold of NFAT3 nuclear intensity (expressed as in figure 5E) of IFN-γ treated cells over untreated (mean ± SD, t-test, **P<0.01; n=5 independent experiments). **(G)** Representative pictures of iPSC-derived neurons LRRK2 KO transfected with NFAT3-GFP plasmid (green) untreated or treated with 200 IU/mL of IFN-γ for 24 hours. Red β-Tubulin III, blue DAPI. **(H)** Quantification of NFAT3 nuclear fluorescent intensity over total cell body fluorescent intensity in transfected iPSC-derived neurons CTRL-1, G2019S-1 and LRRK2 KO untreated or treated with IFN-γ (mean ± SD, t-test, *P<0.05, **P<0.01; n=5 independent experiments).

Next, we questioned whether IFN-γ treatment could affect NFAT3 protein expression levels. In untreated neurons, there were no differences in protein expression between LRRK2 G2019S and isogenic controls. However, stimulation with IFN-γ lead to a significant decrease in NFAT levels independently of LRRK2 genotype (Figure 6A, B). Similarly, cell fractionation experiments showed reduction of NFAT3 protein expression in both cytoplasm and nuclei, upon IFN-γ treatment (Figure 6C). Interestingly, IFN-γ has been shown to activate the proteasome [172]. We then hypothesised that the decreased expression of NFAT3 in the presence of IFN-γ could be due to proteasomal degradation. Indeed, treatment of control neurons with the proteasomal inhibitor MG132 restored total NFAT3 levels (Figure 6D).

We then wondered if other NFAT isoforms could also be affected by the presence of the LRRK2 G2019S mutation. Therefore, we focused on the isoform that is most generally studied in T cells, NFAT1. Unlike for NFAT3, for NFAT1 there are good antibodies also for staining. Thus, by using an Amnis ImageStream flow cytometry, we were able to analyse the nuclear staining of NFAT1 for more than 10’000 β-Tubulin III positive neurons per experiment (Figure 6E). Indeed, we found that NFAT1 translocation was significantly reduced in G2019S-1-derived neurons, compared to their isogenic control (Figure 6F). However, for iPSC-derived neurons we focused on NFAT3, since it’s the most expressed isoform (Figure 5C).

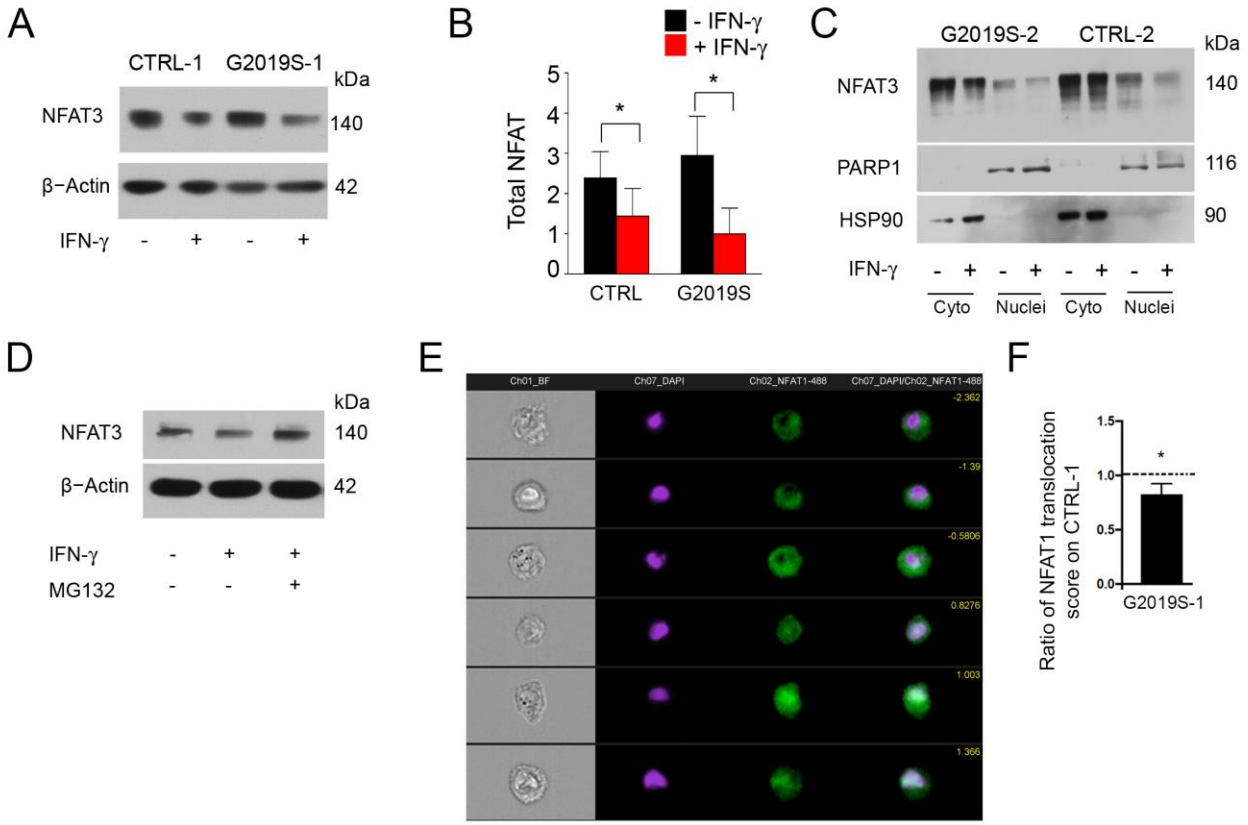

Figure 6. (A-D) IFN-γ induces NFAT3 degradation via the proteasome. (A) Representative western blot showing reduction of total levels of NFAT3 in iPSC-derived neurons after stimulation with IFN-γ 200 IU/mL for 24 hours. **(B)** Quantification of total levels of NFAT3 in CTRL and G2019S neurons untreated or treated with IFN-γ 200 IU/mL for 24 hours (mean + SD, t-test treated vs untreated, *P<0.05; n=5 independent experiments). **(C)** Representative western blot showing expression of NFAT3 in cytosolic and nuclear fraction of iPSC-derived neurons, untreated or treated with IFN-γ 200 IU/mL for 24 hours as indicated. **(D)** Representative western blot showing recovery of NFAT3 levels upon treatment of control neurons with IFN-γ 200 IU/mL after proteasomal inhibition with 20 nM of MG132 for 24 hours. **(E-F) NFAT1 translocation is as well reduced in LRRK2 G2019S neurons. (E)** Representative Image Stream pictures showing examples of NFAT1 (green) nuclear translocation score (in yellow) in β-Tubulin III positive sorted cells. **(F)** Quantification of NFAT1 translocation with Image Stream in β-Tubulin III positive sorted neurons derived from G2019S-1 and the corresponding isogenic control. Data are expressed as ratio of median of NFAT1 translocation score of G2019S-1 over CTRL-1 (mean + SEM, t-test, *P<0.05; n=5).

3.3.1 NFAT1 nuclear localization is dependent on LRRK2 in THP-1 macrophages

As mentioned, NFAT1 is the most studied isoform, mainly in the immune system. To determine whether LRRK2 affects NFAT translocation in another cell type, we studied NFAT1 localization in a monocytic cell line, THP-1 cells. We confirmed that IFN-γ was inducing LRRK2 expression in THP1 differentiated to macrophages (see Material and methods 2.5) by western blot (Figure 7A). Consistent with literature [101], after 72 hours of exposure to 200 IU/mL of IFN-γ, THP-1

macrophages showed increased levels of LRRK2 (Figure 7A). To test the role of LRRK2 in NFAT shuttling in these cells, we generated LRRK2 knockdown (KD) THP-1 monocytes via lentiviral-mediated delivery of shRNAs (see Material and methods 2.6), and verified the LRRK2 KD with qRT-PCR and western blot for LRRK2 (Figure 7B, C). After differentiating these cells to macrophages (see Material and methods 2.5), we performed immunocytochemistry analysis for NFAT1 nuclear localization with or without 1 μM Ionomycin stimulation to promote translocation of the factor (Figure 7D, E, staining and analysis by Dina Ivanyuk). Indeed, we found a significant increase in nuclear translocation of NFAT1 in LRRK2 KD cells, upon Ionomycin stimulation (Figure 7E). These data support the role of LRRK2 in regulating NFAT localization in human cells.

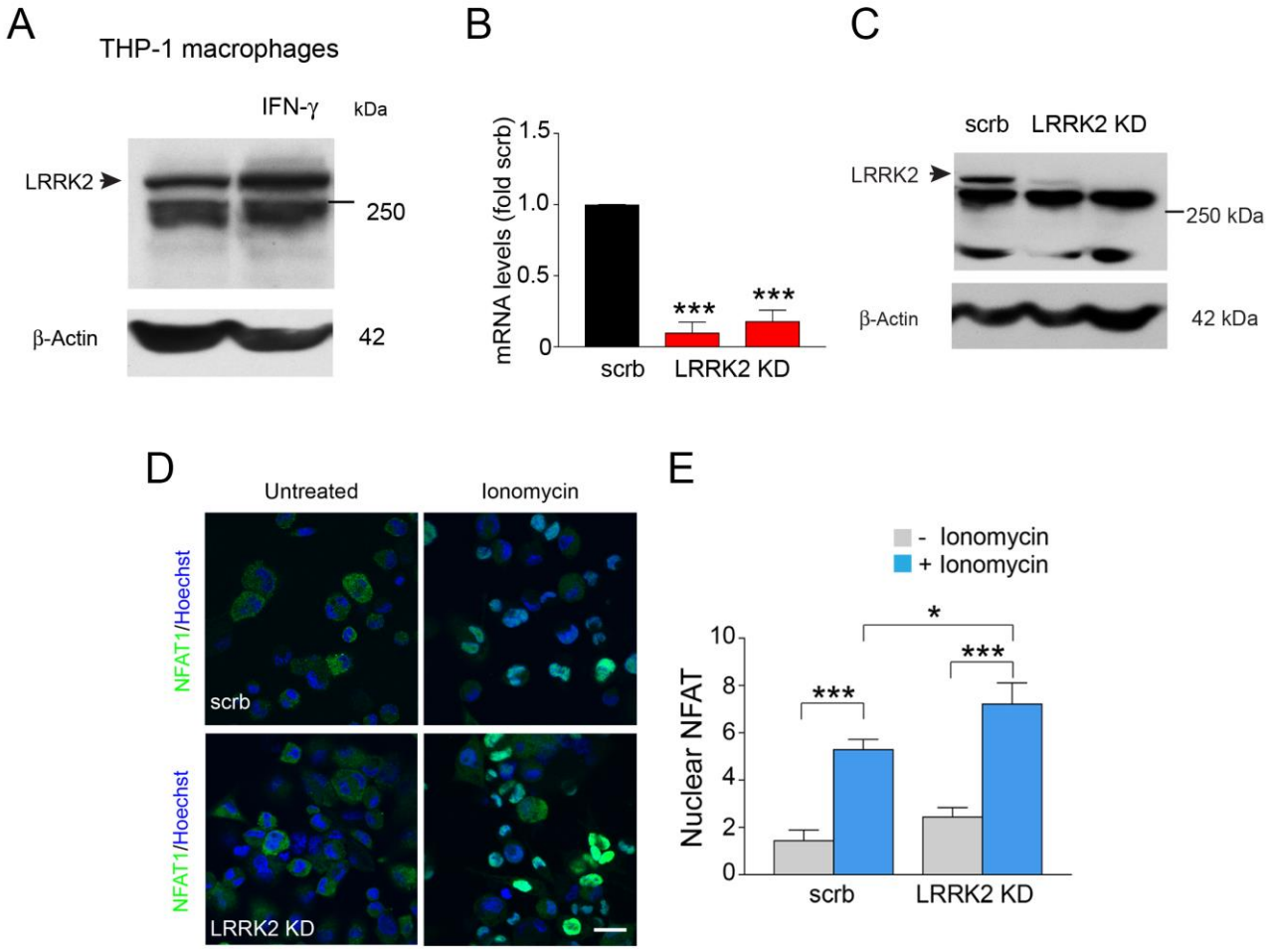

Figure 7. LRRK2 modulates NFAT1 nuclear translocation in THP-1 macrophages. (A) Representative western blot showing LRRK2 levels in THP-1 macrophages with or without stimulation for 72 hours with 200 IU/mL of IFN-γ. **(B)** qRT-PCR showing LRRK2 mRNA levels in THP-1 monocytes transduced with lentiviral vector expressing scramble (scrb), or shRNAs for LRRK2 KD. Data are expressed as fold changes over scrb. (mean + SD, t-test, ***P<0.001; n=3 independent experiments). **(C)** Representative western blot showing LRRK2 levels in THP-1 monocytes scrb and LRRK2 KD. **(D)** Representative pictures of

immunocytochemistry for NFAT1 (green) on THP-1 macrophages scrb and LRRK2 KD with or without treatment with 1 μM Ionomycin for 30 minutes. Nuclei were counterstained with DAPI. Scale bar 20 μm. **(E)** Quantification of NFAT1 fluorescent intensity in the nuclei (mean + SD, one-way ANOVA, Bonferroni post hoc, *P<0.05, ***P<0.001; n=3 independent experiments).

3.4 Potential mechanisms of LRRK2/IFN-γ mediated regulation of NFAT translocation

3.4.1 Calcium homeostasis is altered in LRRK2 G2019S neurons

The canonical pathway for NFAT nuclear translocation is mediated by calcium concentration increase, which leads to activation of the calcium sensitive phosphatase calcineurin. Calcineurin is then dephosphorylating NFAT, exposing its nuclear localization signal, leading to shuttling of NFAT in the nuclei, where it can exert its function as a transcription factor [173]. Therefore, we examined calcium homeostasis in iPSC-derived neurons, to establish if alterations were present based on LRRK2 genotype. Neurons were loaded with Fura-2 and calcium live imaging was performed by Dr. Wadood Haq and Dina Ivanyuk in two different isogenic couples. We discovered that basal levels of cytosolic calcium were higher in G2019S carrying neurons compared to controls (Figure 8A, B). Moreover, after depolarization with KCl, the calcium influx in mutant neurons was significantly lower (Figure 8A, B). Furthermore, the recovery time to get back to baseline was longer for mutant (Figure 8A, B). These data suggest an impairment of intracellular calcium buffering capacity to be present in mutant neurons. We then challenged the Endoplasmic Reticulum (ER) with Sarco-ER Ca2+-ATPase (SERCA) inhibitor thapsigargin (TPH). Indeed, inhibition of SERCA lead to a significantly lower calcium release from the ER in G2019S neurons compared to controls (Figure 8C), which suggests that the ER of mutant neurons has a reduced ability to uptake and to store calcium. Next, we investigated the ER calcium release (stimulated with TPH) after exposure of iPSC-derived neurons to 24 hours of stimulation with 200 IU/mL of IFN-γ. Notably, only control neurons showed significantly less calcium release in IFN-γ treated cells, while treated mutant neurons barely responded to TPH (Figure 8D). These data suggest that the ER calcium storage is already depleted in LRRK2 G2019S neurons.

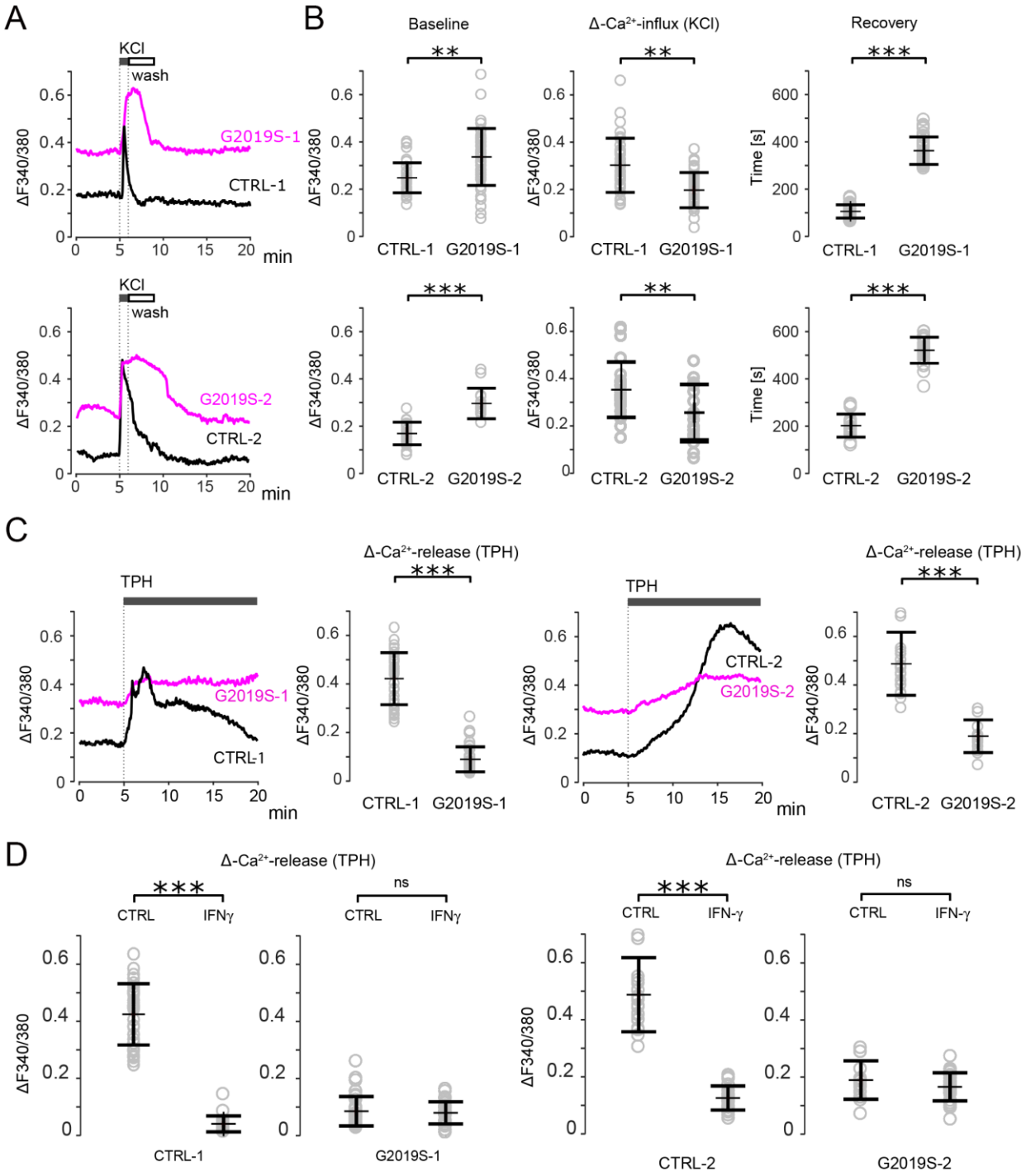

Figure 8. iPSC-derived LRRK2 G2019S neurons show altered calcium homeostasis and response to IFN-γ. (A) Representative calcium traces upon 20 nM KCl stimulation in iPSC-derived neurons of indicated cell lines, measured after Fura-2-AM loading. **(B)** From left to right: quantification of baseline calcium levels before KCl stimulation; quantification of calcium influx after KCl stimulation; recovery time (in seconds) to return to baseline in iPSC-derived neurons (mean ± SD, t-test, ***P<0.001, **P<0.01; n=3 independent experiments, at least 10-15 cells per each cell line per experiment were analysed). **(C)** Representative calcium traces upon 500 nM of TPH stimulation for 15 minutes in iPSC-derived neurons of indicated cell lines, measured after Fura-2-AM loading. Quantification of calcium release from the ER after TPH

stimulation is also shown. (mean ± SD, t-test, ***P<0.001; n=3 independent experiments, at least 10-15 cells per each cell line per experiment were analysed). **(D)** Quantification of calcium release from the ER after TPH stimulation in IFN-γ pretreated or untreated neurons of the indicated cell lines. (mean ± SD, t-test, ***P<0.001; n=3 independent experiments, at least 10-15 cells per each cell line per experiment were analysed).

3.4.2 Microtubule network alterations in LRRK2 G2019S overexpressing cells

LRRK2 is known to interact with several cytoskeletal proteins, including adding post translational modifications such as phosphorylation and acetylation to tubulin [76, 77]. Therefore, we speculated that mutations of LRRK2 might affect the microtubule network. Besides, a recent paper suggested that NFAT translocates into the nuclei along the microtubules [174]. For these reasons, we first tested on HEK NFAT reporter cells whether microtubule disruption mediated by colchicine treatment affected NFAT activity. Indeed, upon colchicine treatment, NFAT activity was significantly reduced (Figure 9A), confirming the importance of microtubules in NFAT shuttling. To evaluate microtubule network differences in the presence of different LRRK2 genotypes, we decided to perform a quantitative analysis at nanoscale resolution, by using direct stochastic optical reconstruction microscopy (dSTORM). We transfected HEK cells with SF-tagged LRRK2 WT or G2019S, and, after 48 hours, we fixed cells with a buffer specific for microtubule preservation. Then, we performed immunocytochemistry for β-tubulin with secondary antibody emission at 647 (Alexa Fluor 647, Figure 9B), necessary for the dSTORM settings, and Flag, to detect cells expressing LRRK2. Only Flag positive cells were imaged for transfected cells. To analyse the microtubule network structure, we employed a recently developed Matlab-based software, SMLM image filament network extractor (SIFNE), that is able to automatically extract microtubule filaments from super-resolution images (Figure 9B) [166]. With this tool, we discovered no differences between control untransfected and transfected cells in terms of number and length of microtubules filaments (Figure 9C, D). However, a significantly higher number of curvatures was detected in cells overexpressing LRRK2 G2019S (Figure 9E), as well as a higher frequency of intersections and branching distributed in the cell periphery (Figure 9F), which suggests a higher network complexity might be present in LRRK2 G2019S cells.

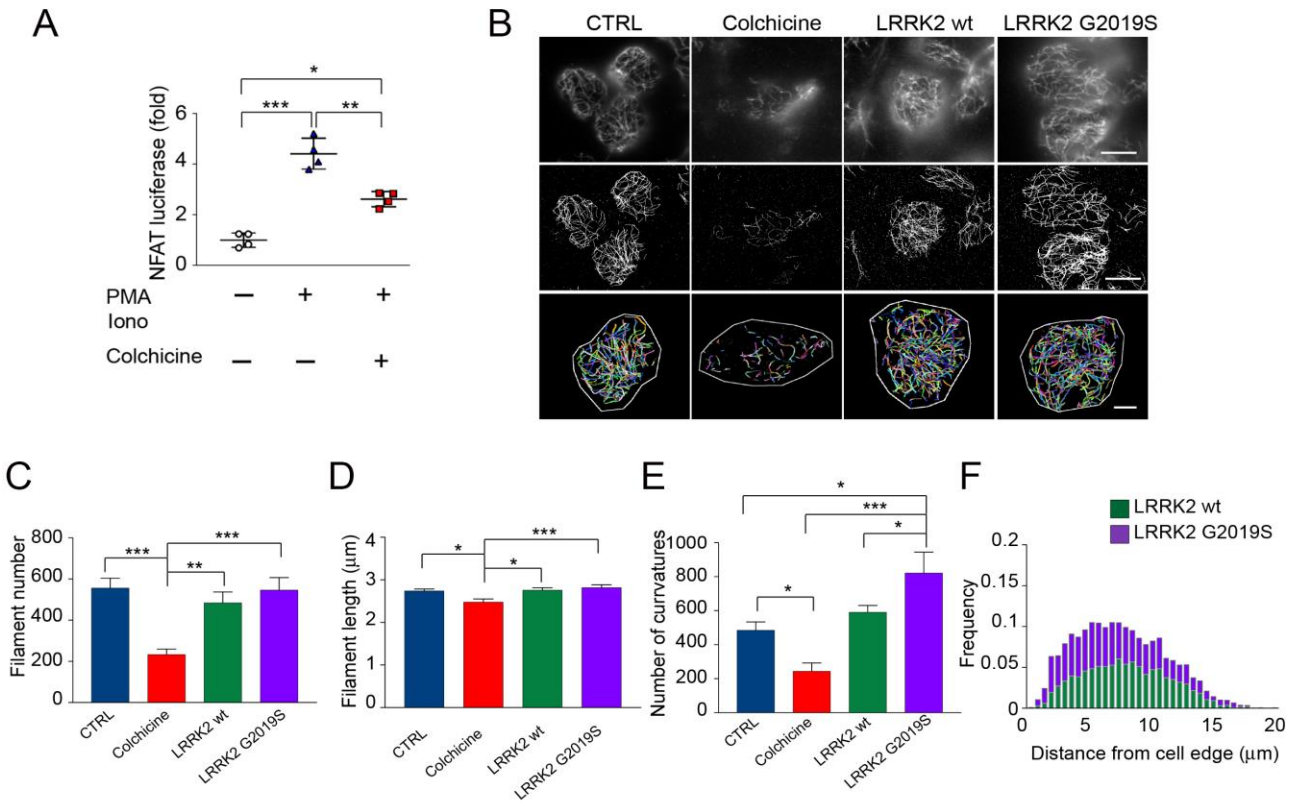

Figure 9. Analysis of microtubule network complexity in HEK cells. (A) Luciferase activity assay in HEK NFAT reporter cells. Where indicated, cells were stimulated with THP-1-PMA 40 ng/mL and Ionomycin 1 µM for 24 hours. Colchicine was applied for 30 minutes at 37 degrees at a concentration of 100 µM where indicated (mean ± SEM, one-way ANOVA, Bonferroni post hoc, ***P<0.001, **P<0.01, *P<0.05; n=4). **(B)** Representative pictures of HEK293 from left to right: untransfected (CTRL), treated with 100 µM colchicine for 30 minutes, transfected with SF-tagged LRRK2 wt or G2019S. Upper panel shows confocal images of β-tubulin staining; middle panel shows dSTORM super-resolution images of microtubule filaments; lower panel shows microtubule filaments extraction obtained through SIFNE analysis. Scale bar 10 µm. **(C)** Analysis of microtubule filaments number (mean + SEM, one-way ANOVA, Bonferroni post hoc, ***P<0.001, **P<0.01; 5 to 8 cells per condition per experiment, n=3 experiments). **(D)** Analysis of microtubule filaments length in µm (mean + SEM, one-way ANOVA, Bonferroni post hoc, ***P<0.001, *P<0.05; 5 to 8 cells per condition per experiment, n=3 experiments). **(E)** Analysis of microtubule filaments number of curvatures (mean + SEM, one-way ANOVA, Bonferroni post hoc, ***P<0.001, *P<0.05; 5 to 8 cells per condition per experiment, n=3 experiments). **(F)** Representative graph of the distribution of microtubule filaments junctions along the cell in LRRK2 WT or G2019S transfected HEK. Junctions are defined as intersecting or branching points (5 to 8 cells per condition per experiment).

Besides what is already known about LRRK2 modulating the cytoskeleton, we focused on another possible way through which NFAT translocation might be affected. In fact, LRRK2 has been shown to be part of the non-coding RNA repressor of NFAT (NRON) complex, which constitutes of a long

non-coding RNA and a complex of 11 proteins that use it as a scaffold [104, 105]. Among these proteins, there is IQ Motif Containing GTPase Activating Protein 1 (IQGAP1), which has very important functions in the regulation of the cytoskeleton of actin and microtubules [175, 176]. In particular, it has been shown that IQGAP1 can act as a scaffold protein for actin-microtubules interaction at the leading edges during migration [177]. We therefore wanted to investigate whether IQGAP1 might be involved in LRRK2/IFN-γ regulation of NFAT translocation and activity. In order to do this, we generated HEK NFAT reporter knockdown for IQGAP1 and verified the knockdown by qRT-PCR and western blot (KD1, KD2, Figure 10A, B). NFAT activity was significantly increased in IQGAP1 KD cells with or without THP-1-PMA and Ionomycin stimulation (Figure 10C, D), consistent with literature, suggesting IQGAP1 is important in retaining NFAT in the cytoplasm [178]. Interestingly, the effect of IFN-γ in reducing NFAT activity previously shown (Figure 5B) was observed only in scrb transduced cells, and was lost in IQGAP1 KD cells (Figure 10E), suggesting IQGAP1 is fundamental for IFN-γ mediated effect on NFAT shuttling. Moreover, IFN-γ effect on SF-tagged LRRK2 WT or G2019S transfected cells was reduced in IQGAP1 KD cells (Figure 10F, G), implicating IQGAP1 has a role in the LRRK2-dependent NFAT modulation.

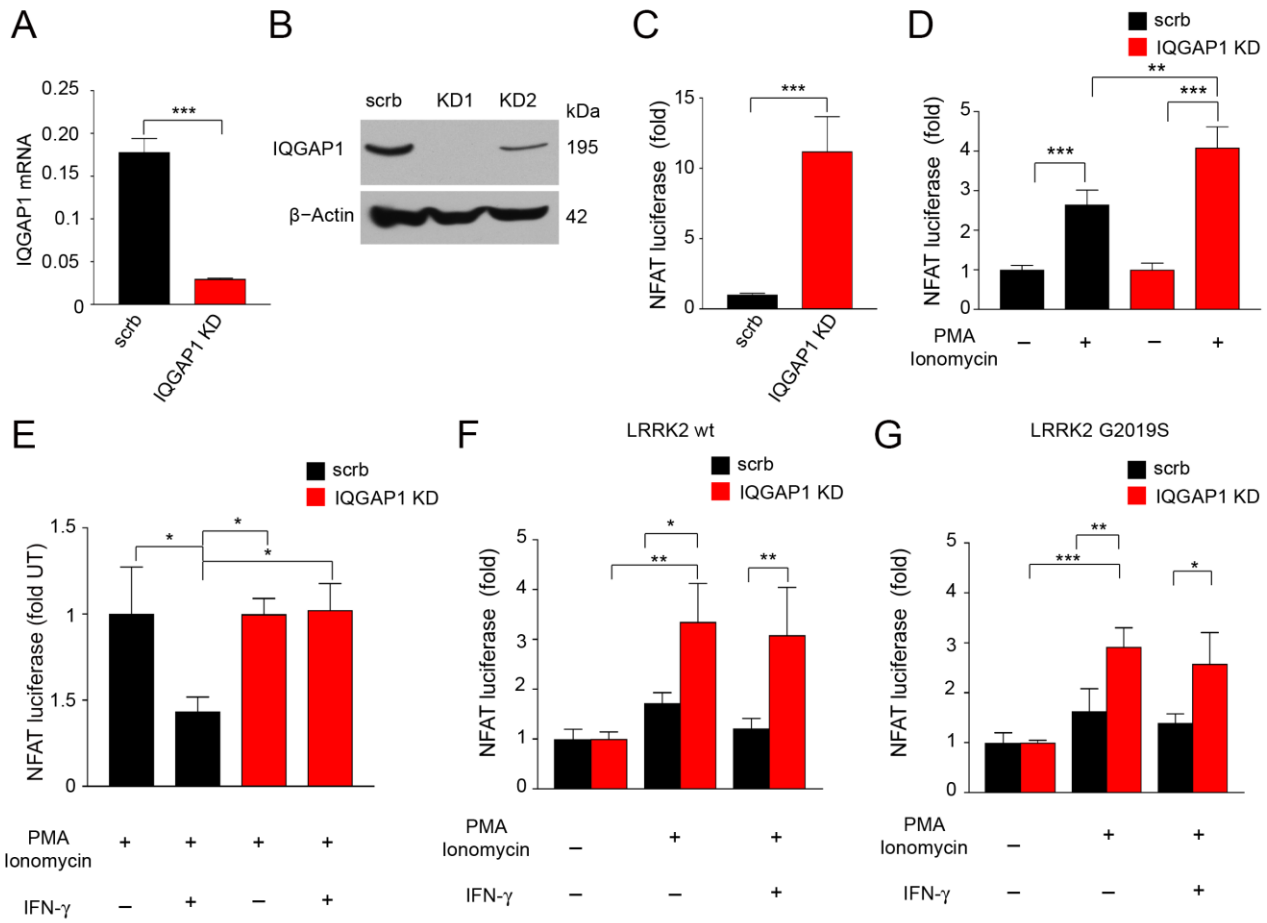

Figure 10. IQGAP1 is fundamental for LRRK2/IFN-γ mediated regulation of NFAT translocation. (A) qRT-PCR showing IQGAP1 mRNA levels in HEK NFAT reporter cells transduced with lentiviral vector expressing scramble (scrb), or shRNAs for IQGAP1 KD. (mean + SD, t-test, ***P<0.001, n=3). **(B)** Representative western blot showing IQGAP1 protein levels in scrb or IQGAP1 KD. **(C)** Luciferase activity assay in HEK NFAT reporter cells scrb or IQGAP1 KD at basal level. Data are expressed as fold changes over scrb (mean + SD, t-test, ***P<0.001, n=3 independent experiments). **(D)** Luciferase activity assay in HEK NFAT reporter cells scrb or IQGAP1 KD untreated or treated with THP-1-PMA 40 ng/mL and Ionomycin 1 μM for 24 hours. Data are expressed as fold changes over corresponding untreated cells (mean + SD, one-way ANOVA, Bonferroni post hoc, ***P<0.001, **P<0.01; n=3 independent experiments). **(E)** Luciferase activity assay in HEK NFAT reporter cells scrb or IQGAP1 KD treated with THP-1-PMA 40 ng/mL and Ionomycin 1 μM for 24 hours, and treated or untreated with IFN-γ 200 IU/mL for 24 hours. Data are expressed as fold changes over corresponding IFN-γ untreated cells (-UT-, mean + SD, one-way ANOVA, Bonferroni post hoc, *P<0.05; n=3). **(F)** Luciferase activity assay in HEK NFAT reporter cells scrb or IQGAP1 KD transfected with SF-tagged LRRK2 WT. Where indicated, cells were treated with THP-1-PMA 40 ng/mL and Ionomycin 1 μM for 24 hours, and/or IFN-γ 200 IU/mL for 24 hours. Data are expressed as fold changes over corresponding LRRK2 WT transfected untreated cells (mean + SD, one-way ANOVA, Bonferroni post hoc, **P<0.01, *P<0.05; n=4). **(G)** Luciferase activity assay in HEK NFAT reporter cells scrb or IQGAP1 KD transfected with SF-tagged LRRK2 G2019S. Where indicated, cells were treated with THP-1-PMA 40 ng/mL and Ionomycin 1 μM for 24 hours, and/or IFN-γ 200 IU/mL for 24 hours. Data are expressed as fold changes over corresponding LRRK2 G2019S transfected untreated cells (mean + SD, one-way ANOVA, Bonferroni post hoc, ***P<0.001, **P<0.01, *P<0.05; n=4).

3.5 IFN-γ leads to reduced neurite length depending on NFAT translocation

We have confirmed that NFAT translocation is impaired in G2019S carrying iPSC-derived neurons, and that this might be due to alterations in the calcium homeostasis and/or microtubule network. We then wondered what functional consequences the NFAT pathway impairment might have on neurons. Since we did not see any differences in cell viability and differentiation potential after stimulation with IFN-γ (Figure 2), we analysed the length of the neurites in iPSC-derived neurons after stimulation with the proinflammatory cytokine (Figure 11A-C). We performed immunocytochemistry for β-Tubulin III, then we quantified neurite length with the ImageJ plugin Simple Neurite Tracer. Indeed, treatment with IFN-γ lead to significantly shorter neurites in control and G2019S mutant lines (Figure 11A, B). According to literature, G2019S carrying neurons already showed shorter neurites than isogenic controls (Figure 11A, B). Importantly, the shortening of the neurites upon IFN-γ treatment was lost in LRRK2 KO iPSC-derived neurons (Figure 11A, C), corroborating the hypothesis that LRRK2 is necessary for IFN-γ mediated effect. Moreover, since NFAT has been shown to be crucial for neurite growth [170], we argued that NFAT signalling

could be the pathway connecting LRRK2 and IFN-γ-dependent neurite deficit. Therefore, we treated our iPSC-derived neurons with a specific inhibitor of NFAT and calcineurin interaction, a peptide called MCV1, the use of which results in blocking NFAT translocation (Figure 11A, D, E). Treatment with MCV1 lead to a significantly shorter neurite length both in control and in LRRK2 mutant neurons (Figure 11A, D), but no effect was observed in the LRRK2 KO lines (Figure 11A, E).

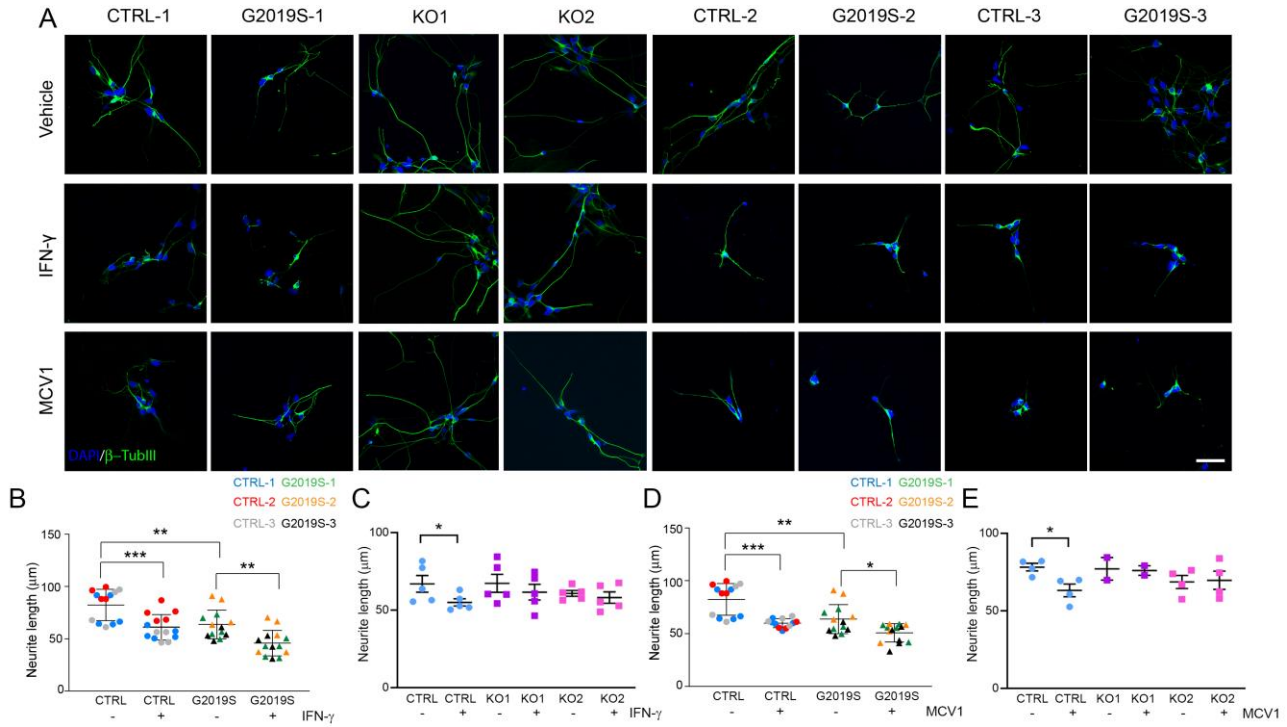

Figure 11. IFN-γ exposure and inhibition of NFAT translocation both reduce neurite length in iPSC-derived neurons. (A) Representative pictures of β-tubulin III immunocytochemistry (green) on iPSC-derived neurons of the indicated lines. Cells were treated with 200 IU/mL of IFN-γ for 24 hours, or with 500 nM of MCV1 (NFAT inhibitor) for 24 hours, or left untreated (vehicle). Nuclei were counterstained with DAPI. Scale bar 50 µm. **(B)** Quantification of neurite length in CTRL vs G2019S neurons with or without treatment with 200 IU/mL of IFN-γ for 24 hours (mean ± SD, t-test, ***P<0.001, **P<0.01; n=5 independent experiments). **(C)** Quantification of neurite length in CTRL-1 vs LRRK2 KO neurons with or without treatment with 200 IU/mL of IFN-γ for 24 hours (mean ± SD, t-test, *P<0.05; n=5 independent experiments). **(D)** Quantification of neurite length in CTRL vs G2019S neurons with or without treatment with 500 nM of MCV1 (NFAT inhibitor) for 24 hours (mean ± SD, t-test, ***P<0.001, **P<0.01, *P<0.05; n=5 independent experiments). **(E)** Quantification of neurite length in CTRL-1 vs LRRK2 KO neurons with or without treatment with 500 nM of MCV1 (NFAT inhibitor) for 24 hours (mean ± SD, t-test, *P<0.05; n=4 independent experiments).

To verify that the neurite length reduction after IFN-γ stimulation was really dependent on NFAT, we pre-treated our cells with Neuregulin 1 (NRG1), which was found to promote NFAT translocation and activity [179]. Therefore, we treated iPSC-derived neurons from one isogenic couple with 200 IU/mL IFN-γ or MCV1 500 nM for 24 hours, with or without pre-treatment with 200 ng/mL of NRG1 for 24 hours before adding the stimulants. Afterwards, we performed immunocytochemistry for β-Tubulin III, then we quantified neurite length with the ImageJ plugin Simple Neurite Tracer. Consistent with the hypothesis, NRG1 pre-treatment lead to recovery of the neurite length upon further treatments with IFN-γ or MCV1, and even to a partial recovery of the basal levels in G2019S carrying neurons (Figure 12A, B). Moreover, to further confirm these results, we performed the rescue experiment by analysing only cells positive for the dopaminergic marker TH (Figure 12C). Indeed, the results were similar, with shortening of neurite upon stimulation with IFN-γ or MCV1, and partial rescue due to pre-treatment with NRG1 (Figure 12C, D).

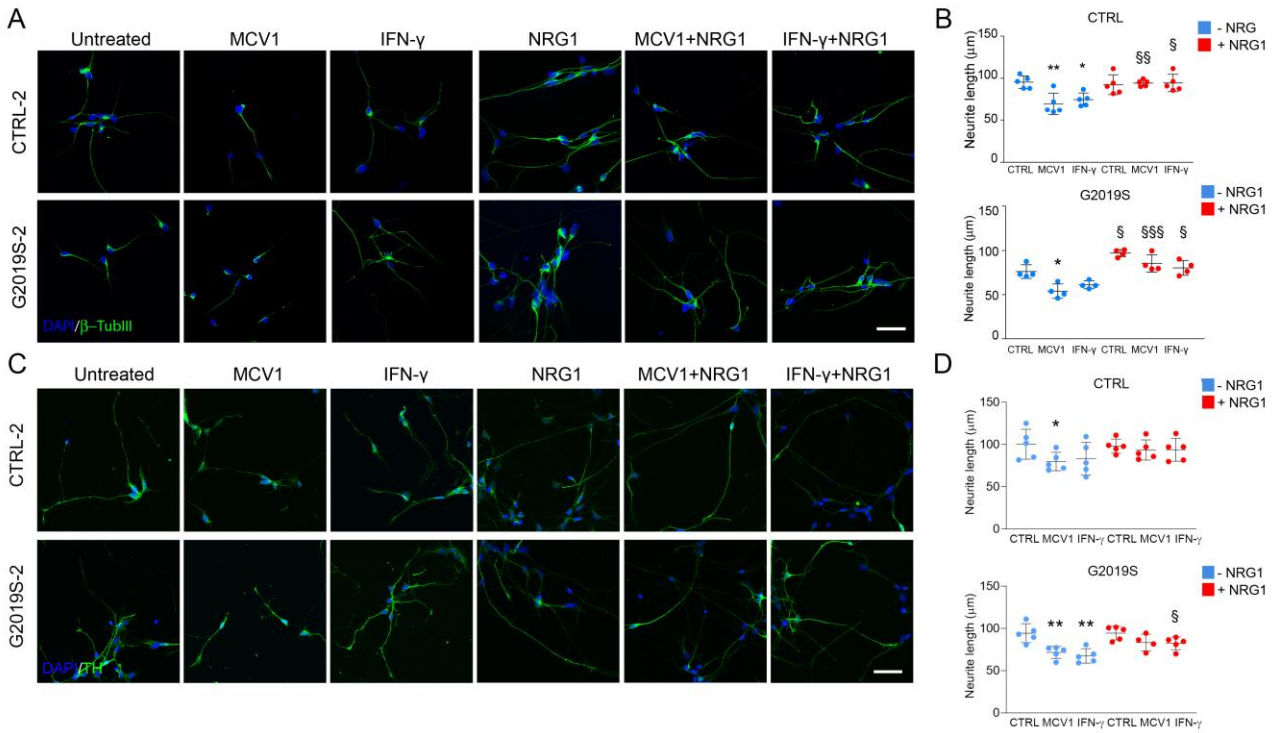

Figure 12. Promoting NFAT translocation rescues neurite shortening. (A) Representative pictures of β-tubulin III immunocytochemistry (green) on iPSC-derived neurons of CTRL-2 and G2019S-2. Cells were treated with 500 nM of MCV1 (NFAT inhibitor) for 24 hours or with 200 IU/mL of IFN-γ for 24 hours, or left untreated. Where indicated, treatment with 200 ng/mL NRG1 for 48 hours was performed. Nuclei were counterstained with DAPI. Scale bar 50 µm. **(B)** Quantification of neurite length in CTRL-2 or G2019S-2 neurons (mean ± SD, one-way ANOVA, Bonferroni post hoc; for MCV1/IFN-γ treatment vs vehicle **P<0.01, *P<0.05; for NRG1 treatment vs corresponding NRG1 untreated §§§P<0.001, §§P<0.01,

§P<0,05; n=5 independent experiments). **(C)** Representative pictures of TH immunocytochemistry (green) on iPSC-derived neurons of CTRL-2 and G2019S-2. Cells were treated with 500 nM of MCV1 (NFAT inhibitor) for 24 hours or with 200 IU/mL of IFN-γ for 24 hours, or left untreated. Where indicated, treatment with 200 ng/mL NRG1 for 48 hours was performed. Nuclei were counterstained with DAPI. Scale bar 50 µm. **(D)** Quantification of neurite length in CTRL-2 or G2019S-2 neurons (mean ± SD, one-way ANOVA, Bonferroni post hoc; for MCV1/IFN-γ treatment vs vehicle **P<0.01, *P<0.05; for NRG1 treatment vs corresponding NRG1 untreated §P<0,05; n=5 independent experiments).

To conclude, we performed neurite outgrowth experiments on iPSC-derived neurons after treatment with IFN-γ (Figure 13A). Quantification of neurite outgrowth showed a similar tendency as the neurite length, with a reduction of neurite growth upon IFN-γ stimulation, only significant in one control line (Figure 13B, C). These results indicate neurite growth might also be affected. It's possible that longer IFN-γ exposure times could lead to a more severe defect in growth.

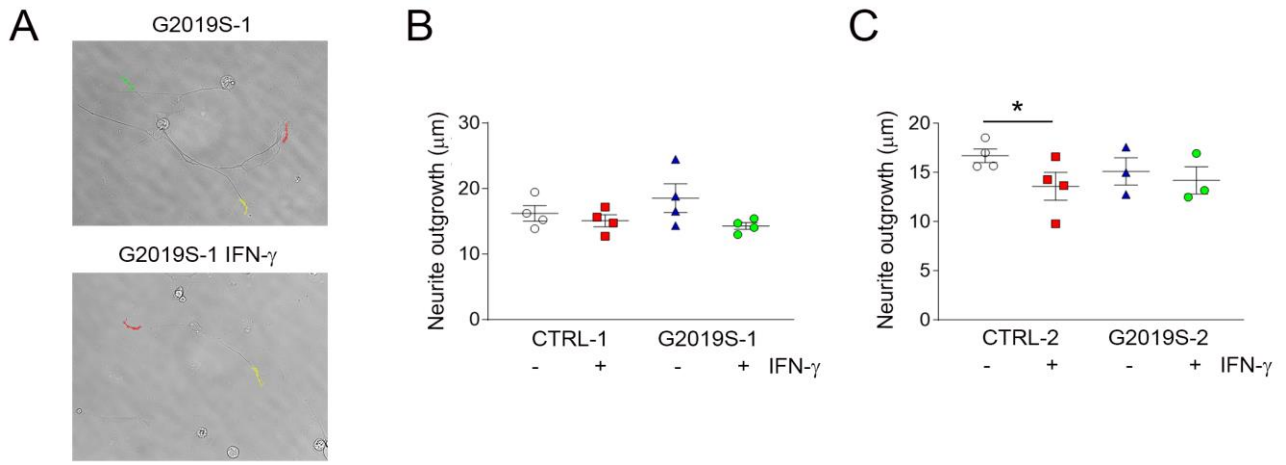

Figure 13. Neurite outgrowth is also altered with IFN-γ treatment. (A) Representative pictures of neurite outgrowth experiment. Traces for growing neurites are colored, and growth was measured with MTrack2 plugin from ImageJ. **(B)** Quantification of neurite outgrowth of iPSC-derived neurons CTRL-1 and G2019S-1 with or without treatment with 200 IU/mL IFN-γ (mean ± SEM; n=4). **(C)** Quantification of neurite outgrowth of iPSC-derived neurons CTRL-2 and G2019S-2 with or without treatment with 200 IU/mL IFN-γ (mean ± SEM, t-test, *P<0.05; n=4).

4. Outlook

Here, we have identified a potential role of neuronal IFN-γ response and the NFAT pathway in PD-related neurodegeneration. Future experiments will assess the NFAT downstream pathway in human neurons via RNA sequencing. This could lead to the identification of novel neurodegenerative pathways.

IFN-γ response could also affect cells belonging to the immune system, in particular the resident innate immune cells of the brain, microglia. Microglia have many roles in the CNS, including sensing the environment for the presence of pathogens, as well as contributing to synaptic pruning and giving trophic support to neurons. When potentially harmful stimuli are detected, microglia reacts by inducing the expression of Toll-like receptors (TLRs), which are sensors for danger/pathogen-associated molecular patterns (DAMPs or PAMPs), and subsequently to their activation, by releasing pro-inflammatory cytokines. Whether microglia express LRRK2 at basal conditions is still controversial [107, 180]. Interestingly, LPS or microbial exposure significantly increases LRRK2 protein expression in microglia, as well as in monocytes and macrophages [107]. Knock-down of LRRK2 or inhibition of its kinase activity have been shown to lead to a reduction of the secretion of pro-inflammatory cytokines in mouse primary microglia [107, 181]. We have also observed a distinct cytokine profile in iPSC-derived microglia from PD patients carrying the G2019S mutation compared to isogenic controls upon LPS stimulation (paper in revision). Furthermore, NFAT translocation was significantly reduced in G2019S microglia compared to control cells. It remains to be elucidated the effect of exposure of microglia cells to IFN-γ on the cytokine profile.

Given that we also detected changes in motility in G2019S microglia compared to isogenic controls, it would be of great interest to analyse more in depth the microtubule cytoskeleton with dSTORM super-resolution imaging, both in microglia, as well as in dopaminergic neurons, derived from human iPSCs form PD patients and isogenic controls.

To further elucidate the communication between neurons and microglia, co-culture experiments combined with 3D systems, such as organoids, will be employed in future experiments. Work from the literature and our lab show that it is possible to generate microglia-like cells from cerebral organoids [182]. Furthermore, microglia can be co-cultured with brain organoids [183, 184].

On another note, LRRK2 kinase activity has been recently associated with the activation of the inflammasome protein Nod-like receptor (NLR) family CARD domain-containing protein 4 (NLRC4) [111]. The NLRC4 inflammasome is activated after recognition of components of

intracellular bacteria, such as *Salmonella Typhimurium*. Upon detection of the PAMP, inflammasome proteins cluster together, through a scaffolding protein named apoptotic speck protein containing a caspase recruitment domain (ASC), to promote the production of active caspase 1, which in turn cleaves and activates the pro-inflammatory cytokines IL-1β and IL-18. Interestingly, increased IL-1β has been detected in CSF, as well as basal ganglia and substantia nigra of PD patients [33, 35, 36]. Moreover, increased serum levels of IL-1β have been quantified in PD patients carrying the G2019S mutation [94]. Data from the literature and our lab suggest that LRRK2 kinase activity plays a key role in NLRC4 activation and cytokine release, both in mouse and human cells (unpublished data) [111]. Thus, it is tempting to speculate that LRRK2-dependent inflammasome activation has an overall relevance for PD onset and progression. Also based on the recent findings showing the relevance of NLRP3 inflammasome in Alzheimer's disease development [185-187], it would be important to evaluate NLRC4 relevance in PD. IPSC-derived microglia would be an excellent model to study the role of LRRK2 in the activation of the NLRC4 inflammasome and its impact on inflammatory reactions.

5. Discussion

The aim of this thesis was to discover new mechanistic insights about how persistent exposure to the pro-inflammatory cytokine IFN-γ affects neurons, in particular in the context of PD. Indeed, we found that the presence of the LRRK2 mutation G2019S is linked to alterations of the IFN-γ response pathway that lead to defects in the activation of NFAT and neurite shortening.

The IFN-γ response has been shown to play a fundamental role in neurodegenerative processes [119]. Evidences from different studies suggest that this cytokine may be involved in PD onset and development [43, 121-123]. Increased IFN-γ levels in the serum [21] and in the substantia nigra [35, 36] of PD patients, combined with animal models suggesting selective DA neuronal cell death as an effect of the cytokine [21, 122, 123], made a compelling argument of IFN-γ being involved in the disease pathophysiology. However, in line with previous findings that show no specific DA neuronal death in the absence of microgliosis [122, 123], we did not observe neuronal death upon IFN-γ stimulation of iPSC-derived neurons. This is also in agreement with the physiological role of IFN-γ in the maintenance of brain homeostasis [118]. Moreover, we have shown that IFN-γ does not affect neuronal differentiation of human iPSCs.

LRRK2 is highly expressed in immune cells [91] and LRRK2 SNPs have been associated with inflammatory diseases such as Crohn's disease. It has been shown that IFN-γ induces LRRK2 expression in cells of the innate immunity [91, 101], due to the presence of an IFN-γ responsive element in the LRRK2 promoter [100]. Notably, LRRK2 regulates the immune responses against pathogens such as *Mycobacterium tuberculosis*, *Listeria monocytogenes* and *Salmonella typhimurium* [103, 111, 113]. Based on these premises, we hypothesized that IFN-γ regulates the LRRK2-dependent response during infections, as well as neuroinflammatory responses. Indeed, we found that IFN-γ increases LRRK2 expression levels also in iPSC-derived neurons, to a comparable extent in control and LRRK2 G2019S lines. To investigate whether LRRK2 modulates IFN-γ response, we first analysed the IFN-γ-dependent response in LRRK2 G2019S and isogenic control neurons. Interestingly, IFN-γ treatment in control neurons led to a significant upregulation of genes implicated in stress responses and inflammasome assembly (*EIF2AK2*), apoptosis (*IRF1, SOCS1*), axonal regeneration (*AKT3, SOCS1*) and brain development (*AKT3*). When comparing the effect of IFN-γ treatment in control and LRRK2 G2019S neurons, we found a significant upregulation of AKT3 mRNA levels in LRRK2 G2019S compared to control neurons; however, the AKT activation state, evaluated by the presence of the phosphorylation, was significantly downregulated in G2019S carrying neurons, suggesting that the increased mRNA transcription might be a compensatory mechanism for the reduced protein activity. Interestingly, human macrophages

stimulated with IFN-γ have shown similar results in terms of reduced activation of AKT [188]. Besides, LRRK2 has been already found to interact with and phosphorylate AKT, and that mutations of LRRK2 disturb this process [189, 190]. Our results suggest that the LRRK2 mutation affects the IFN-γ-dependent response by lowering the activation of AKT.

Importantly, AKT is a major regulator of the pathway that modulates NFAT activity [191], through its negative phosphorylation of GSK-3β [168], which, when active, is negatively phosphorylating NFAT, leading to NFAT retrotranslocation from the nuclei to the cytoplasm [169, 192]. Interestingly, IFN-γ stimulation of human macrophages has shown downregulation of GSK-3β negative phosphorylation [188], suggesting that this protein hyperactivation might be responsible for a lower IFN-γ-dependent NFAT activity in immune cells. It is well established that NFAT regulates immune cell functions, such as T cell anergy and metabolism, as well as cytokine production [193]. However, the functional role of NFAT activation is relatively unexplored. NFAT is known to play a key role in neuronal outgrowth and development. In particular, NFAT1, NFAT3 and NFAT4 have been found to be necessary for axonal outgrowth in response to netrins and neurotrophins in mouse primary cultures [170]. Besides, NFAT2 regulates neurite outgrowth of dopaminergic neurons differentiated from SH-SY5Y cells [194]. Moreover, NFAT3 has a role in lithium-induced neuroprotection in cerebellar granule cells [171] and it has an antiapoptotic function in cortical neurons [195]. Furthermore, NFAT1/3/4 mutant mice showed defects in axon growth and sensory axon projection [170]. In addition, NFAT pathway activation has been found to be necessary for olfactory neurons axon terminal remodelling in a zebrafish model [196]. Inhibition of NFAT activity has also been shown to negatively affect NPC proliferation and viability [197]. Taken together, these findings highlight the potential role of NFAT in neurite outgrowth and brain function. Consistently with the paper from Liu et al. that showed LRRK2-dependent negative regulation of NFAT translocation in immune cells, we found that LRRK2 inhibits NFAT nuclear shuttling in iPSC-derived neurons and HEK overexpressing cells, and that the G2019S mutation significantly exacerbates this defect. In line with the IFN-γ-mediated increased expression of LRRK2 already discussed, treatment with the pro-inflammatory cytokine lead to further negative regulation of NFAT activity and translocation. This effect was further exacerbated in LRRK2 mutant cells by the downregulation of AKT3 activity.

Interestingly, we discovered that IFN-γ treated neurons, both control and G2019S, had lower protein levels of NFAT3. Since it has been shown that IFN-γ activates proteasomal degradation of specific targets [172], we hypothesised that NFAT3 reduced expression upon treatment could be due to this process. This mechanism could be mediated by SOCS1 [198]. However, there is another

possible pathway that could lead to NFAT3 degradation. Indeed, AKT1 has been found to promote NFAT1 proteasomal degradation in breast cancer cell lines [199, 200], and this mechanism could be exploited in other cell types by other isoforms, such as AKT3. Indeed, proteasome inhibition restored basal levels of NFAT3 expression. The exact pathway involved in this process still remains to be elucidated.

Of note, iPSC-derived neurons carrying the G2019S mutation showed reduced NFAT1 translocation, as well as NFAT3, suggesting that this regulatory mechanism could be applied also to other NFAT isoforms. The group of Timmusk et al. has shown that different NFAT isoforms have different kinetics of translocation upon calcium influx: in rat primary hippocampal neurons the NFAT1 orthologous protein translocates in the nucleus faster than the NFAT3 orthologous. Moreover, depending on the cell type investigated, different NFAT isoforms were activated at different levels, with NFAT3 and NFAT4 orthologous proteins more highly induced in neurons, and NFAT2 and NFAT4 in HEK293 cells [201]. Besides, the same group proposes that this cell type-dependent role of different NFAT isoforms is due to cell type-dependent different sumoylation [202]. Here, we also showed that THP1 monocytic cell lines knockdown for LRRK2 displayed an increased NFAT1 nuclear localization, which corroborates the idea that LRRK2 controls the activity of NFAT in different cell types, and with different scopes. For example, in monocytes and macrophages LRRK2 could be involved in monitoring cytokines production, as it has been shown that LPS-treated LRRK2 mutant cells produce more pro-inflammatory cytokines [99], but also in skewing the differentiation process [203].

LRRK2 has been shown to retain NFAT in the cytoplasm through binding to the NRON complex [104]. To further investigate possible mechanisms of NFAT modulation, we also focused on other aspects of the NFAT pathway. As mentioned, calcium concentration increase leads to NFAT nuclear translocation and activity [204]. Interestingly, response to calcium influx has been shown to be reduced in LRRK2 G2019S mutant iPSCs-derived sensory neurons [74]. Therefore, we performed calcium imaging experiments in control and carrying the LRRK2 G2019S iPSC-derived neurons. We found that the LRRK2 G2019S mutation increased calcium levels and defects in calcium buffering capacity, which is in line with a recent paper [75]. IFN-γ is known to generate calcium transients in different cell types, including neurons [205-207]. However, little is known about the effect of the prolonged exposure to IFN-γ. In line with the reduced NFAT translocation observed in mutant neurons, we showed that 24 hours treatment with IFN-γ leads to complete depletion of the ER calcium storage. Therefore, the LRRK2 G2019S mutation synergizes with IFN-γ into regulating NFAT translocation also through alteration of calcium levels.

Several studies indicate that LRRK2 is interacting and regulating cytoskeletal proteins [76, 77, 208]. Interestingly, about 40% of the interactome of LRRK2 is associated with the cytoskeleton [209]. In particular, some studies have investigated the influence of a LRRK2 mutation on the cytoskeletal modulation. For example, Caesar and colleagues have shown that human fibroblasts carrying the G2019S mutation migrate more than controls [76]. However, LRRK2 G2019S iPSC-derived monocytes and microglia displayed defects in migration compared to controls [108, 203], suggesting that impaired cytoskeletal dynamics is a general feature of the disease, but might lead to cell-type dependent effects. Moreover, Gillardon has shown that LRRK2 interacts with tubulin and facilitates tubulin polymerization in a kinase dependent way [76, 78, 210]. Gillardon suggests that the enhanced phosphorylation of tubulin might lead to less dynamic microtubules, which could in turn result in the neurite outgrowth deficit that is present in G2019S carrying neurons [78, 158]. Indeed, a fragmented microtubule network has been reported in overexpressing G2019S LRRK2 Drosophila neurons [211]. Based on these premises, we investigated the microtubule network of HEK293 cells overexpressing wildtype or mutant LRRK2 with super-resolution microscopy analysis coupled with microtubules single filament detection made possible by a recently developed Matlab-based software, SIFNE [166]. With this method, we detected alterations in the G2019S overexpressing cells in terms of higher complexity of the network, especially in the cell periphery. Importantly, we showed that microtubules disruption mediated by colchicine treatment lead to lower NFAT activity, which is consistent with literature reports indicating that NFAT translocates into the nuclei along the microtubules [174]. Interestingly, the AKT/GSK-3β/NFAT pathway itself has been proposed to be involved in cytoskeletal regulation [200]. In fact, breast cancer cell motility is reduced with activation of AKT and subsequent inactivation of GSK-3β, leading to NFAT degradation via the proteasome [200]. However, this mechanism might also be cell-type specific and should be further characterized in neurons. Intriguingly, neurons derived from iPSC from PD patients carrying Parkin mutations have been shown to recover their neurite shortening phenotype upon microtubule stabilization mediated by taxol, which confirms Parkin as a microtubule stabilizer [148]. To conclude, we hypothesize that microtubules alterations induced by the LRRK2 mutations lead to NFAT translocation defects.

Since IQGAP1 is a scaffolding protein that takes part in the NRON complex and is implicated in cytoskeletal remodelling, we speculated that it might be the link between LRRK2 and IFN-γ-mediated regulation of NFAT translocation. In particular, IQGAP1 has been shown to regulate actin cytoskeleton during migration in different cell types [177, 212]. Moreover, Watanabe and colleagues discovered that IQGAP1 is fundamental for microtubule and actin mutual organization at the leading edge of the cell [177]. Importantly, IQGAP1 has been shown to be involved in neuronal

survival and outgrowth. For example, overexpression of IQGAP1 increases neurite growth in a mouse neuroblastoma cell line [213], while knockdown of IQGAP1 leads to reduced neuronal motility [214]. IQGAP1 regulates this process through complexing, upon increased intracellular calcium levels, with the known actin regulator Cdc42, with Lissencephaly 1 (Lis1), a fundamental protein in neurogenesis and neuronal migration, and with CLIP-170, thereby linking the actin cytoskeleton with the microtubules network [214]. Moreover, IQGAP1 has been shown to be important for NPCs, as knockout mice showed impaired VEGF-dependent NPCs migration and differentiation [215]. IQGAP1 knockout mice also displayed decreased dendritic spines number and density [216], further consolidating its role in cytoskeletal regulation in neurons. To study IQGAP1 role in LRRK2/IFN-γ-dependent NFAT shuttling, we have generated HEK293 NFAT reporter cell line knockdown for IQGAP1. Consistent with literature, knockdown of IQGAP1 showed increased NFAT activity [178]. Interestingly, IFN-γ treatment reduced NFAT shuttling only in the presence of normal IQGAP1 levels, suggesting IQGAP1 is fundamental in the LRRK2/IFN-γ-dependent regulation of NFAT translocation. Notably, a recent publication has implicated IFN-γ in regulating breast cancer cell cytoskeleton through increasing IQGAP1 post-translational modification ISGylation [217].

Consistent with the important role of NFAT in neurite growth and neuronal development [170], NFAT translocation inhibition lead to neurite shortening in our iPSC-derived neurons, recovered with stimulation of the shuttling mediated by Neuregulin 1 [179]. This shortening is exacerbated by the presence of the LRRK2 G2019S mutation. Importantly, IFN-γ treatment displayed reduction of neurite length similar to NFAT inhibitor exposure, recovered as well with Neuregulin 1. This corroborates our findings that IFN-γ modulates NFAT pathway to eventually cause neurite shortening. Indeed, LRRK2 G2019S have been shown in multiple studies to have shorter neurites [74, 75, 158, 218, 219]. Interestingly, Lin and colleagues showed that Lovastatin treatment protects G2019S dopaminergic neurons from neurite shortening by increasing AKT activity, thereby decreasing GSK-3β activation [220]. Concerning the role of LRRK2 kinase activity in this pathway, most reports suggest that the negative effect on neurite length is kinase dependent, by showing a rescue of this phenotype upon treatment with various specific LRRK2 kinase inhibitors [74, 75, 158]. However, other papers report that the G2019S effect on neurite length is kinase independent. For example, Skibinski and colleagues demonstrated that LRRK2 levels are more important than its kinase activity in terms of neurite length and neurotoxicity [156]. Few papers have shown increased basal levels of LRRK2 G2019S expression compared to controls [221, 222]. Interestingly, LRRK2 degradation is modulated by chaperon-mediated-autophagy (CMA), and CMA has been shown to be impaired in the presence of the LRRK2 mutation [221]. Indeed, Khurana and colleagues have

shown increased LRRK2 expression in G2019S carrying dopaminergic neurons [222]. However, we did not see differences in LRRK2 expression in our iPSC-derived neurons at basal level, but the IFN-γ-mediated increase of LRRK2 expression might be responsible for neurite defects, via NFAT-mediated mechanisms in the cytoplasm. Of note, another paper with iPSCs-derived neurons from idiopathic PD patients showed that LRRK2 kinase inhibition did not ameliorate neurite shortening [223], suggesting the increased kinase activity might be a potential target only for G2019S mutant patients. Clinical trials to test this hypothesis are currently ongoing. Our conclusion is that impairment in NFAT translocation contributes to LRRK2-dependent neurite growth defects and that a pro-inflammatory environment could aggravate such defects.

It remains to be elucidated whether potentiation of NFAT translocation could be a possible therapeutic approach. Interestingly, accumulation of misfolded proteins like amyloid β leads to calcium deregulation through ER stress, causing cytotoxicity calcineurin-dependent [224-226]. Moreover, hyperactivation of calcineurin has been shown to provoke apoptosis through NFAT sustained activity [227]. Besides, few papers show that NFAT activation is detrimental in neurodegenerative disorders. In fact, Hudry and colleagues demonstrated that constitutive NFAT activation leads to spine loss and simplified dendritic branching *in vitro* in primary cultures and *in vivo* in mice models of Alzheimer's disease [226]. In addition, Luo and his group reported that α-synuclein enhances calcineurin activity, and therefore NFAT activity, in HEK293 cells overexpressing A53T mutant α-synuclein, or in A53T transgenic mice. Indeed, inhibition of calcineurin increased viability of dopaminergic neurons in primary culture [228]. Therefore, NFAT modulation seems to have similar negative effects on neurons, whether its activity is enhanced or reduced, as we showed. This suggests that a tight regulation of the pathway is fundamental for neuronal survival and homeostasis, and that NFAT regulation is not a foreseeable therapeutic strategy.

However, another potential approach could be the modulation of downstream targets of the NFAT pathway in neurons, in line with the important role of NFAT in neurite length regulation. Unexpectedly, in PC12 cells and murine cortical neurons, overexpression of NFAT3 has been shown to negatively modulate the mRNA levels of growth-associated protein 43 (*GAP43*), a gene known to associate with nerve growth and plasticity [229]. Moreover, the repressive effect was specific for *GAP43*, as *IL-2* expression was not altered in this model [229]. Besides, other NFAT targets identified in PC12 plasma membrane Ca2+-ATPases (PMCA) 2 and 3 deficient cells were *Vamp1* and *Vamp2*, genes involved in the secretory machine, including in dopamine secretion regulation [230]. In this experimental setup, NFAT shuttling repression with VIVIT lead to

increased mRNA expression of *Vamp1* and *Vamp2* [230]. As mentioned, it is likely that the NFAT pathway needs tight regulation to properly exert its function. A further investigation of the NFAT dependent genes in DA neurons is needed to design any therapeutic approach.

Interestingly, with ageing a progressive senescence of the immune cells occurs, which leads to increased production of pro-inflammatory cytokines, among which is IFN-γ [231]. However, the source of IFN-γ is not clear yet. Indeed, Dulken and colleagues recently showed a clonal expansion of T cells expressing IFN-γ at high levels in mice brain at old age, compared to younger ones, and reported that this was causative for the lower proliferation levels in the aged neurogenic niche [232]. Since T cells have been found to infiltrate in PD brains [28] and they are likely involved in PD pathogenesis [233, 234], it is tempting to speculate that another detrimental role of these cells towards dopaminergic neurons could be the production of IFN-γ, which increases LRRK2 levels. This hypothesis, though, needs further investigation.

In conclusion, we have shown that IFN-γ synergizes with the LRRK2 mutation G2019S to render neurons more vulnerable to inflammation. Moreover, this pathway is of potential interest for idiopathic PD patients, as it could hypothetically link inflammation and neurodegeneration, through the NFAT pathway regulation, in a not yet discovered way.

6. References

1. De Cicco, S., et al., *Interferon-γ signaling synergizes with LRRK2 in human neurons and microglia.* bioRxiv, 2020: p. 2020.01.30.925222.
2. Kalia, L.V. and A.E. Lang, *Parkinson's disease.* Lancet, 2015. **386**(9996): p. 896-912.
3. Reeve, A., E. Simcox, and D. Turnbull, *Ageing and Parkinson's disease: why is advancing age the biggest risk factor?* Ageing Res Rev, 2014. **14**: p. 19-30.
4. Spillantini, M.G., et al., *Alpha-synuclein in Lewy bodies.* Nature, 1997. **388**(6645): p. 839-40.
5. Kish, S.J., K. Shannak, and O. Hornykiewicz, *Uneven pattern of dopamine loss in the striatum of patients with idiopathic Parkinson's disease. Pathophysiologic and clinical implications.* N Engl J Med, 1988. **318**(14): p. 876-80.
6. Nandhagopal, R., et al., *Longitudinal evolution of compensatory changes in striatal dopamine processing in Parkinson's disease.* Brain, 2011. **134**(Pt 11): p. 3290-8.
7. Postuma, R.B., et al., *Identifying prodromal Parkinson's disease: pre-motor disorders in Parkinson's disease.* Mov Disord, 2012. **27**(5): p. 617-26.
8. Tanner, C.M. and S.M. Goldman, *Epidemiology of Parkinson's disease.* Neurol Clin, 1996. **14**(2): p. 317-35.
9. Van Den Eeden, S.K., et al., *Incidence of Parkinson's disease: variation by age, gender, and race/ethnicity.* Am J Epidemiol, 2003. **157**(11): p. 1015-22.
10. Jafari, S., et al., *Head injury and risk of Parkinson disease: a systematic review and meta-analysis.* Mov Disord, 2013. **28**(9): p. 1222-9.
11. Jang, H., et al., *Viral parkinsonism.* Biochim Biophys Acta, 2009. **1792**(7): p. 714-21.
12. von Economo, C.F., *Die encephalitis lethargica*. Vol. 31. 1918: F. Deuticke.
13. Martyn, C.N. and C. Osmond, *Parkinson's disease and the environment in early life.* J Neurol Sci, 1995. **132**(2): p. 201-6.
14. Sandy, M.S., et al., *Role of active oxygen in paraquat and 1-methyl-4-phenyl-1,2,3,6-tetrahydropyridine (MPTP) cytotoxicity.* Basic Life Sci, 1988. **49**: p. 795-801.
15. Ballard, P.A., J.W. Tetrud, and J.W. Langston, *Permanent human parkinsonism due to 1-methyl-4-phenyl-1,2,3,6-tetrahydropyridine (MPTP): seven cases.* Neurology, 1985. **35**(7): p. 949-56.
16. Ramsay, R.R., et al., *Interaction of 1-methyl-4-phenylpyridinium ion (MPP+) and its analogs with the rotenone/piericidin binding site of NADH dehydrogenase.* J Neurochem, 1991. **56**(4): p. 1184-90.
17. Noyce, A.J., et al., *Meta-analysis of early nonmotor features and risk factors for Parkinson disease.* Ann Neurol, 2012. **72**(6): p. 893-901.
18. Dobbs, R.J., et al., *Association of circulating TNF-alpha and IL-6 with ageing and parkinsonism.* Acta Neurol Scand, 1999. **100**(1): p. 34-41.
19. Stypula, G., et al., *Evaluation of interleukins, ACTH, cortisol and prolactin concentrations in the blood of patients with parkinson's disease.* Neuroimmunomodulation, 1996. **3**(2-3): p. 131-4.
20. Rentzos, M., et al., *Circulating interleukin-15 and RANTES chemokine in Parkinson's disease.* Acta Neurol Scand, 2007. **116**(6): p. 374-9.
21. Mount, M.P., et al., *Involvement of interferon-gamma in microglial-mediated loss of dopaminergic neurons.* J Neurosci, 2007. **27**(12): p. 3328-37.
22. Hisanaga, K., et al., *Increase in peripheral CD4 bright+ CD8 dull+ T cells in Parkinson disease.* Arch Neurol, 2001. **58**(10): p. 1580-3.
23. Fiszer, U., et al., *gamma delta+ T cells are increased in patients with Parkinson's disease.* J Neurol Sci, 1994. **121**(1): p. 39-45.
24. Baba, Y., et al., *Alterations of T-lymphocyte populations in Parkinson disease.* Parkinsonism Relat Disord, 2005. **11**(8): p. 493-8.
25. McGeer, P.L., et al., *Reactive microglia are positive for HLA-DR in the substantia nigra of Parkinson's and Alzheimer's disease brains.* Neurology, 1988. **38**(8): p. 1285-91.
26. Damier, P., et al., *Glutathione peroxidase, glial cells and Parkinson's disease.* Neuroscience, 1993. **52**(1): p. 1-6.
27. Lin, L.F., et al., *GDNF: a glial cell line-derived neurotrophic factor for midbrain dopaminergic neurons.* Science, 1993. **260**(5111): p. 1130-2.
28. Brochard, V., et al., *Infiltration of CD4+ lymphocytes into the brain contributes to neurodegeneration in a mouse model of Parkinson disease.* J Clin Invest, 2009. **119**(1): p. 182-92.

29. Cheray, M. and B. Joseph, *Epigenetics Control Microglia Plasticity.* Front Cell Neurosci, 2018. **12**: p. 243.
30. Yamada, T., et al., *Histological and biochemical pathology in a family with autosomal dominant Parkinsonism and dementia.* Neurology Psychiatry and Brain Research, 1993. **2**(1): p. 26-35.
31. Le, W., D. Rowe, and W. Xie. *Activated microglia induce dopaminergic cell injury in vitro*. in *XIII International Congress on Parkinson's disease. Parkinson Relat Disord Vancouver*. 1999.
32. Jenner, P., *Oxidative stress in Parkinson's disease.* Ann Neurol, 2003. **53 Suppl 3**: p. S26-36; discussion S36-8.
33. McGeer, P.L., K. Yasojima, and E.G. McGeer, *Inflammation in Parkinson's disease.* Adv Neurol, 2001. **86**: p. 83-9.
34. Sriram, K., et al., *Mice deficient in TNF receptors are protected against dopaminergic neurotoxicity: implications for Parkinson's disease.* Faseb j, 2002. **16**(11): p. 1474-6.
35. Hunot, S., et al., *FcepsilonRII/CD23 is expressed in Parkinson's disease and induces, in vitro, production of nitric oxide and tumor necrosis factor-alpha in glial cells.* J Neurosci, 1999. **19**(9): p. 3440-7.
36. Mogi, M., et al., *p53 protein, interferon-gamma, and NF-kappaB levels are elevated in the parkinsonian brain.* Neurosci Lett, 2007. **414**(1): p. 94-7.
37. Kruger, R., et al., *Genetic analysis of immunomodulating factors in sporadic Parkinson's disease.* J Neural Transm (Vienna), 2000. **107**(5): p. 553-62.
38. McGeer, P.L., K. Yasojima, and E.G. McGeer, *Association of interleukin-1 beta polymorphisms with idiopathic Parkinson's disease.* Neurosci Lett, 2002. **326**(1): p. 67-9.
39. Liberatore, G.T., et al., *Inducible nitric oxide synthase stimulates dopaminergic neurodegeneration in the MPTP model of Parkinson disease.* Nat Med, 1999. **5**(12): p. 1403-9.
40. McGeer, P.L., et al., *Presence of reactive microglia in monkey substantia nigra years after 1-methyl-4-phenyl-1,2,3,6-tetrahydropyridine administration.* Ann Neurol, 2003. **54**(5): p. 599-604.
41. Wu, D.C., et al., *Blockade of microglial activation is neuroprotective in the 1-methyl-4-phenyl-1,2,3,6-tetrahydropyridine mouse model of Parkinson disease.* J Neurosci, 2002. **22**(5): p. 1763-71.
42. Polymeropoulos, M.H., et al., *Mutation in the alpha-synuclein gene identified in families with Parkinson's disease.* Science, 1997. **276**(5321): p. 2045-7.
43. Nalls, M.A., et al., *Expanding Parkinson's disease genetics: novel risk loci, genomic context, causal insights and heritable risk.* bioRxiv, 2018.
44. Sidransky, E. and G. Lopez, *The link between the GBA gene and parkinsonism.* Lancet Neurol, 2012. **11**(11): p. 986-98.
45. Zimprich, A., et al., *Mutations in LRRK2 cause autosomal-dominant parkinsonism with pleomorphic pathology.* Neuron, 2004. **44**(4): p. 601-7.
46. West, A.B., et al., *Parkinson's disease-associated mutations in leucine-rich repeat kinase 2 augment kinase activity.* Proc Natl Acad Sci U S A, 2005. **102**(46): p. 16842-7.
47. Lewis, P.A., et al., *The R1441C mutation of LRRK2 disrupts GTP hydrolysis.* Biochem Biophys Res Commun, 2007. **357**(3): p. 668-71.
48. Guaitoli, G., et al., *Structural model of the dimeric Parkinson's protein LRRK2 reveals a compact architecture involving distant interdomain contacts.* Proc Natl Acad Sci U S A, 2016. **113**(30): p. E4357-66.
49. Giasson, B.I., et al., *Biochemical and pathological characterization of Lrrk2.* Ann Neurol, 2006. **59**(2): p. 315-22.
50. Biskup, S., et al., *Localization of LRRK2 to membranous and vesicular structures in mammalian brain.* Ann Neurol, 2006. **60**(5): p. 557-69.
51. Sharma, S., et al., *LRRK2 expression in idiopathic and G2019S positive Parkinson's disease subjects: a morphological and quantitative study.* Neuropathol Appl Neurobiol, 2011. **37**(7): p. 777-90.
52. Steger, M., et al., *Phosphoproteomics reveals that Parkinson's disease kinase LRRK2 regulates a subset of Rab GTPases.* Elife, 2016. **5**.
53. Waschbusch, D., et al., *LRRK2 transport is regulated by its novel interacting partner Rab32.* PLoS One, 2014. **9**(10): p. e111632.
54. Gloeckner, C.J., et al., *The Parkinson disease-associated protein kinase LRRK2 exhibits MAPKKK activity and phosphorylates MKK3/6 and MKK4/7, in vitro.* J Neurochem, 2009. **109**(4): p. 959-68.

55. Berger, Z., K.A. Smith, and M.J. Lavoie, *Membrane localization of LRRK2 is associated with increased formation of the highly active LRRK2 dimer and changes in its phosphorylation.* Biochemistry, 2010. **49**(26): p. 5511-23.
56. Kett, L.R., et al., *LRRK2 Parkinson disease mutations enhance its microtubule association.* Hum Mol Genet, 2012. **21**(4): p. 890-9.
57. Heo, H.Y., K.S. Kim, and W. Seol, *Coordinate Regulation of Neurite Outgrowth by LRRK2 and Its Interactor, Rab5.* Exp Neurobiol, 2010. **19**(2): p. 97-105.
58. Beilina, A., et al., *Unbiased screen for interactors of leucine-rich repeat kinase 2 supports a common pathway for sporadic and familial Parkinson disease.* Proc Natl Acad Sci U S A, 2014. **111**(7): p. 2626-31.
59. Atashrazm, F., et al., *LRRK2-mediated Rab10 phosphorylation in immune cells from Parkinson's disease patients.* Mov Disord, 2019. **34**(3): p. 406-415.
60. Ysselstein, D., et al., *LRRK2 kinase activity regulates lysosomal glucocerebrosidase in neurons derived from Parkinson's disease patients.* Nat Commun, 2019. **10**(1): p. 5570.
61. Tong, Y., et al., *Loss of leucine-rich repeat kinase 2 causes age-dependent bi-phasic alterations of the autophagy pathway.* Mol Neurodegener, 2012. **7**: p. 2.
62. Manzoni, C., et al., *mTOR independent regulation of macroautophagy by Leucine Rich Repeat Kinase 2 via Beclin-1.* Sci Rep, 2016. **6**: p. 35106.
63. Schapansky, J., et al., *Membrane recruitment of endogenous LRRK2 precedes its potent regulation of autophagy.* Hum Mol Genet, 2014. **23**(16): p. 4201-14.
64. Manzoni, C., et al., *Inhibition of LRRK2 kinase activity stimulates macroautophagy.* Biochim Biophys Acta, 2013. **1833**(12): p. 2900-2910.
65. Saez-Atienzar, S., et al., *The LRRK2 inhibitor GSK2578215A induces protective autophagy in SH-SY5Y cells: involvement of Drp-1-mediated mitochondrial fission and mitochondrial-derived ROS signaling.* Cell Death Dis, 2014. **5**: p. e1368.
66. Stafa, K., et al., *Functional interaction of Parkinson's disease-associated LRRK2 with members of the dynamin GTPase superfamily.* Hum Mol Genet, 2014. **23**(8): p. 2055-77.
67. Wang, X., et al., *LRRK2 regulates mitochondrial dynamics and function through direct interaction with DLP1.* Hum Mol Genet, 2012. **21**(9): p. 1931-44.
68. Smith, G.A., et al., *Fibroblast Biomarkers of Sporadic Parkinson's Disease and LRRK2 Kinase Inhibition.* Mol Neurobiol, 2016. **53**(8): p. 5161-77.
69. Su, Y.C. and X. Qi, *Inhibition of excessive mitochondrial fission reduced aberrant autophagy and neuronal damage caused by LRRK2 G2019S mutation.* Hum Mol Genet, 2013. **22**(22): p. 4545-61.
70. Grunewald, A., et al., *Does uncoupling protein 2 expression qualify as marker of disease status in LRRK2-associated Parkinson's disease?* Antioxid Redox Signal, 2014. **20**(13): p. 1955-60.
71. Hsieh, C.H., et al., *Functional Impairment in Miro Degradation and Mitophagy Is a Shared Feature in Familial and Sporadic Parkinson's Disease.* Cell Stem Cell, 2016. **19**(6): p. 709-724.
72. Cherra, S.J., 3rd, et al., *Mutant LRRK2 elicits calcium imbalance and depletion of dendritic mitochondria in neurons.* Am J Pathol, 2013. **182**(2): p. 474-84.
73. Verma, M., et al., *Mitochondrial Calcium Dysregulation Contributes to Dendrite Degeneration Mediated by PD/LBD-Associated LRRK2 Mutants.* J Neurosci, 2017. **37**(46): p. 11151-11165.
74. Schwab, A.J. and A.D. Ebert, *Neurite Aggregation and Calcium Dysfunction in iPSC-Derived Sensory Neurons with Parkinson's Disease-Related LRRK2 G2019S Mutation.* Stem Cell Reports, 2015. **5**(6): p. 1039-1052.
75. Korecka, J.A., et al., *Neurite Collapse and Altered ER Ca(2+) Control in Human Parkinson Disease Patient iPSC-Derived Neurons with LRRK2 G2019S Mutation.* Stem Cell Reports, 2019. **12**(1): p. 29-41.
76. Caesar, M., et al., *Leucine-rich repeat kinase 2 functionally interacts with microtubules and kinase-dependently modulates cell migration.* Neurobiol Dis, 2013. **54**: p. 280-8.
77. Law, B.M., et al., *A direct interaction between leucine-rich repeat kinase 2 and specific beta-tubulin isoforms regulates tubulin acetylation.* J Biol Chem, 2014. **289**(2): p. 895-908.
78. Gillardon, F., *Leucine-rich repeat kinase 2 phosphorylates brain tubulin-beta isoforms and modulates microtubule stability--a point of convergence in parkinsonian neurodegeneration?* J Neurochem, 2009. **110**(5): p. 1514-22.

79. Esteves, A.R., et al., *The Upshot of LRRK2 Inhibition to Parkinson's Disease Paradigm.* Mol Neurobiol, 2015. **52**(3): p. 1804-1820.
80. Godena, V.K., et al., *Increasing microtubule acetylation rescues axonal transport and locomotor deficits caused by LRRK2 Roc-COR domain mutations.* Nat Commun, 2014. **5**: p. 5245.
81. Li, X., et al., *Enhanced striatal dopamine transmission and motor performance with LRRK2 overexpression in mice is eliminated by familial Parkinson's disease mutation G2019S.* J Neurosci, 2010. **30**(5): p. 1788-97.
82. Ramonet, D., et al., *Dopaminergic neuronal loss, reduced neurite complexity and autophagic abnormalities in transgenic mice expressing G2019S mutant LRRK2.* PLoS One, 2011. **6**(4): p. e18568.
83. Schuepbach, W.M., et al., *Neurostimulation for Parkinson's disease with early motor complications.* N Engl J Med, 2013. **368**(7): p. 610-22.
84. Song, B., et al., *Human autologous iPSC-derived dopaminergic progenitors restore motor function in Parkinson's disease models.* J Clin Invest, 2020. **130**(2): p. 904-920.
85. Kim, J.H., et al., *Dopamine neurons derived from embryonic stem cells function in an animal model of Parkinson's disease.* Nature, 2002. **418**(6893): p. 50-6.
86. Ben-Hur, T., et al., *Transplantation of human embryonic stem cell-derived neural progenitors improves behavioral deficit in Parkinsonian rats.* Stem Cells, 2004. **22**(7): p. 1246-55.
87. Johnston, L.C., et al., *Clinically relevant effects of convection-enhanced delivery of AAV2-GDNF on the dopaminergic nigrostriatal pathway in aged rhesus monkeys.* Hum Gene Ther, 2009. **20**(5): p. 497-510.
88. Sardi, S.P., et al., *Glucosylceramide synthase inhibition alleviates aberrations in synucleinopathy models.* Proc Natl Acad Sci U S A, 2017. **114**(10): p. 2699-2704.
89. Fischer, T., et al., *Evaluation of Glucosylceramide Synthase (GCS) Inhibition for GBA-Associated Parkinson's Disease (P3.051).* Neurology, 2018. **90**(15 Supplement): p. P3.051.
90. Taymans, J.M. and E. Greggio, *LRRK2 Kinase Inhibition as a Therapeutic Strategy for Parkinson's Disease, Where Do We Stand?* Curr Neuropharmacol, 2016. **14**(3): p. 214-25.
91. Hakimi, M., et al., *Parkinson's disease-linked LRRK2 is expressed in circulating and tissue immune cells and upregulated following recognition of microbial structures.* Journal of neural transmission, 2011. **118**(5): p. 795-808.
92. Thevenet, J., et al., *Regulation of LRRK2 expression points to a functional role in human monocyte maturation.* PLoS One, 2011. **6**(6): p. e21519.
93. Cook, D.A., et al., *LRRK2 levels in immune cells are increased in Parkinson's disease.* NPJ Parkinsons Dis, 2017. **3**: p. 11.
94. Dzamko, N., D.B. Rowe, and G.M. Halliday, *Increased peripheral inflammation in asymptomatic leucine-rich repeat kinase 2 mutation carriers.* Mov Disord, 2016. **31**(6): p. 889-97.
95. Mira, M.T., et al., *Susceptibility to leprosy is associated with PARK2 and PACRG.* Nature, 2004. **427**(6975): p. 636-40.
96. Barrett, J.C., et al., *Genome-wide association defines more than 30 distinct susceptibility loci for Crohn's disease.* Nat Genet, 2008. **40**(8): p. 955-62.
97. Hui, K.Y., et al., *Functional variants in the LRRK2 gene confer shared effects on risk for Crohn's disease and Parkinson's disease.* Sci Transl Med, 2018. **10**(423).
98. Umeno, J., et al., *Meta-analysis of published studies identified eight additional common susceptibility loci for Crohn's disease and ulcerative colitis.* Inflamm Bowel Dis, 2011. **17**(12): p. 2407-15.
99. Gillardon, F., R. Schmid, and H. Draheim, *Parkinson's disease-linked leucine-rich repeat kinase 2(R1441G) mutation increases proinflammatory cytokine release from activated primary microglial cells and resultant neurotoxicity.* Neuroscience, 2012. **208**: p. 41-8.
100. Gardet, A., et al., *LRRK2 Is Involved in the IFN-{gamma} Response and Host Response to Pathogens.* J Immunol, 2010.
101. Kuss, M., E. Adamopoulou, and P.J. Kahle, *Interferon-gamma induces leucine-rich repeat kinase LRRK2 via extracellular signal-regulated kinase ERK5 in macrophages.* J Neurochem, 2014. **129**(6): p. 980-7.
102. Brockmann, K., et al., *Inflammatory profile in LRRK2-associated prodromal and clinical PD.* J Neuroinflammation, 2016. **13**(1): p. 122.

103. Zhang, Q., et al., *Commensal bacteria direct selective cargo sorting to promote symbiosis.* Nat Immunol, 2015. **16**(9): p. 918-26.
104. Liu, Z., et al., *The kinase LRRK2 is a regulator of the transcription factor NFAT that modulates the severity of inflammatory bowel disease.* Nature immunology, 2011. **12**(11): p. 1063-70.
105. Wong, A.Y.W., et al., *Leucine-Rich Repeat Kinase 2 Controls the Ca(2+)/Nuclear Factor of Activated T Cells/IL-2 Pathway during Aspergillus Non-Canonical Autophagy in Dendritic Cells.* Front Immunol, 2018. **9**: p. 210.
106. Russo, I., et al., *Leucine-rich repeat kinase 2 positively regulates inflammation and down-regulates NF-kappaB p50 signaling in cultured microglia cells.* J Neuroinflammation, 2015. **12**: p. 230.
107. Moehle, M.S., et al., *LRRK2 inhibition attenuates microglial inflammatory responses.* The Journal of neuroscience : the official journal of the Society for Neuroscience, 2012. **32**(5): p. 1602-11.
108. Choi, I., et al., *LRRK2 G2019S mutation attenuates microglial motility by inhibiting focal adhesion kinase.* Nat Commun, 2015. **6**: p. 8255.
109. Ma, B., et al., *LRRK2 modulates microglial activity through regulation of chemokine (C-X3-C) receptor 1 -mediated signalling pathways.* Hum Mol Genet, 2016. **25**(16): p. 3515-3523.
110. Dzamko, N., et al., *The IkappaB kinase family phosphorylates the Parkinson's disease kinase LRRK2 at Ser935 and Ser910 during Toll-like receptor signaling.* PLoS One, 2012. **7**(6): p. e39132.
111. Liu, W., et al., *LRRK2 promotes the activation of NLRC4 inflammasome during Salmonella Typhimurium infection.* J Exp Med, 2017. **214**(10): p. 3051-3066.
112. Shutinoski, B., et al., *Lrrk2 alleles modulate inflammation during microbial infection of mice in a sex-dependent manner.* Sci Transl Med, 2019. **11**(511).
113. Hartlova, A., et al., *LRRK2 is a negative regulator of Mycobacterium tuberculosis phagosome maturation in macrophages.* Embo j, 2018. **37**(12).
114. Weindel, C.G., et al., *LRRK2 maintains mitochondrial homeostasis and regulates innate immune responses to Mycobacterium tuberculosis.* Elife, 2020. **9**.
115. Isaacs, A. and J. Lindenmann, *Virus interference. I. The interferon.* Proc R Soc Lond B Biol Sci, 1957. **147**(927): p. 258-67.
116. Kawanokuchi, J., et al., *Production of interferon-gamma by microglia.* Mult Scler, 2006. **12**(5): p. 558-64.
117. Makela, J., et al., *Interferon-gamma produced by microglia and the neuropeptide PACAP have opposite effects on the viability of neural progenitor cells.* PLoS One, 2010. **5**(6): p. e11091.
118. Deczkowska, A., K. Baruch, and M. Schwartz, *Type I/II Interferon Balance in the Regulation of Brain Physiology and Pathology.* Trends Immunol, 2016. **37**(3): p. 181-192.
119. Mathys, H., et al., *Temporal Tracking of Microglia Activation in Neurodegeneration at Single-Cell Resolution.* Cell Rep, 2017. **21**(2): p. 366-380.
120. Olah, M., et al., *A single cell-based atlas of human microglial states reveals associations with neurological disorders and histopathological features of the aging brain.* bioRxiv, 2018.
121. Liscovitch, N. and L. French, *Differential Co-Expression between alpha-Synuclein and IFN-gamma Signaling Genes across Development and in Parkinson's Disease.* PLoS One, 2014. **9**(12): p. e115029.
122. Chakrabarty, P., et al., *Interferon-gamma induces progressive nigrostriatal degeneration and basal ganglia calcification.* Nat Neurosci, 2011. **14**(6): p. 694-6.
123. Strickland, M.R., et al., *Ifngr1 and Stat1 mediated canonical Ifn-gamma signaling drives nigrostriatal degeneration.* Neurobiol Dis, 2018. **110**: p. 133-141.
124. Kozina, E., et al., *Mutant LRRK2 mediates peripheral and central immune responses leading to neurodegeneration in vivo.* Brain, 2018. **141**(6): p. 1753-1769.
125. Barcia, C., et al., *IFN-gamma signaling, with the synergistic contribution of TNF-alpha, mediates cell specific microglial and astroglial activation in experimental models of Parkinson's disease.* Cell Death Dis, 2011. **2**: p. e142.
126. Filiano, A.J., et al., *Unexpected role of interferon-gamma in regulating neuronal connectivity and social behaviour.* Nature, 2016. **535**(7612): p. 425-9.
127. Li, H., et al., *Modeling Parkinson's Disease Using Patient-specific Induced Pluripotent Stem Cells.* J Parkinsons Dis, 2018. **8**(4): p. 479-493.
128. Takahashi, K. and S. Yamanaka, *Induction of pluripotent stem cells from mouse embryonic and adult fibroblast cultures by defined factors.* Cell, 2006. **126**(4): p. 663-76.

129. Takahashi, K., et al., *Induction of pluripotent stem cells from adult human fibroblasts by defined factors.* Cell, 2007. **131**(5): p. 861-72.
130. Kunisato, A., et al., *Generation of induced pluripotent stem cells by efficient reprogramming of adult bone marrow cells.* Stem Cells Dev, 2010. **19**(2): p. 229-38.
131. Aasen, T., et al., *Efficient and rapid generation of induced pluripotent stem cells from human keratinocytes.* Nat Biotechnol, 2008. **26**(11): p. 1276-84.
132. Nakagawa, M., et al., *Generation of induced pluripotent stem cells without Myc from mouse and human fibroblasts.* Nat Biotechnol, 2008. **26**(1): p. 101-6.
133. Yu, J., et al., *Induced pluripotent stem cell lines derived from human somatic cells.* Science, 2007. **318**(5858): p. 1917-20.
134. Wu, X., et al., *Transcription start regions in the human genome are favored targets for MLV integration.* Science, 2003. **300**(5626): p. 1749-51.
135. Brambrink, T., et al., *Sequential expression of pluripotency markers during direct reprogramming of mouse somatic cells.* Cell Stem Cell, 2008. **2**(2): p. 151-9.
136. Stadtfeld, M., et al., *Induced pluripotent stem cells generated without viral integration.* Science, 2008. **322**(5903): p. 945-9.
137. Fusaki, N., et al., *Efficient induction of transgene-free human pluripotent stem cells using a vector based on Sendai virus, an RNA virus that does not integrate into the host genome.* Proc Jpn Acad Ser B Phys Biol Sci, 2009. **85**(8): p. 348-62.
138. Okita, K., et al., *Generation of mouse induced pluripotent stem cells without viral vectors.* Science, 2008. **322**(5903): p. 949-53.
139. Zhou, H., et al., *Generation of induced pluripotent stem cells using recombinant proteins.* Cell Stem Cell, 2009. **4**(5): p. 381-4.
140. Warren, L., et al., *Highly efficient reprogramming to pluripotency and directed differentiation of human cells with synthetic modified mRNA.* Cell Stem Cell, 2010. **7**(5): p. 618-30.
141. Kriks, S., et al., *Dopamine neurons derived from human ES cells efficiently engraft in animal models of Parkinson's disease.* Nature, 2011. **480**(7378): p. 547-51.
142. Reinhardt, P., et al., *Derivation and expansion using only small molecules of human neural progenitors for neurodegenerative disease modeling.* PLoS One, 2013. **8**(3): p. e59252.
143. Flierl, A., et al., *Higher vulnerability and stress sensitivity of neuronal precursor cells carrying an alpha-synuclein gene triplication.* PLoS One, 2014. **9**(11): p. e112413.
144. Oliveira, L.M., et al., *Elevated alpha-synuclein caused by SNCA gene triplication impairs neuronal differentiation and maturation in Parkinson's patient-derived induced pluripotent stem cells.* Cell Death Dis, 2015. **6**: p. e1994.
145. Chung, C.Y., et al., *Identification and rescue of alpha-synuclein toxicity in Parkinson patient-derived neurons.* Science, 2013. **342**(6161): p. 983-7.
146. Ryan, S.D., et al., *Isogenic human iPSC Parkinson's model shows nitrosative stress-induced dysfunction in MEF2-PGC1alpha transcription.* Cell, 2013. **155**(6): p. 1351-64.
147. Jiang, H., et al., *Parkin controls dopamine utilization in human midbrain dopaminergic neurons derived from induced pluripotent stem cells.* Nat Commun, 2012. **3**: p. 668.
148. Ren, Y., et al., *Parkin mutations reduce the complexity of neuronal processes in iPSC-derived human neurons.* Stem Cells, 2015. **33**(1): p. 68-78.
149. Shaltouki, A., et al., *Mitochondrial alterations by PARKIN in dopaminergic neurons using PARK2 patient-specific and PARK2 knockout isogenic iPSC lines.* Stem Cell Reports, 2015. **4**(5): p. 847-59.
150. Chung, S.Y., et al., *Parkin and PINK1 Patient iPSC-Derived Midbrain Dopamine Neurons Exhibit Mitochondrial Dysfunction and alpha-Synuclein Accumulation.* Stem Cell Reports, 2016. **7**(4): p. 664-677.
151. Morais, V.A., et al., *PINK1 loss-of-function mutations affect mitochondrial complex I activity via NdufA10 ubiquinone uncoupling.* Science, 2014. **344**(6180): p. 203-7.
152. Burbulla, L.F., et al., *Dopamine oxidation mediates mitochondrial and lysosomal dysfunction in Parkinson's disease.* Science, 2017. **357**(6357): p. 1255-1261.
153. Schondorf, D.C., et al., *iPSC-derived neurons from GBA1-associated Parkinson's disease patients show autophagic defects and impaired calcium homeostasis.* Nat Commun, 2014. **5**: p. 4028.

154. Schondorf, D.C., et al., *The NAD+ Precursor Nicotinamide Riboside Rescues Mitochondrial Defects and Neuronal Loss in iPSC and Fly Models of Parkinson's Disease.* Cell Rep, 2018. **23**(10): p. 2976-2988.
155. Nguyen, H.N., et al., *LRRK2 mutant iPSC-derived DA neurons demonstrate increased susceptibility to oxidative stress.* Cell Stem Cell, 2011. **8**(3): p. 267-80.
156. Skibinski, G., et al., *Mutant LRRK2 toxicity in neurons depends on LRRK2 levels and synuclein but not kinase activity or inclusion bodies.* J Neurosci, 2014. **34**(2): p. 418-33.
157. Sanchez-Danes, A., et al., *Disease-specific phenotypes in dopamine neurons from human iPS-based models of genetic and sporadic Parkinson's disease.* EMBO Mol Med, 2012. **4**(5): p. 380-95.
158. Reinhardt, P., et al., *Genetic correction of a LRRK2 mutation in human iPSCs links parkinsonian neurodegeneration to ERK-dependent changes in gene expression.* Cell Stem Cell, 2013. **12**(3): p. 354-67.
159. Sanders, L.H., et al., *LRRK2 mutations cause mitochondrial DNA damage in iPSC-derived neural cells from Parkinson's disease patients: reversal by gene correction.* Neurobiol Dis, 2014. **62**: p. 381-6.
160. Smits, L.M., et al., *Modeling Parkinson's disease in midbrain-like organoids.* NPJ Parkinsons Dis, 2019. **5**: p. 5.
161. Berry, B.J., et al., *Advances and Current Challenges Associated with the Use of Human Induced Pluripotent Stem Cells in Modeling Neurodegenerative Disease.* Cells Tissues Organs, 2018. **205**(5-6): p. 331-349.
162. Kyttala, A., et al., *Genetic Variability Overrides the Impact of Parental Cell Type and Determines iPSC Differentiation Potential.* Stem Cell Reports, 2016. **6**(2): p. 200-12.
163. Hu, B.Y., et al., *Neural differentiation of human induced pluripotent stem cells follows developmental principles but with variable potency.* Proc Natl Acad Sci U S A, 2010. **107**(9): p. 4335-40.
164. Carcamo-Orive, I., et al., *Analysis of Transcriptional Variability in a Large Human iPSC Library Reveals Genetic and Non-genetic Determinants of Heterogeneity.* Cell Stem Cell, 2017. **20**(4): p. 518-532.e9.
165. Kilpinen, H., et al., *Common genetic variation drives molecular heterogeneity in human iPSCs.* Nature, 2017. **546**(7658): p. 370-375.
166. Zhang, Z., Y. Nishimura, and P. Kanchanawong, *Extracting microtubule networks from superresolution single-molecule localization microscopy data.* Mol Biol Cell, 2017. **28**(2): p. 333-345.
167. Rusinova, I., et al., *Interferome v2.0: an updated database of annotated interferon-regulated genes.* Nucleic Acids Res, 2013. **41**(Database issue): p. D1040-6.
168. Cross, D.A., et al., *Inhibition of glycogen synthase kinase-3 by insulin mediated by protein kinase B.* Nature, 1995. **378**(6559): p. 785-9.
169. Beals, C.R., et al., *Nuclear export of NF-ATc enhanced by glycogen synthase kinase-3.* Science, 1997. **275**(5308): p. 1930-4.
170. Graef, I.A., et al., *Neurotrophins and netrins require calcineurin/NFAT signaling to stimulate outgrowth of embryonic axons.* Cell, 2003. **113**(5): p. 657-70.
171. Benedito, A.B., et al., *The transcription factor NFAT3 mediates neuronal survival.* J Biol Chem, 2005. **280**(4): p. 2818-25.
172. Floyd, Z.E. and J.M. Stephens, *Interferon-gamma-mediated activation and ubiquitin-proteasome-dependent degradation of PPARgamma in adipocytes.* J Biol Chem, 2002. **277**(6): p. 4062-8.
173. Beals, C.R., et al., *Nuclear localization of NF-ATc by a calcineurin-dependent, cyclosporin-sensitive intramolecular interaction.* Genes Dev, 1997. **11**(7): p. 824-34.
174. Aguera-Gonzalez, S., et al., *Adenomatous Polyposis Coli Defines Treg Differentiation and Anti-inflammatory Function through Microtubule-Mediated NFAT Localization.* Cell Rep, 2017. **21**(1): p. 181-194.
175. Brown, M.D. and D.B. Sacks, *IQGAP1 in cellular signaling: bridging the GAP.* Trends Cell Biol, 2006. **16**(5): p. 242-9.
176. Hedman, A.C., J.M. Smith, and D.B. Sacks, *The biology of IQGAP proteins: beyond the cytoskeleton.* EMBO Rep, 2015. **16**(4): p. 427-46.

177. Watanabe, T., et al., *Interaction with IQGAP1 links APC to Rac1, Cdc42, and actin filaments during cell polarization and migration*. Dev Cell, 2004. **7**(6): p. 871-83.
178. Sharma, S., et al., *Dephosphorylation of the nuclear factor of activated T cells (NFAT) transcription factor is regulated by an RNA-protein scaffold complex.* Proc Natl Acad Sci U S A, 2011. **108**(28): p. 11381-6.
179. Kao, S.C., et al., *Calcineurin/NFAT signaling is required for neuregulin-regulated Schwann cell differentiation.* Science, 2009. **323**(5914): p. 651-4.
180. Miklossy, J., et al., *LRRK2 expression in normal and pathologic human brain and in human cell lines.* J Neuropathol Exp Neurol, 2006. **65**(10): p. 953-63.
181. Russo, I., et al., *Transcriptome analysis of LRRK2 knock-out microglia cells reveals alterations of inflammatory- and oxidative stress-related pathways upon treatment with alpha-synuclein fibrils.* Neurobiol Dis, 2019. **129**: p. 67-78.
182. Ormel, P.R., et al., *Microglia innately develop within cerebral organoids.* Nat Commun, 2018. **9**(1): p. 4167.
183. Song, L., et al., *Functionalization of Brain Region-specific Spheroids with Isogenic Microglia-like Cells.* Sci Rep, 2019. **9**(1): p. 11055.
184. Abreu, C.M., et al., *Microglia Increase Inflammatory Responses in iPSC-Derived Human BrainSpheres.* Front Microbiol, 2018. **9**: p. 2766.
185. Luciunaite, A., et al., *Soluble Abeta oligomers and protofibrils induce NLRP3 inflammasome activation in microglia*. J Neurochem, 2019: p. e14945.
186. Ising, C., et al., *NLRP3 inflammasome activation drives tau pathology.* Nature, 2019. **575**(7784): p. 669-673.
187. Tejera, D., et al., *Systemic inflammation impairs microglial Abeta clearance through NLRP3 inflammasome*. Embo j, 2019. **38**(17): p. e101064.
188. Hu, X., et al., *IFN-gamma suppresses IL-10 production and synergizes with TLR2 by regulating GSK3 and CREB/AP-1 proteins.* Immunity, 2006. **24**(5): p. 563-74.
189. Ohta, E., et al., *LRRK2 directly phosphorylates Akt1 as a possible physiological substrate: impairment of the kinase activity by Parkinson's disease-associated mutations.* FEBS Lett, 2011. **585**(14): p. 2165-70.
190. Chuang, C.L., et al., *Genetic dissection reveals that Akt is the critical kinase downstream of LRRK2 to phosphorylate and inhibit FOXO1, and promotes neuron survival.* Hum Mol Genet, 2014. **23**(21): p. 5649-58.
191. Reif, K., S. Lucas, and D. Cantrell, *A negative role for phosphoinositide 3-kinase in T-cell antigen receptor function.* Curr Biol, 1997. **7**(5): p. 285-93.
192. Antos, C.L., et al., *Activated glycogen synthase-3 beta suppresses cardiac hypertrophy in vivo.* Proc Natl Acad Sci U S A, 2002. **99**(2): p. 907-12.
193. Vaeth, M. and S. Feske, *NFAT control of immune function: New Frontiers for an Abiding Trooper.* F1000Res, 2018. **7**: p. 260.
194. Lim, J., H.S. Choi, and H.J. Choi, *Estrogen-related receptor gamma regulates dopaminergic neuronal phenotype by activating GSK3beta/NFAT signaling in SH-SY5Y cells.* J Neurochem, 2015. **133**(4): p. 544-57.
195. Vashishta, A., et al., *Nuclear factor of activated T-cells isoform c4 (NFATc4/NFAT3) as a mediator of antiapoptotic transcription in NMDA receptor-stimulated cortical neurons.* J Neurosci, 2009. **29**(48): p. 15331-40.
196. Yoshida, T. and M. Mishina, *Distinct roles of calcineurin-nuclear factor of activated T-cells and protein kinase A-cAMP response element-binding protein signaling in presynaptic differentiation.* J Neurosci, 2005. **25**(12): p. 3067-79.
197. Serrano-Perez, M.C., et al., *NFAT transcription factors regulate survival, proliferation, migration, and differentiation of neural precursor cells.* Glia, 2015. **63**(6): p. 987-1004.
198. Zhang, J.G., et al., *The conserved SOCS box motif in suppressors of cytokine signaling binds to elongins B and C and may couple bound proteins to proteasomal degradation.* Proc Natl Acad Sci U S A, 1999. **96**(5): p. 2071-6.
199. Yoeli-Lerner, M., et al., *Akt blocks breast cancer cell motility and invasion through the transcription factor NFAT.* Mol Cell, 2005. **20**(4): p. 539-50.

200. Yoeli-Lerner, M., et al., *Akt/protein kinase b and glycogen synthase kinase-3beta signaling pathway regulates cell migration through the NFAT1 transcription factor.* Mol Cancer Res, 2009. **7**(3): p. 425-32.
201. Vihma, H., et al., *Regulation of different human NFAT isoforms by neuronal activity.* J Neurochem, 2016. **137**(3): p. 394-408.
202. Vihma, H. and T. Timmusk, *Sumoylation regulates the transcriptional activity of different human NFAT isoforms in neurons.* Neurosci Lett, 2017. **653**: p. 302-307.
203. Speidel, A., et al., *Leucine-Rich Repeat Kinase 2 Influences Fate Decision of Human Monocytes Differentiated from Induced Pluripotent Stem Cells.* PLoS One, 2016. **11**(11): p. e0165949.
204. Hogan, P.G., et al., *Transcriptional regulation by calcium, calcineurin, and NFAT.* Genes Dev, 2003. **17**(18): p. 2205-32.
205. Aas, V., K. Larsen, and J.G. Iversen, *IFN-gamma induces calcium transients and increases the capacitative calcium entry in human neutrophils.* J Interferon Cytokine Res, 1998. **18**(3): p. 197-205.
206. Franciosi, S., et al., *Interferon-gamma acutely induces calcium influx in human microglia.* J Neurosci Res, 2002. **69**(5): p. 607-13.
207. Mizuno, T., et al., *Interferon-gamma directly induces neurotoxicity through a neuron specific, calcium-permeable complex of IFN-gamma receptor and AMPA GluR1 receptor.* FASEB J, 2008. **22**(6): p. 1797-806.
208. Civiero, L., et al., *The role of LRRK2 in cytoskeletal dynamics.* Biochem Soc Trans, 2018. **46**(6): p. 1653-1663.
209. Manzoni, C., et al., *Computational analysis of the LRRK2 interactome.* PeerJ, 2015. **3**: p. e778.
210. Gillardon, F., *Interaction of elongation factor 1-alpha with leucine-rich repeat kinase 2 impairs kinase activity and microtubule bundling in vitro.* Neuroscience, 2009. **163**(2): p. 533-9.
211. Lin, C.H., et al., *LRRK2 G2019S mutation induces dendrite degeneration through mislocalization and phosphorylation of tau by recruiting autoactivated GSK3ss.* J Neurosci, 2010. **30**(39): p. 13138-49.
212. Liu, Y., et al., *IQGAP1 regulates actin cytoskeleton organization in podocytes through interaction with nephrin.* Cell Signal, 2015. **27**(4): p. 867-77.
213. Li, Z., et al., *IQGAP1 promotes neurite outgrowth in a phosphorylation-dependent manner.* J Biol Chem, 2005. **280**(14): p. 13871-8.
214. Kholmanskikh, S.S., et al., *Calcium-dependent interaction of Lis1 with IQGAP1 and Cdc42 promotes neuronal motility.* Nat Neurosci, 2006. **9**(1): p. 50-7.
215. Balenci, L., et al., *IQGAP1 regulates adult neural progenitors in vivo and vascular endothelial growth factor-triggered neural progenitor migration in vitro.* J Neurosci, 2007. **27**(17): p. 4716-24.
216. Gao, C., et al., *IQGAP1 regulates NR2A signaling, spine density, and cognitive processes.* J Neurosci, 2011. **31**(23): p. 8533-42.
217. Tecalco-Cruz, A.C., et al., *Interplay between interferon-stimulated gene 15/ISGylation and interferon gamma signaling in breast cancer cells.* Cell Signal, 2019. **54**: p. 91-101.
218. Lavalley, N.J., et al., *14-3-3 Proteins regulate mutant LRRK2 kinase activity and neurite shortening*. Hum Mol Genet, 2016. **25**(1): p. 109-22.
219. Borgs, L., et al., *Dopaminergic neurons differentiating from LRRK2 G2019S induced pluripotent stem cells show early neuritic branching defects.* Sci Rep, 2016. **6**: p. 33377.
220. Lin, C.H., et al., *Lovastatin protects neurite degeneration in LRRK2-G2019S parkinsonism through activating the Akt/Nrf pathway and inhibiting GSK3beta activity.* Hum Mol Genet, 2016. **25**(10): p. 1965-1978.
221. Orenstein, S.J., et al., *Interplay of LRRK2 with chaperone-mediated autophagy.* Nat Neurosci, 2013. **16**(4): p. 394-406.
222. Khurana, V., et al., *Genome-Scale Networks Link Neurodegenerative Disease Genes to alpha-Synuclein through Specific Molecular Pathways.* Cell Syst, 2017. **4**(2): p. 157-170.e14.
223. Marrone, L., et al., *Generation of iPSCs carrying a common LRRK2 risk allele for in vitro modeling of idiopathic Parkinson's disease.* PLoS One, 2018. **13**(3): p. e0192497.
224. Dineley, K.T., et al., *Amyloid-beta oligomers impair fear conditioned memory in a calcineurin-dependent fashion in mice.* J Neurosci Res, 2010. **88**(13): p. 2923-32.

225. Mukherjee, A., et al., *Calcineurin inhibition at the clinical phase of prion disease reduces neurodegeneration, improves behavioral alterations and increases animal survival.* PLoS Pathog, 2010. **6**(10): p. e1001138.
226. Hudry, E., et al., *Inhibition of the NFAT pathway alleviates amyloid beta neurotoxicity in a mouse model of Alzheimer's disease.* J Neurosci, 2012. **32**(9): p. 3176-92.
227. Shah, S.Z., et al., *A central role for calcineurin in protein misfolding neurodegenerative diseases.* Cell Mol Life Sci, 2017. **74**(6): p. 1061-1074.
228. Luo, J., et al., *A calcineurin- and NFAT-dependent pathway is involved in alpha-synuclein-induced degeneration of midbrain dopaminergic neurons.* Hum Mol Genet, 2014. **23**(24): p. 6567-74.
229. Nguyen, T., et al., *NFAT-3 is a transcriptional repressor of the growth-associated protein 43 during neuronal maturation.* J Biol Chem, 2009. **284**(28): p. 18816-23.
230. Kosiorek, M., et al., *Calcineurin/NFAT signaling represses genes Vamp1 and Vamp2 via PMCA-dependent mechanism during dopamine secretion by Pheochromocytoma cells.* PLoS One, 2014. **9**(3): p. e92176.
231. Deleidi, M., M. Jaggle, and G. Rubino, *Immune aging, dysmetabolism, and inflammation in neurological diseases.* Front Neurosci, 2015. **9**: p. 172.
232. Dulken, B.W., et al., *Single-cell analysis reveals T cell infiltration in old neurogenic niches.* Nature, 2019.
233. Sommer, A., et al., *Th17 Lymphocytes Induce Neuronal Cell Death in a Human iPSC-Based Model of Parkinson's Disease.* Cell Stem Cell, 2018. **23**(1): p. 123-131 e6.
234. Sulzer, D., et al., *T cells from patients with Parkinson's disease recognize alpha-synuclein peptides.* Nature, 2017. **546**(7660): p. 656-661.

Acknowledgements

I would like to thank Dr. Michela Deleidi for providing the tools for me to achieve my doctoral degree in her lab, and for making me learn a lot in this journey of 4 years.

I would like to thank all the colleagues that I had along me in this journey.

In particular, David for teaching me all about work and life, and for having been a great friend in times of need.

Dina, for being the most amazing special person I have ever met, I hope you never change.

Katha, for being one of the strongest person I know, always listening and supporting me.

Vasiliki, for making life at work a little better with her sense of humor.

And last but not least, Pascale, for being the best person (and scientist) I have ever met, and will probably ever meet.

I also want to thank my mom, dad, sister Sabrina and Teo, plus the new additions of Lisa and Luca, for always being supportive no matter where life was leading me. I love you, and I am proud of being your daughter.

To conclude, I would like to thank my boyfriend Andy, for sticking around during the ups and downs of my PhD, and for still supporting me. You are the best boyfriend.